CALCULATION OF SOLID PARTICLE EROSION IN A MULTISTAGE TURBINE

by

Mustafa Erten

B.S. in M.E., Boğaziçi University, 1981

Submitted to the Institute for Graduate Studies in Science and Engineering in partial fulfillment of the requirements for the degree of Master of Science in Mechanical Engineering

Boğaziçi University

1983

ABSTRACT

This thesis presents a computer package developed to calculate the blade erosion rates in multistage turbines that use particle-laden hot expansion gases. This package is an extension of the single-stage erosion code presented in an earlier work. The present package calculates gas flow and particle trajectories in each stage. The calculated particle outlet conditions of given stage are processed statistically to generate the particle inlet conditions to the next stage enabling trajectory and erosion calculations to be advanced beyond a single turbine stage. The package allows erosion predictions to be obtained either based on the semiempirical erosion formula presented earlier or by using an improved model which relies upon direct interpolation of available experimental data.

This computer package has been applied to a four-stage electric utility gas turbine. Erosion damage primarily occurs at the leading and trailing edges of the blades and is usually confined to pressure surfaces. It is found that, in addition to the first stage rotor blades, as indicated in earlier studies, the second stage rotor and the second and third stage stator blades may also be exposed to critical erosion damage. The useful life of the machine appears to be dictated by the thinning of the first stage rotor trailing edge, but the other high erosion points indicated by this study should also be effectively protected for feasible turbine operation. Recommended methods of controlling blade erosion and some general guidelines for the design of an erosion resistant turbine are indicated.

ÖZET

Bu tezde parçacık yüklü sıcak gaz kullanan çok kademeli türbinlerde meydana gelen kanat erozyon hızlarını hesaplamak için geliştirilen bir bilgisayar paketi sunulmaktadır. Bu paket daha önce sunulan tek kademeli erozyon programının bir uzantısı olarak geliştirilmiştir. Yeni pakette her kademenin gaz ve parçacık akışları hesaplanmaktadır. Verilen bir kademenin çıkışında hesaplanan parçacık özellikleri bir sonraki kademenin girişindeki parçacık özelliklerini elde etmek için istatistiki bir işlemden geçirilmekte ve böylelikle parçacık yörünge ve kanat erozyon hesapları bir tek türbin kademesinden öteye götürülebilmektedir. Erozyon hesabı daha önce sunulan yarı ampirik erozyon formülü ile veya mevcut deneysel datanın doğrudan interpolasyonu ile daha hassas bir biçimde yapılabilmektedir.

Bu bilgisayar paketinin elektrik üretiminde kullanılan dört kademeli bir gaz türbinine uygulanması sunulmaktadır. Sonuçlardan erozyon hasarının özellikle kanatların hucum ve firar kenarlarında oluştuğu ve genellikle basınç yüzeylerine tesir ettiği anlaşılmaktadır. Daha önceki çalışmaların gösterdiği gibi birinci kademe rotor kanatlarının aşırı bir erozyona maruz kaldığı gözlenmiş, ancak ilaveten ikinci kademe rotor ve ikinci, üçüncü kademe stator kanatlarında da kritik erozyon hasarı olduğu saptanmıştır. Türbinin faydalı ömrünün birinci kademe rotor kanatlarının firar kenarlarındaki inceleme ile sınırlandığı sonucuna varılmış fakat diğer yüksek erozyon bölgelerinin de etkin bir etkin bir biçimde korunması gereği ortaya çıkmıştır. Kanat erozyonu kontrolu ve erozyona dayanıklı bir türbin tasarımı hususlarında tavsiyeler belirtilmiştir.

ACKNOWLEDGEMENTS

I am indebted to my thesis supervisor Doç. Dr. Muhsin Mengütürk for his invaluable suggestions, guidance and encouragement during the development of this study. I would like to express my sincere gratitudes to him for his patience and goodwill that he has shown throughout my graduate studies.

I also wish to express my gratitudes to Dr. Doğan Güneş who made many suggestions and help for the improvement of the study which were gratefully appreciated.

I would like to extend my appreciation to my chief Mr. Necdet Arseven and my fellows at TSKB A.Ş. for their continous help, especially to Mr. Y.Selim Aygüney and also to Mr. Kağan Önal. My thanks to Miss. Bakiye Takmaz for her patience in typing the manuscript.

Support of Boğaziçi University Computer Center is gratefully acknowledged.

And last, I would like to express my deepest gratitudes to my family for their encouragement, support and precious help, especially to my sisters Miss. H.Gelengül Erten and Miss. Ç.Ferah Erten.

İstanbul, Nov. 1983
Mustafa Erten

TABLE OF CONTENTS

LIST OF FIGURES

Page

LIST OF TABLES

LIST OF SYMBOLS

$A_1, A_2, B_1, C_1, C_2, C_3$	Coefficients defined by Eq. 23
B	Hardness of target
BHN	Brinell hardness number
b	Blade chord
C, CK	Constants
C_D	Drag coefficient
DPH	Diamond-pyramid hardness
d_p	Particle diameter
E	Volume of material (m^3) removed per kg particle
E	Volume of material (m^3) removed in 10,000 hours
F_1	Surface properties
F_2	Surface shape
F_3	Particle shape
F_4	Particle strength
F_5	Particle concentration
F_6	Nature of the carrier gas
$f_1(I), f_2(I)$	Dimensionless functions of mass and dimensions of particle
$f_1(m'), f_2(m')$	Functions of flaw parameter of the weibull fracture strength distribution
G	Coefficient defined by Eq.19
H	Effective hardness of dust

H_v	Vickers diamond pyramid hardness number
K, K_1, K_2, K_3, K_{12}	Constants
$K_1, K_2, K_3, K_4, K_5, K_6$	Coefficients defined by Eq.25
K_1', K_2'	Coefficients defined by Table 2
k	Quantity involving material constant
M	Particle mass
m	Erosion velocity exponent
m_1, m_2	Coefficients defined by Eq.23
N	Number of blades
n	Coefficient defined by Eq.27
p	Constant plastic flow stress
Q	Erosion rate
Q_{BS}	Erosion rate for brittle materials
Q_{c1}, Q_{c2}	Cutting wear
Q_D	Deformation wear
Q_{DS}	Erosion rate for ductile materials
Q_t	Total wear
Q_W	Weight of metal loss
R	Degree of roundness of a particle in one plane
r	Radial coordinate
r_p	Average radius of particle
R_T	Tangential restitution ratio
St_{avg}	Average stokes number
T_g	Gas temperature
t	Time
t_n	Final time step
t_{n-1}	Initial time step
Δt	Time interval

Δt_n	Current time interval
V	Particle velocity
V_{avg}	Average gas velocity
$\vec{V}_g$	Absolute gas velocity vector
V_{n1}	Particle normal velocity before impact
V_{n2}	Particle normal velocity after impact
$\vec{V}_p$	Absolute particle velocity vector
V_{t1}	Particle tangential velocity before impact
V_{t2}	Particle tangential velocity after impact
W_i	Percent by weight of commercial abrasive particles corresponding to ith substance in the fly ash
W_p	Weight of impacting particles
W_r, W_x, W_θ	Relative gas velocity components in r,x,θ directions
X	Axial coordinate of fixed reference frame
x	Axial coordinate of rotating reference frame
Y	Coordinate of fixed reference frame
Z	Coordinate of fixed reference frame

Greek Symbols

α	Angle through which the flow is turned
β	Angle of attack
β_g	Inlet gas angle
β_o	Reference angle Eq.3,Eq.7,Eq.27
β_{max}	Maximum erosion angle
β_p	Inlet particle angle

β_1	Acute angle between the velocity vector and the tangent surface before impact
β_2	Acute angle between the velocity vector and the tangent surface after impact
δ	Deviation of particles from the gas flow at inlet
ε	Energy needed to remove a unit volume of material from the surface by cutting
ε'	Erosion due to unit mass of commercial abrasive particle
θ	Circumferential coordinate
μ_g	Gas viscosity
ξ	Erosion resistance per unit volume of target
σ_s	Stress level in the surface
ρ_g	Gas density
ρ_p	Particle density
ϕ	Energy needed to remove a unit volume of material from the surface by cutting
ψ	Erosion constant
Ω_p	Particle rotation at impingement
ω_j	Per cent by weight of commercial abrasive particle

I. INTRODUCTION

The escalating cost of petroleum together with the uncertanities in its availability has directed attention to coal as an alternative source of energy for future power plants.

In order for coal to widely substitute petroleum, more efficient and nonpolluting ways of obtaining power from coal must be found than the traditional system of burning pulverized coal in steam turbine plants. In this regard pressurized fluidized-bed combustion and low BTU coal gasification processes are under consideration for use in combined-cycle plants where part of the power will be generated by passing the combusted coal gas through a gas turbine.

One of the problems associated with this scheme is that the particulate matter contained in the hot expansion gas is likely to cause turbine blade erosion. Unless the gas is adequately filtered, significant amounts of particles ranging in size from 1to 10 μm can still pass through and enter the turbine. These particles may erode the blade surfaces and result in an unacceptably short operating life or mechanical failure without any warning.

The trival solution to this problem is to reduce the particulate content to negligible proportions by extensive filtration. However, hot-gas particle filters are very expensive and therefore, it is desirable to know in advance

how much filtration is required for economical plant operation. It is also desirable to achieve further reduction in filtration costs by taking special design precautions to ruggedize turbines against particle erosion.

Ability to theortically calculate turbine erosion is vital to determination of the particle filtration requirements and the development of an erosion resistant turbine design.

The most complete work about turbine blade erosion was reported by Mengütürk and Sverdrup {1}. The computer model developed by them enables calculation of erosion in an axial turbine stage. They reported erosion calculations for the first stage of a large electric utility gas turbine. However, it is not clear whether the critical erosion does indeed occur in the first stage. A more comprehensive analysis that considers all stages of a multistage turbine is necessary.

The aim of this thesis, is to modify the existing model which predicts the erosion in a single stage, and extend its applicability to a multistage turbine.

For this purpose, the existing program TPART was modified in such a way that it follows particles based on the gas flow solution of the TSONIC program developed by Katsanis {2} and stores impact data for further use in final erosion computations. The modified program is designed to carry out these trajectory calculations stage by stage. The calculated particle exit conditions of a given stage are processed statistically to generate the inlet conditions of the next stage. This procedure enables trajectory calculations to be advanced beyond a single turbine stage and represents the major extension to the single stage capability of the original TPART program. Moreover, the numerical integration procedure used is replaced by a "piecewise exact solution" (PES) technique (Mengütürk and Güneş {3}) that increases the speed of calculations considerably and the erosion calculation routines originally built in the program are removed and recomplied in a separate auxiliary

program TPER. The TPER program accepts impact data calculated and stored by TPART program and calculates erosion damage based on any desired erosion data. These modifications allow erosion prediction to be obtained for different blade materials without having to repeat the costly trajectory calculations.

The model described above was used to predict blade erosion of a 65 MW four stage electric utiliy gas turbine.

II. BACKGROUND

Theoretical prediction of turbine blade erosion requires calculation of particle trajectories in turbine blade passages. Erosion rates can be calculated by combining the calculated impact conditions with experimental data concerning erosion resistance of the blade material. Previous work on particle dynamics and erosion is summarized below.

2.1 PARTICLE DYNAMICS

In their pioneering work Lapple and Shepherd {4} developed equations governing particle motion in a fluid flow in the presence of viscous drag force only. Davies and Peetz{5} calculated particle trajectories around a cylinder by assuming Stokes' drag law. Heywood {6} described a procedure for calculating the uniform velocity attained by particles under steady conditions. Techniques for determining trajectories of particles experiencing unsteady two-dimensional motion were deseribed by Holland-Batt {7}. Tabakoff and Hussein.{8.9} investigated particle trajectories and effect of particle concentration, mean diameter and material density on flow properties by using an experimental cascade. Hussein and Tabakoff {10} presented a computer model to calculate trajectories of solid particles in turbine and compressor blade passages. A theoretical analysis was also described by Morsi and Alexander {11} to determine particle trajectories around

isolated symmetrical and cambered airfoils.

Ulke and Rouleau {12} studied the effect of secondary flows on the motions of particles in an axial gas turbine and indicated that turbine secondary flows must be given serious consideration in particle trajectory calculations since these flows may significantly affect the paths and distribution of particles through the blade rows.

In an analytical investigation of particle trajectories in cascades of airfoils Dring, et al {13} calculated location, velocity, and angle of particle impacts on turbine blades. Results were compared with experimentally determined trajectories.

Using a computer model, similar in scope to that of Mengütürk and Sverdrup {1}, Lord and Singh {14} calculated particle trajectories in blade passages.

Flow visualization techniques were developed by Suo, et al {15} and used to study particle trajectories near an airfoil with a film-cooled leading edge. The results indicated that turbine airfoil leading edge film cooling in a gas turbine engine may deflect particles up to at least 5.8 μm in diameter when the cooling air velocity is at least 0.67 times the approach velocity.

Mengütürk, et al {16} studied the effect of blade boundary layer on particle trajectories. It is noted that the boundary layer effect on the trajectories of particles smaller than 6 μm is important and that an accurate assessment of turbine erosion and deposition requires inclusion of the boundary layer effect.

2.2 EROSION OF METALS

The erosion phenomenon was described by Finnie, Wolak and Kabil {17} as the removal of material from a solid surface by the action of impinging solid or liquid particles. This type of wear arises in many industrial operations and also finds useful application as a material removal process. To understand erosion, or any other type of wear, one must identify and analyze the mechanism or mecanisms by which material is being removed. The practical experience with erosion indicated that there are at least two types of material behavior. Ductile materials undergo weight loss by a process of plastic deformation in which material is removed by the displacing or cutting action of the particle. This type of wear exists if particles strike a body at an acute angle, scratching out some material from the surface. Brittle materials exhibit a different mechanism of erosion primarily because they fracture immediately after elastic deformation without going through any plastic deformation. In the brittle erosion case, material is removed by the intersection of cracks which radiate out from the point of impact of the eroding particles. As it is also seen from Figure 1 ductile and brittle materials respond to erosion in very different ways. Departures from ideally ductile or ideally brittle behavior can be discussed in a qualitative manner. The ductile mode is characterized by the maximum erosion occuring at some intermediate angle between 0-90 degrees, usually 20-30 degrees. The brittle mode is characterized by the erosion rate increasing with increasing impingement angle, up to a maximum at normal (90 degrees) impingement.

As a result of reviewing the extensive literature about metal erosion by particle impact, it could be concluded that, erosion is at least function of particle velocity, particle size and shape, particle and target hardness, temperature, angle of attack and thermal conductivity. However,

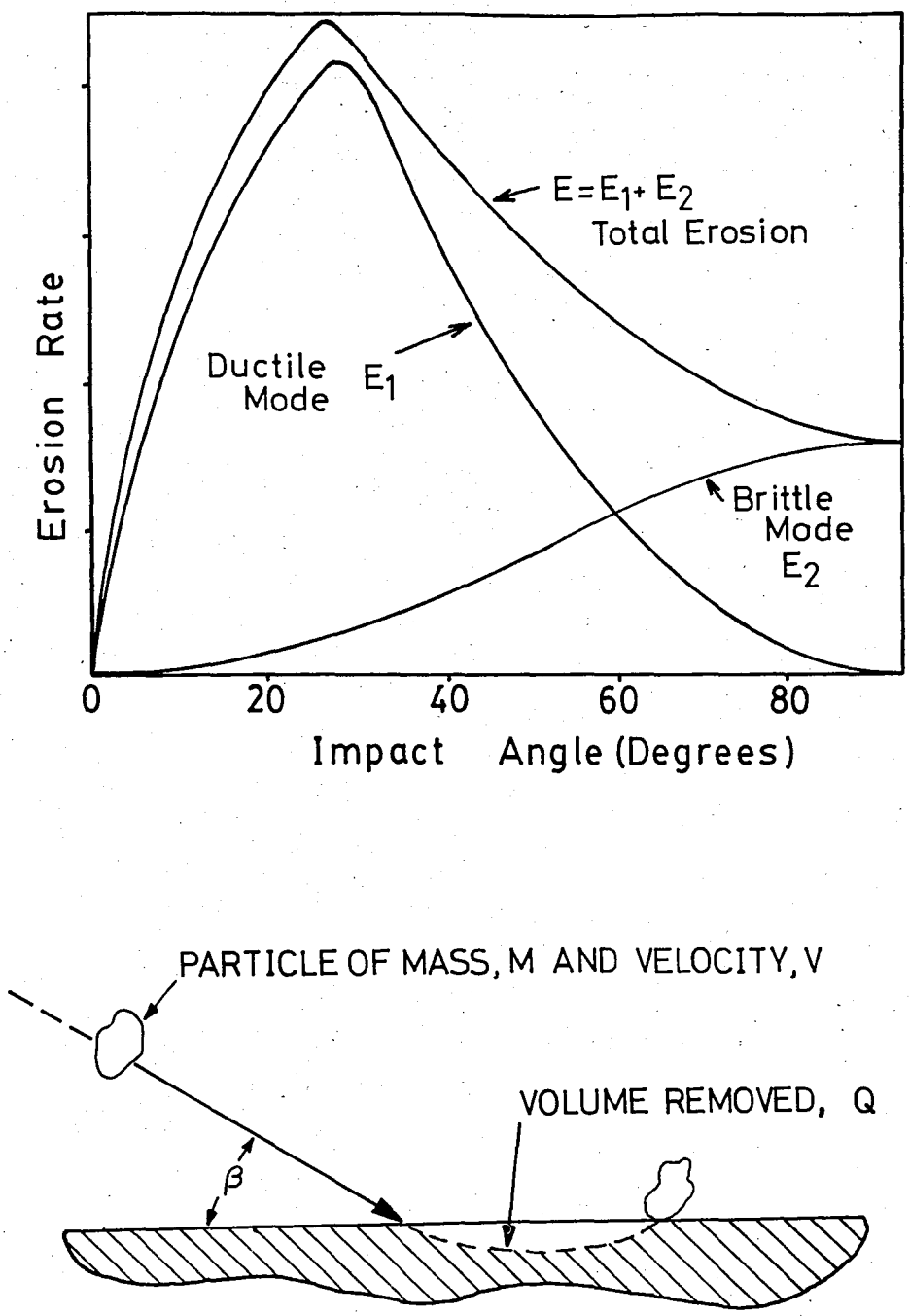

FIGURE 1 - Modes of erosion and principle of material removal for ductile material

most attempts to formulate erosion relate it to two main parameters, namely angle of attack and impact velocity raised to an exponent m. All other variables are lumped into constants of the erosion system considered. In general,

$$Q = C\ f\ (\beta, V^m) \qquad (1)$$

where, Q is the erosion rate, C is the system constant, β is the angle of attack and V is the particle velocity raised to a power m.

Table 1 summarizes experimental results obtained by various investigators and formulations proposed.

Although the velocity exponent m is proposed to fall between 2 and 3 for an extensive range of particle and target combinations, Head and Harr {29} suggested greater than 3 and Smeltzer, Gulden and Crompton {30}suggested less than 2. The maximum erosion angle, β_{max} is usually between 20^o-$40^o$for ductile materials and 90^o for brittle materials.

No definitive explanation on temperature dependence of erosion has been given. Tilly {44} concluded that erosion may increase or decrease with temperature depending on the material properties but the extent of the change is small in relation to the normal operational range of the alloy. Neilson and Gilchrist {45}proposed a linear relationship between initial target temperature and weight loss of target plate. Ives, et al {35} remarked that the effect of temperature and environment on erosion is difficult to establish because it varies among different alloys. Gat and Tabakoff {46} obtained similar results and stated that erosion damage may increase or decrease as the temperature increases, depending upon the angle at which particles strike the material surface and upon the test temperature with respect to the thermal properties of material. Wakeman and Tabakoff{39} stated that the erosion rate as a function of temperature

TABLE 1- Summary of Experimental Results and Formulations About Erosion

Year	Reference	Particle-Target	β_{max}	m	Formulation
49	Stoker {18}	Silicasand-Blackiron	20	2.2-3	
58	Finnie {19}	SiC-Cu,Al, SAE1020 Steel	17	2.0	
60	Finnie {20}	SiC-Cu,Al, SAE1020 Steel	15-20	2.0	$Q \simeq \frac{MV^2}{8p}(\sin 2\beta - 3\sin^2\beta)$ $\beta \leq 18.5^0$ (2)
					$Q \simeq \frac{MV}{24p}\cos^2\beta$ $\beta \leq 18.5^0$
60	Bitter {21}	Cast iron-Al	15	2.0	$Q_{c_1} = \frac{2MC(V\sin\beta - K)^2}{\sqrt{V\sin\beta}}(V\cos\beta - \frac{C(V\sin\beta - K)^2}{\sqrt{V\sin\beta}}\phi)$
	{22}	SiC-Al	12	2.0	
		SiC-Cu	13	2.0	
		SiC-SAE1055(as received)	25	2.0	$Q_{c_2} = \frac{1}{2\phi} M\{V^2\cos^2\beta - K_1(V\sin\beta - K)^{3/2}\}$
		SiC-SAE1055(fully hardened)	50	2.0	$Q_D = \frac{1}{2\varepsilon} M(V\sin\beta - K)^2$ (3)
					$Q_t = Q_D + Q_{c_1}$ $\beta \leq \beta_o$
					Q_{c_2} $\beta \geq \beta_o$
65	Wood and Espenschade	Silicasand-C1050 Steel	20	2.0	
		Silicasand-Stainless Steel	20	2.0	$Q = f_1(I) f_2(I) \frac{MV^2}{p}\cos^2\beta$ (4)
		Silicasand-Al	20	2.0	

TABLE 1 (Cont'd)

Year	Reference	Particle-Target	β_{max}	m	Formulation
66	Sheldon and Finnie {24}	SiC-Brittle Material	-	-	$Q=kr_p f_1(m')_V f_2(m')$ (5)
67	Finnie,et al {17}	SiC-C1213 Steel	22	2.28	$Q=\frac{MV^2}{24}(BHN)f(\beta)$ (6)
		SiC-C1045 Steel	22	2.28	
		SiC-Al	18	2.26	
		SiC-Tool Steel	22	2.35	
68	Neilson and Gilchirst {25}	Al_2O_3-Al	20	2.0	$Q=\frac{1/2MV^2\cos^2\beta\sin n\beta}{\phi}+\frac{1/2M(V\sin\beta-K)^2}{\varepsilon}\ \beta\leq\beta_o$ (7)
		Al_2O_3-Glass	90	2.0	
		Al_2O_3-Steel	20	2.0	$Q=\frac{1/2MV^2\cos^2\beta}{\phi}+\frac{1/2M(V\sin\beta-K)^2}{\varepsilon}\ \beta\geq\beta_o$
		Al_2O_3-Ceramic	90	2.0	for $\beta=\beta_o$, $\beta_o=\frac{\pi}{2n}$
68	Sage {26}	Sand and Dust-Chromium Steel	-	2.3	$Q=V^{2.3}\ dp\ (DPH)^{2.3}$ (8)

TABLE 1 (Cont'd)

Year	Reference	Particle-Target	β_{max}	m	Formulation
70	Tilly and Sage {27}	Quartz-Al Alloy	30	2.0-2.3	
		Quartz-Mg Alloy	30	2.0-2.3	
		Quartz-Co Alloy	30	2.0-2.3	
		Glass sphere-Al	90	2.4-2.4	
70	Brasinikas {28}	Coal ash-18/8 Stainless S.	35-50	2.3-3.4	
		Coal ash-Bright Mild S.	35-50	2.3-3.4	$Q=-0.45d_p-0.13\ d_p^2\ 0.25\ d_p^3$
		Coal ash-HS31	35-50	2.3-2.4	
		Coal ash-Crown Max	35-50	2.3-3.4	$m>4$ at 540^0C (9)
		Coal ash-C242	35-60	2.3-3.4	
		Silicasand-SS18/8	37	2.3	
70	Head and Harr {29}	Silicasand-Al Alloy	30	4.34	$Q_{DS}=\frac{V^{4.34}\beta^{0.46}H^{0.10}\xi^{0.21}}{R^{2.34}B^{2.48}}$
		Glassbeads-Al Alloy	45	4.34	
		Silicasand-Stainless S.	30	4.34	$Q_{BS}=\frac{V^{3.06}\beta^{2.68}H^{2.08}\xi^{0.03}}{B^{3.64}}$ (10)
		Glassbeads-Stainless S.	45	4.34	
		Silicasand-Glass plate	90	3.06	
		Glassbeads-Glass plate	90	3.06	

TABLE 1 (Cont'd)

Year	Reference	Particle-Target	β_{max}	m	Formulation
70	Smeltzer, et al {30}	Silicasand-Al Alloy	38	0-1.64	$Q=Cf(\beta)^{i}$ (11)
		Al_2O_3-Al Alloy	32	0-1.22	
		Silicasand-Stainless S.	38	0-1.14	
		Al_2O_3-Stainless S.	30	0-1.14	
72	Finnie {31}	-	13	2.4	$Q_{DS}=f(\beta,\Omega_p,V,d_p,\sigma_s,T_g,F_1,F_2,F_3,F_4,F_5,F_6)$ (12)
72	Sheldon and Kanhere {32}	SiC-Al, Cu, Steel	-	2.36-3.0	$Q=d_p^3 V^3 (\rho_p)^{3/2}/H_v^{3/2}$ (13)
		Glass-Al	-	2.4	
74	Grant and Tabakoff {33}	Al_2O_3,SiO_2-2024 Al	20-90	2.8-4.0	$Q=K_1 f'(\beta) V^2 \cos^2\beta\{1-R_T^2\} + f(V_n)$ $R_T=1-0.0016V\sin\beta$ $f'(\beta)=1+CK(K_{12}\sin 2\beta_o)^2$ $f(V_n)=K_3(V\sin\beta)^4$ (14)

TABLE 1 (Cont'd)

Year	Reference	Particle-Target	β_{max}	m	Formulation
75	Frass {34}	Silicaflour-C1050 Steel	35	-	
77	Ives,et al {35}	SiC, SiO_2, Al_2O_3 Stainless S., Nickel	20	2.-3.	
77	Young and Ruff {36}	Al_2O_3-304 Steel	20	2.9 (25 C)	
			10	- (500 C)	
79	Tabakoff, et al {37}	Coal ash-2024Al, 304SS,6Al-4V-Ti	20	2.0	Eq.14 with $f'(\beta)=\{1+CK\{K_{12}\sin(90/\beta_o)\beta\}\}^2$ (15)
79	Maji and Sheldon {38}	Steel particles-Al	-	2.0-2.7	

TABLE 1 (Cont'd)

Year	Reference	Particle-Target	β_{max}	m	Formulation
79	Wakeman and Tabakoff {39}	Quartz sand-Ti6-4	30-35	-	
		INCO 718			
79	Raask {40}	Quartz-Mild Steel	36	2.5	$Q_w = CW_p V^{2.5}$ (16)
79	Tabakoff,et al {41}	Coal ash, quartz san			
		304SS,	25	-	
		RENE41	30	-	
		Ti6-4	30	-	
		INCO718	35	-	
80	Raj and Moskowitz {42}	Alumina powder-Nichrome	30-60	3.57	
		V-Cb	30-60	3.57	
80	Kotwal and Tabakoff {43}	Four types fly ash-SS304 RENE41 INCO718	-	-	$Q = \psi \sum_{i=1}^{m} \sum_{j=1}^{n} W_i (\varepsilon'_{ij}\ \omega_j)$ (17)

is relatively constant for each material up to a temperature, which is unique to the material, beyond which it increases rapidly. A rather more detailed explanation about temperature dependence of erosion was given later by Gat and Tabakoff {47}. Briefly, as temperature increases metal resistance to erosion may increase or decrease, but at the homologous temperature (the actual temperature of material divided by its melting temperature) above 0.5, in general, decreasing resistance to erosion is dominant.

Concerning the effect of concentration on erosion Wood and Espenschade {23} noted that the relationship between concentration of dust in the airstream and the erosion loss is not a linear one, the average erosion loss per impact being greater at low dust concentrations than at the higher concentrations. However, Newhart{48} stated that the total erosion is indepenedent of dust concetration within realistic limits, and is a direct function of the total weight ingested of any given particle size for a given gas turbine.

Sheldon {49} showed that the material initial hardness had an effect on erosion and that the fully work hardened target hardness should be considered rather than the annealed hardness of the surface. He postulated that erosion work hardened the surface to a very high degree and that the depth of cut by each impact would progressively decrease as erosion progressed and finally reach a steady state. Therefore, work hardening and annealing properties of the material should be considered. It may be possible that some materials reach high surface hardness after erosion and at high temperatures annealing may occur and increase erosion.

III. ANALYSIS

The present analysis is carried out in three main steps:

i. Calculation of the gas flow through the stator and the rotor blade passages of the given multistage turbine.

ii. Calculation of particle trajectories in the blade passages and determination of particle impacts with blade surfaces

iii. Calculation of the erosion rates caused by impacting particles

In the following, each step is discussed in some detail.

3.1. CALCULATION OF GAS FLOW

The solution for the gas flow in the blade passages is obtained from the computer program TSONIC developed by Katsanis {2}. The input description for this program is given in Appendix A. The solution method is based on the following assumptions;

1. The flow is steady relative to the blade
2. The fluid is a perfect gas with zero viscosity

3. The flow is isentropic and free of vortices
4. The velocity component normal to the blade to blade surface is zero.
5. The stagnation temperature is uniform across the inlet
6. The velocity magnitude and direction are uniform
7. The flow is essentially subsonic with only locally supersonic spots.

If the flow is transonic, the solution is obtained in two stages; (1) the weight flow is reduced sufficiently so the flow is completely subsonic throughout the passage and a solution is obtained to the stream function equation based on this reduced weight flow, and (2) the velocity distribution is determined based on the actual weight flow by means of a velocity gradient method.

The calculated velocities and densities at the grid points of the finite difference mesh used are stored for subsequent use in the trajectory calculations.

3.2 CALCULATION OF PARTICLE TRAJECTORIES

For particle trajectory calculations the computer program TPART developed by Mengütürk and Sverdrup {1} is used with some modifications.

The equations of motion of particle moving in the gas stream are {1}

$$\begin{aligned} \ddot{x} &= G(W_x - \dot{x}) \\ \ddot{\theta} &= \frac{G}{r}(W_\theta - r\dot{\theta}) - \frac{2\dot{r}}{r}(\dot{\theta}+\omega) \\ \ddot{r} &= G(W_r - \dot{r}) + r(\dot{\theta}+\omega)^2 \end{aligned} \qquad (18)$$

where, $$G = \frac{18\,\mu_g}{d_p^2 \rho_p} f(Re) \qquad (19)$$

$$f(Re) = C_D \frac{Re}{24} \qquad (20)$$

and $$Re = \frac{\rho_g\, d_p\, |\vec{V}_g - \vec{V}_p|}{\mu_g} \qquad (21)$$

The moving coordinate system with respect to which these equations are written is illustrated in Figure 2. In the above x denotes the axial coordinate, θ the tangential distance in radians measured from the blade leading edge, r the radial coordinate, W_x , W_θ and W_r are the components of the gas velocity along the respective coordinates. In addition, μ_g denotes gas viscocity, d_p particle diameter, Re particle Reynolds number, ρ_p particle density, ρ_g gas density, $\vec{V}_g$ absolute gas velocity vector and $\vec{V}_p$ absolute particle velocity vector. C_D is the drag coefficient for a spherical particle and equal to 24/Re for Stokes flow. For large Re, experimental correlations obtained by Morsi and Alexander {11}are used.

The main modifications made in the TPART program are as follows;

i. Mengütürk and Sverdrup {1} solved Eqs. (18) by using a numerical method based on a finite difference integration technique. This technique utilizes the HAMMNG predictor corrector algorithm which is essentially a fourth-order Runge-Kutta scheme. However, the highly time consuming nature of the HAMMNG method makes it difficult to solve equations of motion economically. Therefore, this method has been replaced

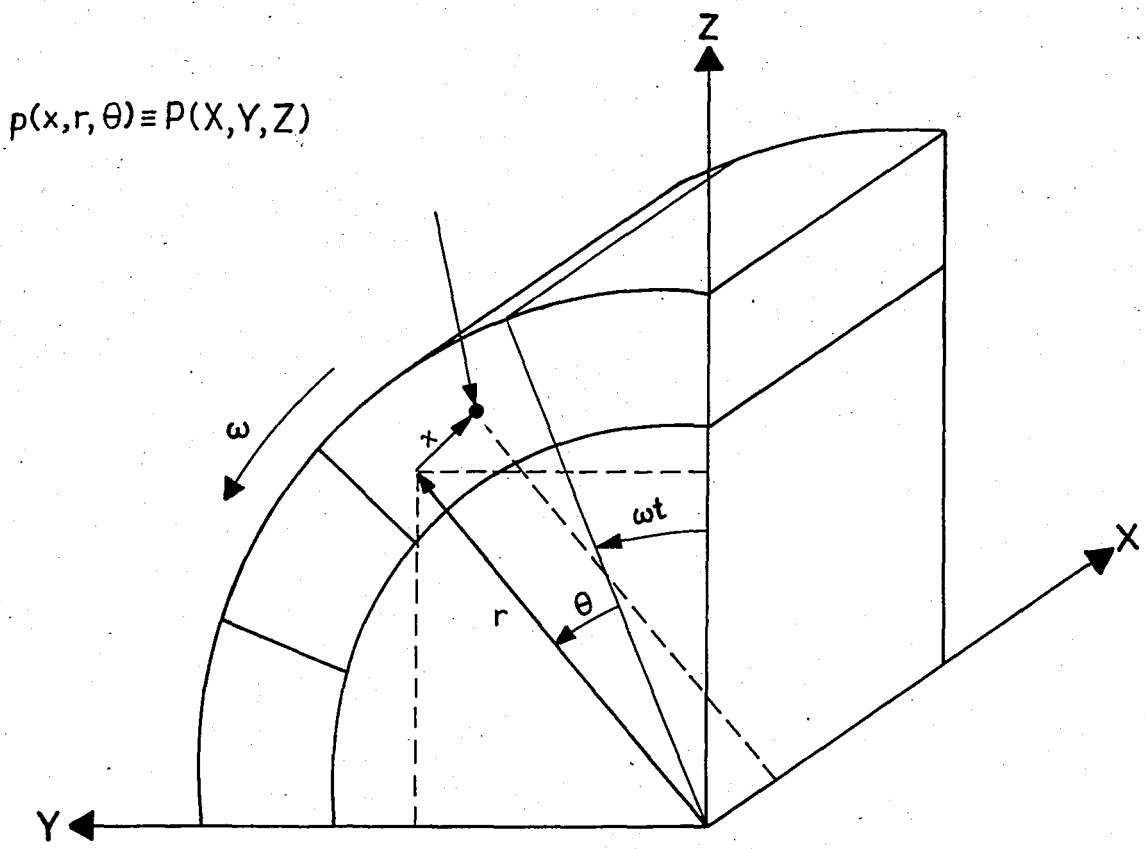

FIGURE 2 - The coordinate system for the particle motion in an axial turbomachine

by the more economical PES (piecewise exact solution) method developed by Mengütürk and Güneş [3]. The PES method of integration seeks exact solution to an approximate form of the governing equation set in small time intervals. In a given time interval Eqs. (18) may be linearized and uncoupled as follows

$$\begin{aligned} \ddot{r} + A_1\dot{r} + B_1 r &= C_1 \\ \ddot{\theta} + A_2\dot{\theta} &= C_2 \qquad t_{n-1} \le t \le t_n \\ \ddot{x} + A_1\dot{x} &= C_3 \end{aligned} \tag{22}$$

where the subscripts (n-1) and (n) refer, respectively, to the initial and final points of the n'th integration step and

$$\begin{aligned} A_1 &= G_{n-1} \\ A_2 &= \left(G + \frac{2\dot{r}}{r}\right)_{n-1} \\ B_1 &= -(\dot{\theta}_{n-1} + \omega)^2 \\ C_1 &= (GW_r)_{n-1} \\ C_2 &= \left(\frac{G}{r} W_\theta\right)_{n-1} - 2\left(\frac{\dot{r}}{r}\right)_{n-1}\omega \\ C_3 &= (GW_x)_{n-1} \end{aligned} \tag{23}$$

The exact solution to Eqs (22) in the current time interval, i.e. the piecewise exact solution to Eqs (18), is given by

$$\begin{aligned} r &= K_1 e^{m_1 \Delta t} + K_2 e^{m_2 \Delta t} + \frac{C_1}{B_1} \\ \theta &= K_3 e^{-A_2 \Delta t} + K_4 + \frac{C_2}{A_2}\,\Delta t \\ x &= K_5 e^{-A_1 \Delta t} + K_6 + \frac{C_3}{A_1}\,\Delta t \end{aligned} \tag{24}$$

where,

$$m_{1,2} = \frac{-A_1 \pm \sqrt{A_1^2 - 4B_1}}{2}$$

$$K_1 = \frac{\dot{r}_{n-1} - r_{n-1} m_1 + \frac{C_1}{B_1} m_2}{m_1 - m_2}$$

$$K_2 = \frac{\dot{r}_{n-1} - r_{n-1} m_1 + \frac{C_1}{B_1} m_1}{m_2 - m_1}$$

$$K_3 = \frac{C_2}{A_2^2} - \frac{\dot{\theta}_{n-1}}{A_2} \qquad (25)$$

$$K_4 = \theta_{n-1} - \frac{C_2}{A_2^2} + \frac{\dot{\theta}_{n-1}}{A_2}$$

$$K_5 = \frac{C_3}{A_1^2} - \frac{\dot{x}_{n-1}}{A_1}$$

$$K_6 = x_{n-1} - \frac{C_3}{A_1^2} + \frac{\dot{x}_{n-1}}{A_1}$$

$$\Delta t = t - t_{n-1}$$

and $\Delta t_n = t_n - t_{n-1}$ represents the current time interval.

In order to advance integration a step further, the solution at $\Delta t = \Delta t_n$ is used as initial condition for the next step.

ii. Particle impact-rebound data is changed. Mengütürk and Sverdrup {1} used Hussein's{50} experimental impact rebound correlations for poppy seeds and corn cups impacting stainless steel. In the present study the following correlations recently

presented by Tabakoff and Hamed{51} for erosive quartz and aluminia particles impacting stainless steel, titanium and aluminium alloys at high speeds are used, Figure (3).

$$\frac{V_{n2}}{V_{n1}} = 1.0 - 0.41598\,\beta_1 - 0.4994\beta_1^2 + 0.292\beta_1^3$$
$$\frac{V_{t2}}{V_{t1}} = 1.0 - 2.12\beta_1 + 3.0775\beta_1^2 - 1.1\beta_1^3 \qquad (26)$$

iii. The capability of the TPART program is extended to the calculation of particle trajectories in successive turbine stages. The old version of the program calculated trajectories only for a single stage. In a given stage this program assigns nine uniformly distributed tangential positions at the rotor inlet to each particle traversing the preceding stator passage. This is done to account for the relative rotation between the stator and the rotor blades. It is argued that, due to rotation, any circumferential position has equal probability at the rotor inlet provided that sufficiently long time is allowed. Therefore, with respect to a multistage application the number of particle trajectories to be calculated would increase exponentially with the successive number of stages. For example, 10 particles entering the first stage stator would produce 90 trajectories in the first stage rotor, 810 trajectories in the second stage stator, 7290 trajectories in the second stage rotor and so on. Instead of this, the new version of the TPART program handles 100 particles with some given distribution at the first stage stator. At rotor entry a random tangential position is assigned to each particle, since at the entry tangential position of particles is statistically random. The same procedure is repeated for the other stages in the same manner. This random entry assignment is performed by the

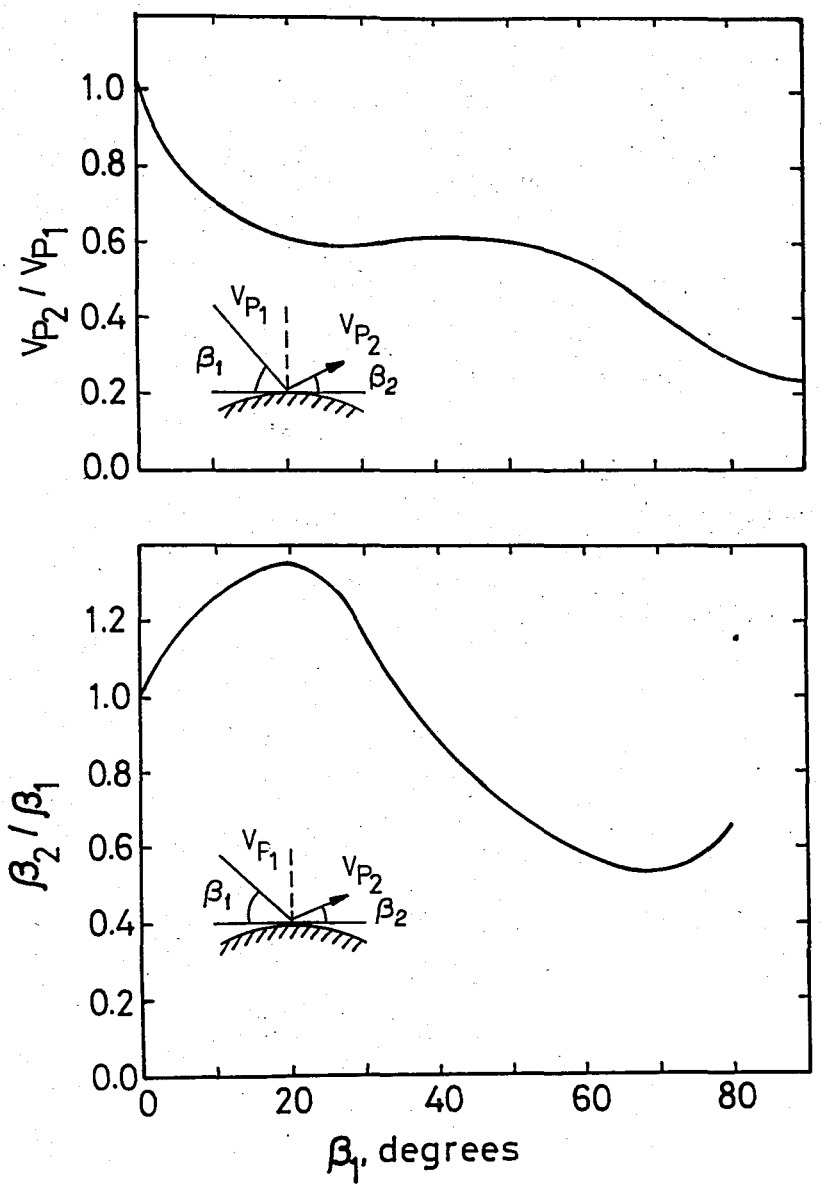

FIGURE 3 - Particle impact-rebound data

random number generator subprogram (RANDU) available on the existing computer system.

The TPART program uses the gas flow solutions given by the TSONIC program and calculates particle trajectories through a turbine stage. The blade surface impact data (i.e. impact location, impact velocity and angle) are stored for use in erosion calculations. The particle exit conditions are also stored to generate the inlet conaitions for the next stage.

The input description of the TPART program is given in Appendix B.

3.3 CALCULATION OF EROSION RATES

A computer program TPER is developed to calculate blade erosion rates based on the impact data obtained by the TPART program. The input description of TPER program is given in Appendix C.

Separation of the erosion calculation routines from the TPART program allows erosion predictions to be obtained for as many different blade materials as desired (provided, of course, basic experimental data concerning erosion resistance of these materials is available) without having to repeat the costly trajectory calculations.

In the applications considered in the present study (see Chapter 4) erosion rates for four different materials have been obtained. The first two materials are some hypothetical blade alloys the erosion resistances of which are assumed to be represented by the following semiempirical erosion model suggested by Mengütürk and Sverdrup{1}.

$$
\begin{aligned}
&Q=K_1'(V\cos\beta)^m \sin n\beta + K_2'(V\sin\beta)^m && \text{for } \beta \le \beta_o \\
&Q=K_1'(V\cos\beta)^m + K_2'(V\sin\beta)^m && \text{for } \beta \ge \beta_o \\
&n=\pi/2\beta_o
\end{aligned}
\qquad (27)
$$

where the first part of both equations represents the ductile mode (Figure 1) and the second the brittle mode. An approximate velocity exponent of 2.5 was assumed. Table 2 shows the erosion coefficients K_1', K_2' and the reference angle β_o. These parameters have been obtained based on experimental data given for silicon carbide particles eroding a nickel cobalt alloy with 99 per cent (Ni+Co) by assuming that SiC particles are approximately 25 times as erosive as coal ash particles eroding typical blade alloys. To investigate the effect of ductile/brittle nature of the blade material two cases have been considered having maximum erosion angles of 20 and 90 degrees (Table 2) with constant maximum erosion rate.

Table 2 - Erosion Coefficients Estimated for Coal Ash Particles Eroding Typical Blade Material for Two Different Maximum Erosion Angles {1}

β_{max} degrees	β_o degrees	Erosion Coefficients K_1'	$\frac{m^3/kg}{(m/sec)^{2.5}}$ K_2'
20	22.7	6.51×10^{-14}	1.87×10^{-14}
90	90	0	5.60×10^{-14}

Owing to its complexity the erosion phenomenon is very little understood. The semi-empirical erosion model of Mengütürk and Sverdrup {1} simplifies this phenomenon by lumping the effects of all material and environmental parameters which are, as yet impossible to generalize, into the coefficients K_1', K_2' and m. Therefore, its applicability is limited to a short range of operational conditions (to a single stage at the best). Although it is possible to eliminate this drawback by changing model coefficients in short

intervals on the basis of experimental results covering a range of ambient conditions, this approach would be cumbersome. If such experimental data is available, it would be more practical and even more accurate to utilize the given data directly by interpolation. The remaining two materials considered in the present study illustrate the interpolation approach. These materials are stainless steel 304 and Rene 41. The experimental results for a range of impact velocities and temperatures for these materials were obtained by Tabakoff, et al {41}, {52}. These four models are illustrated in figures D1 through D4 in Appendix D.

IV. RESULTS AND DISCUSSIONS

The multistage turbine erosion program package developed in this study was applied to a four stage electric utility gas turbine rated to drive a 65 MW generator. The first stage stator and rotor blade erosion rates of the same turbine calculated by the single-stage erosion program were previously reported by Mengütürk and Sverdrup [1].

Figures 4 through 11 show typical midspan trajectories of 3 μm and 12 μm coal ash particles (density 2.5gm/cc) through the four stages (i.e. eight blade rows) of turbine. By virtue of their low inertia, the 3 μm particles can follow the gas stream closely, and most of them avoid collision with the blade surfaces. On the other hand, it is noted that the 12 μm particles exhibit considerable deviation from the gas flow and are involved in frequent impactions with the blades, usually on the pressure surfaces except near the leading edges.

Capture efficiency is defined as the ratio of the amount of particles impacting the blade to the total amount entering the passage. Figure 12 shows the stator and rotor blade capture efficencies for all the stages as a function of particle diameter. In the size range considered, 3-12 μm, the capture efficiencies generally increase with the particle diameter, except in the final row. The capture efficiency of the fourth stage rotor blades starts to decrease for particles larger than 10 μm which, due to their accumulated deviations in the preceding rows, are directed at decreasing

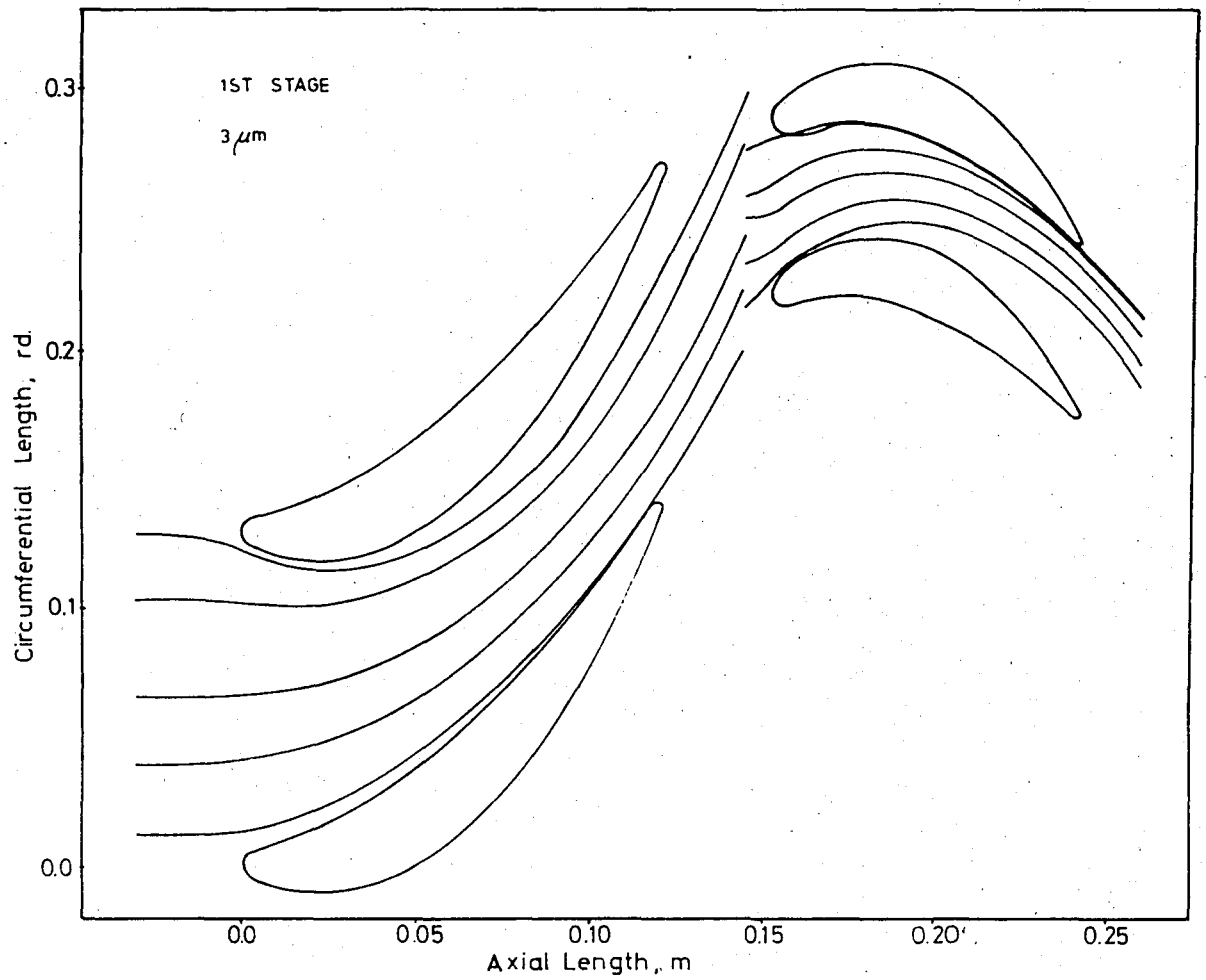

FIGURE 4 - Trajectories of 3μm particles in the first stage

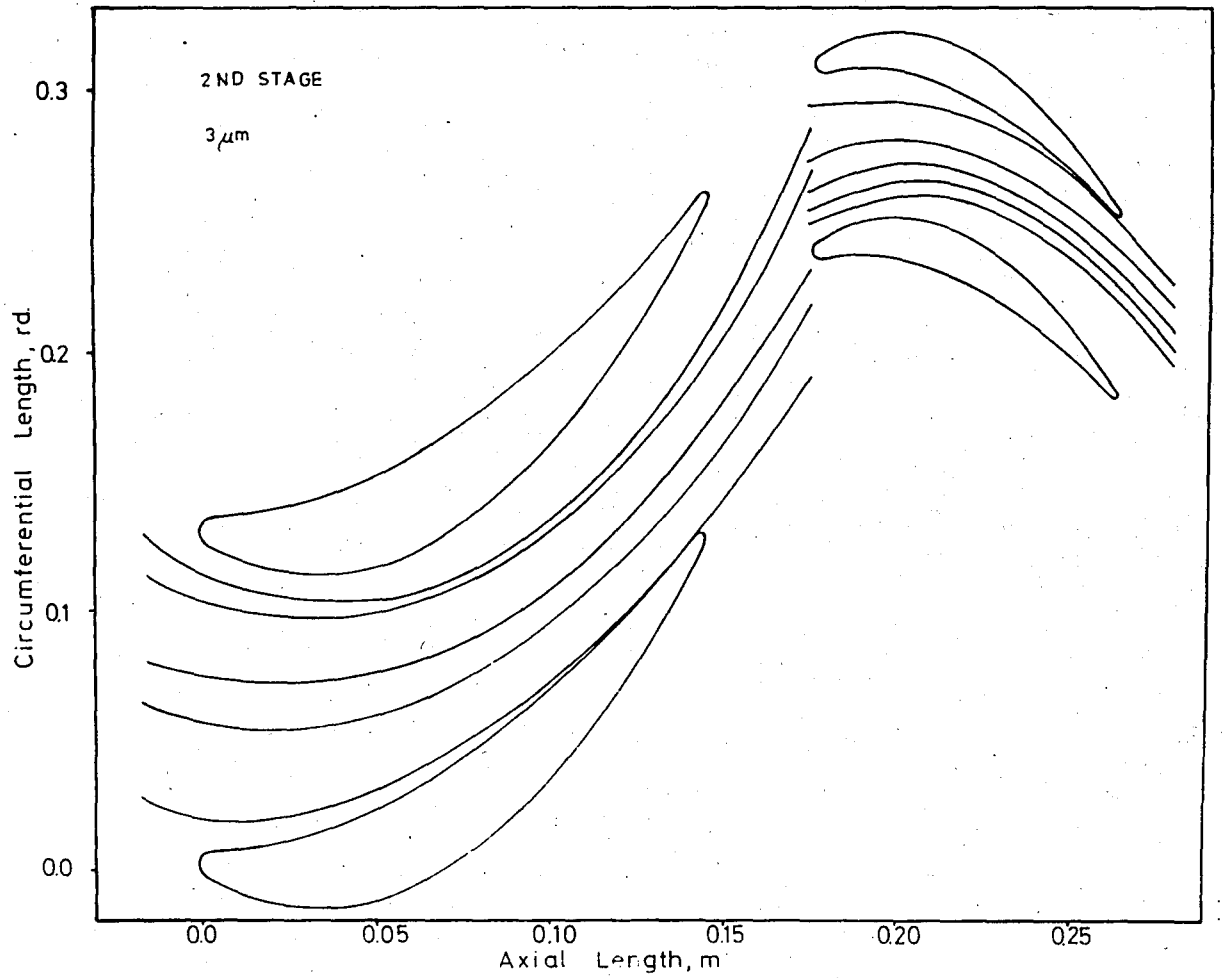

FIGURE 5 - Trajectories of 3μm particles in the second stage

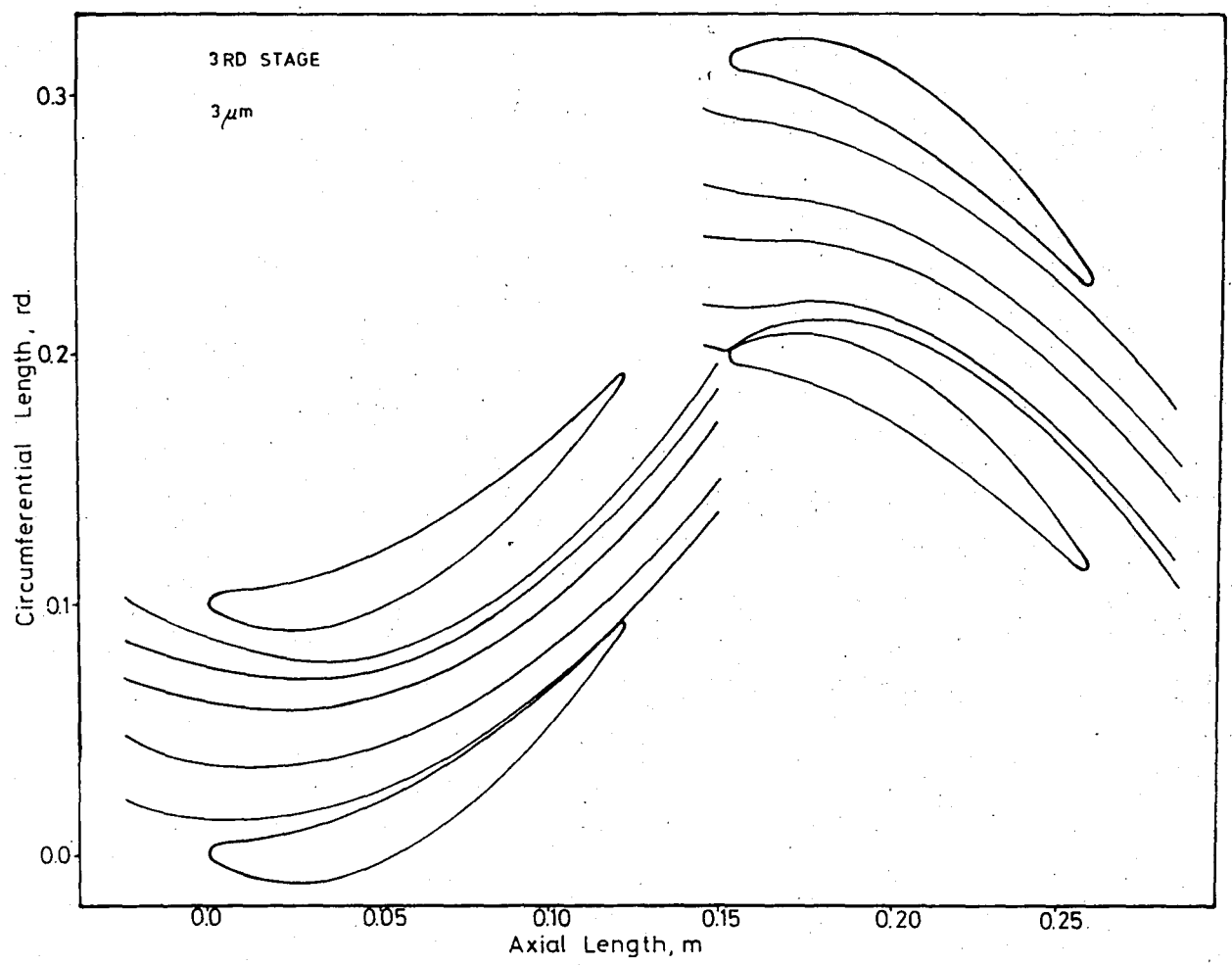

FIGURE 6 - Trajectories of 3μm particles in the third stage

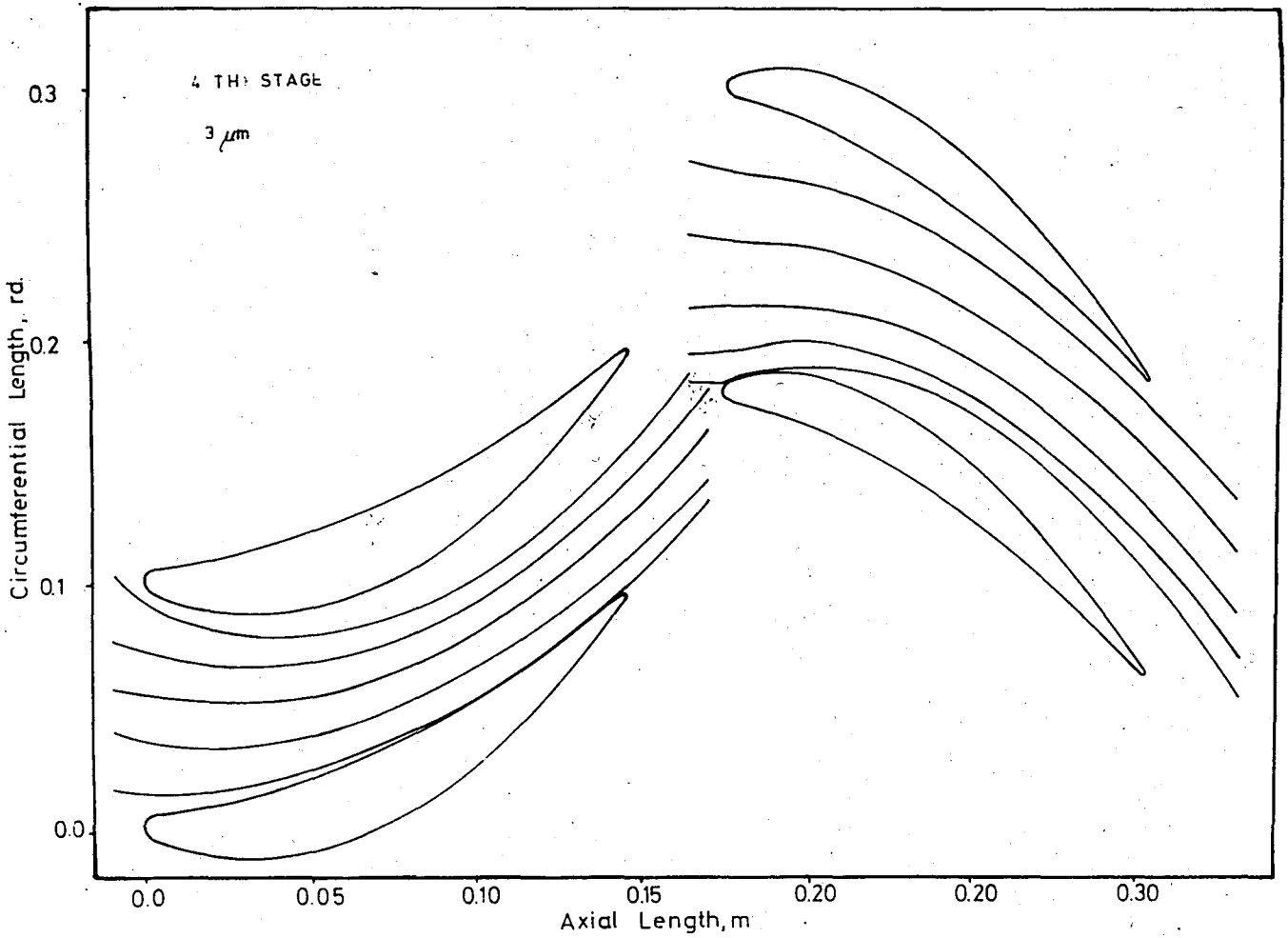

FIGURE 7 - Trajectories of 3μm particles in the fourth stage

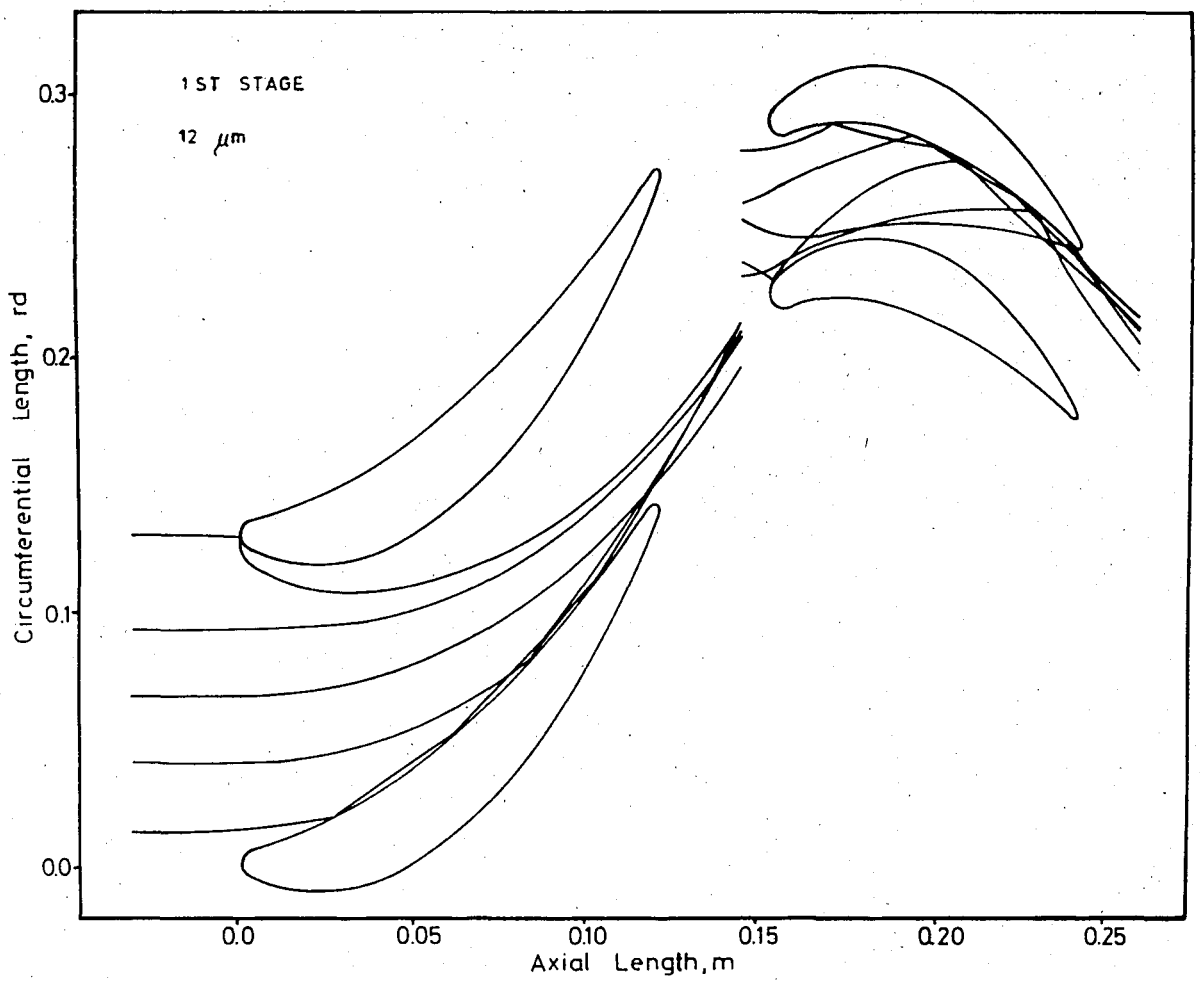

FIGURE 8 - Trajectories of 12μm particles in the first stage

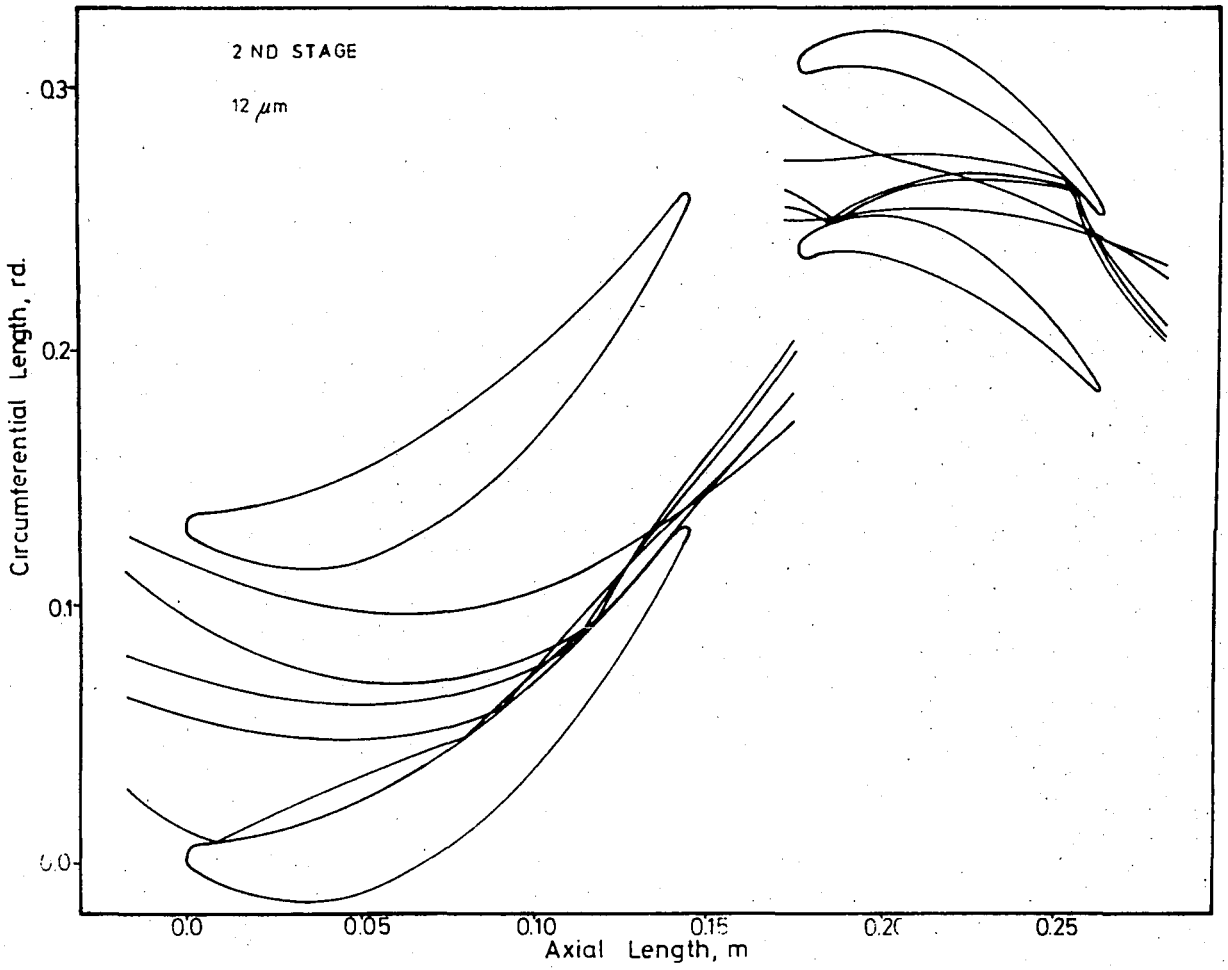

FIGURE 9 - Trajectories of 12μm particles in the second stage

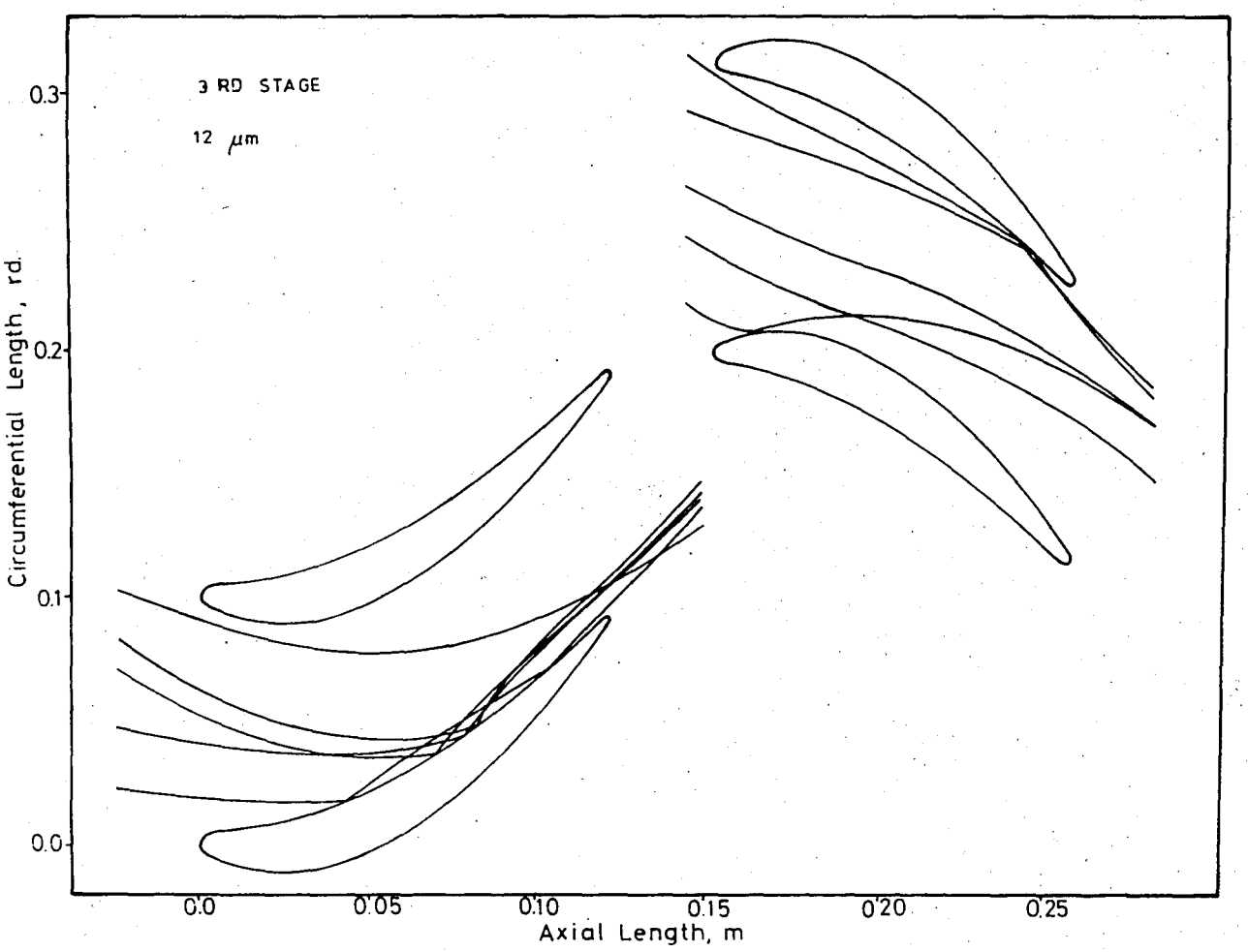

FIGURE 10 - Trajectories of 12μm particles in the third stage

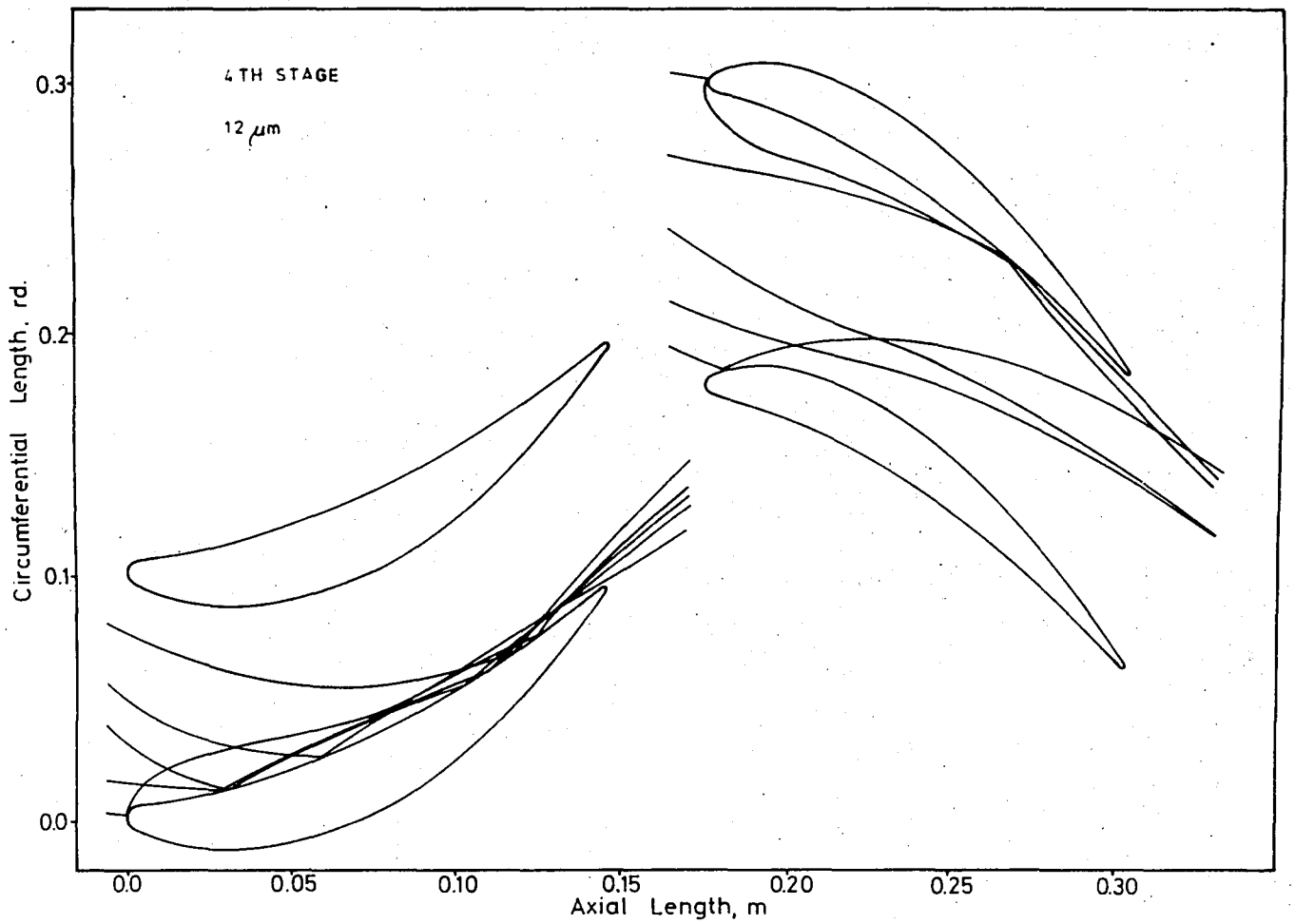

FIGURE 11 - Trajectories of 12μm particles in the fourth stage

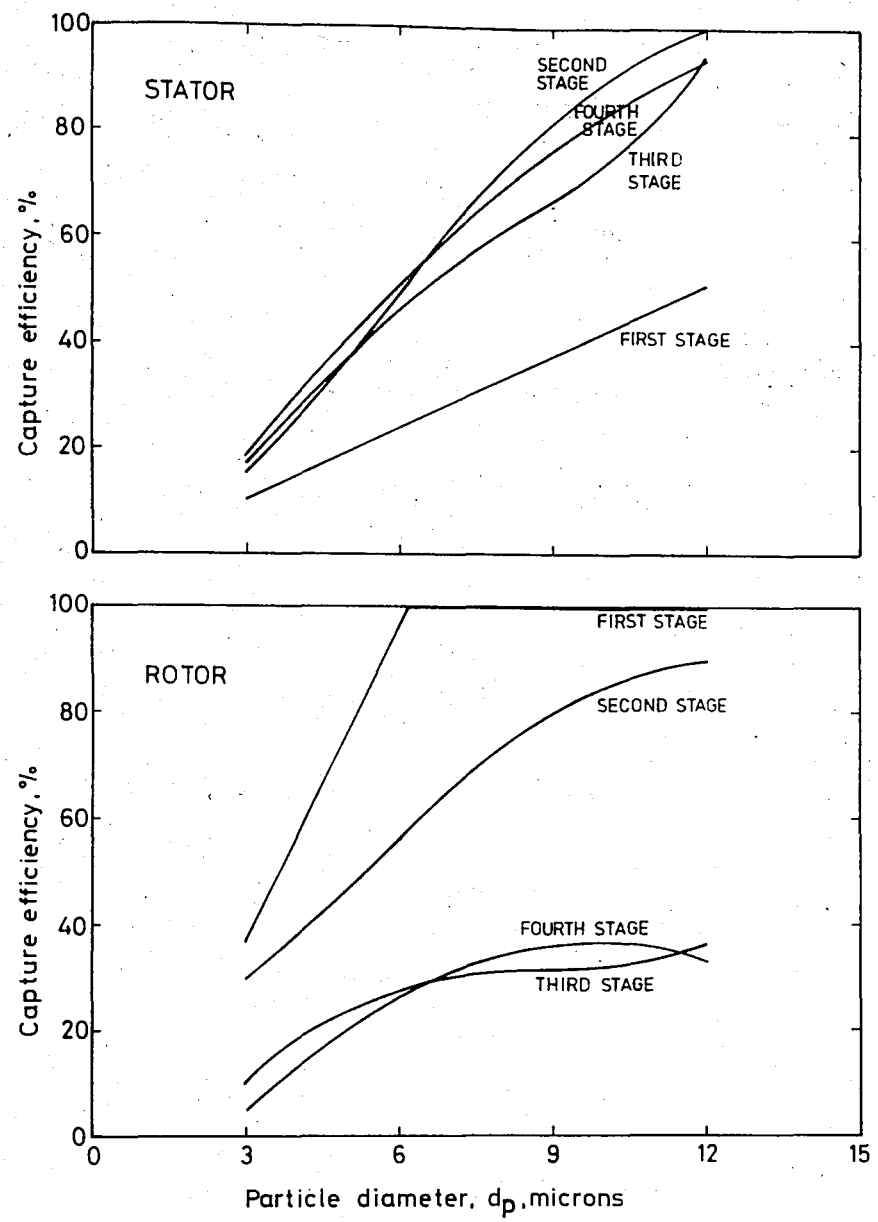

FIGURE 12 - Capture efficiencies as a function of particle size

angles of attack to the blade surfaces.

Some general features of the particle motion through the blade passages can be tied in with the following nondimensional parameters, the blade average stokes number,

$St_{avg}=\frac{\rho_p d_p^2 V_{avg}}{\mu_g b}$ where V_{avg} is the average gas velocity in the passage and b the blade chord, the angle through which the flow is turned, α, the number of blades in the given row, N, and the deviation of particles from the gas flow at the passage inlet that may be expressed by the angle $\delta=\beta_p-\beta_g$ where β_p and β_g denote particle deviation in a given blade passage increases with all these parameters (except perhaps the inlet particle deviation which might sometimes reduce the capture efficiency as in the fourth stage rotor discussed above). The fact that the stokes number is proportional to the square of particle diameter is the explanation for the strong diameter dependence observed in Figures 4 through 12. The first stage rotor has the maximum capture efficiency, because the velocities, the turning angle and the number of blades are relatively large in this row and the blades are relatively small.

The above generalization carries important design implications. An erosion resistant turbine should incorporate the following design features. The annulus area should be large so that the throughflow velocities are low. To decrease stage loadings (turning angles), the number of stages should be increased and work should be uniformly distributed between stages. The blade chords should be large and the number of blades in each row should be minimized.

The main parameters that affect local erosion rates are the particle impact velocity and angle. Figures 13 through 20 show particle impact velocities and angles as a function of the axial distance from the leading edge of each blade.

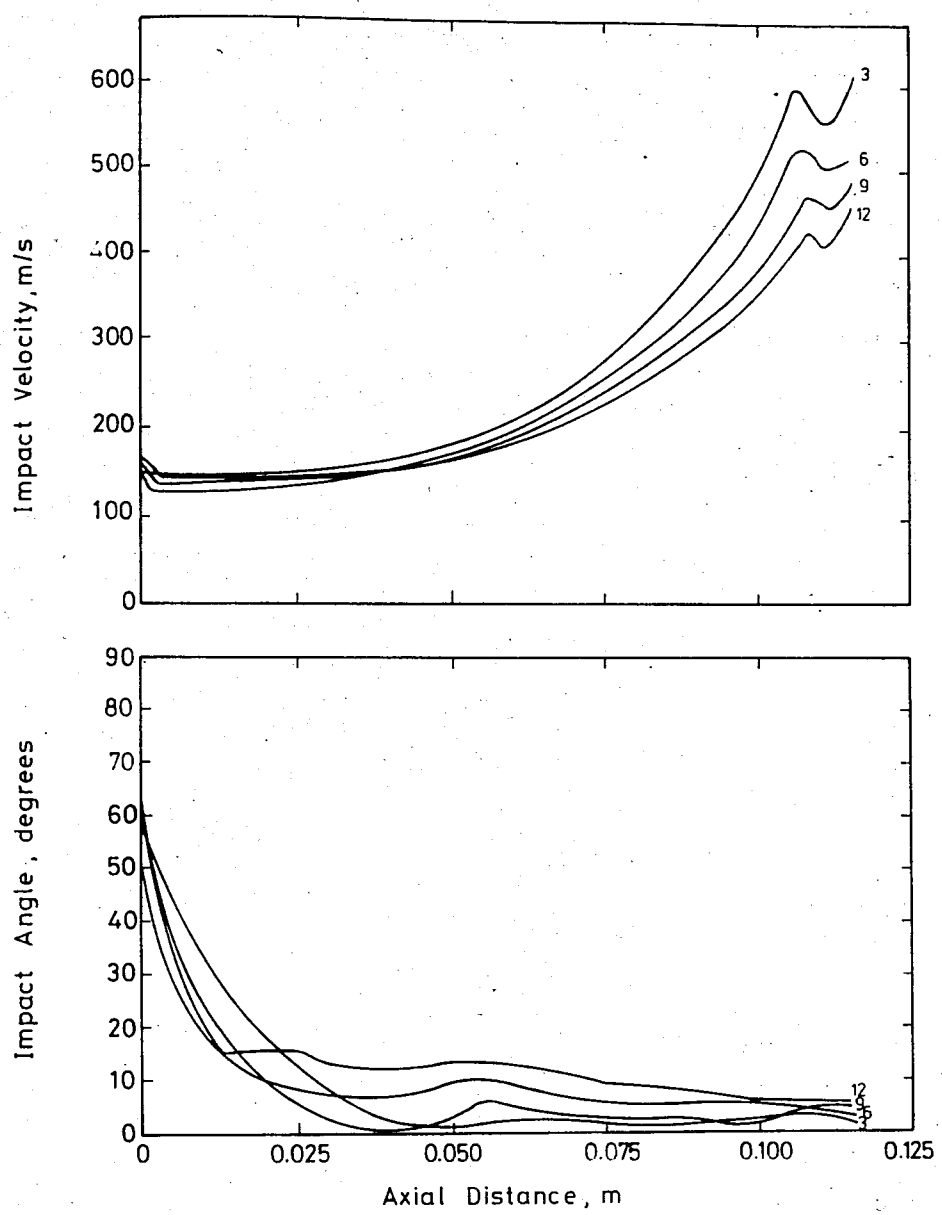

FIGURE 13 - Particle impact angles and velocities for the first stage stator

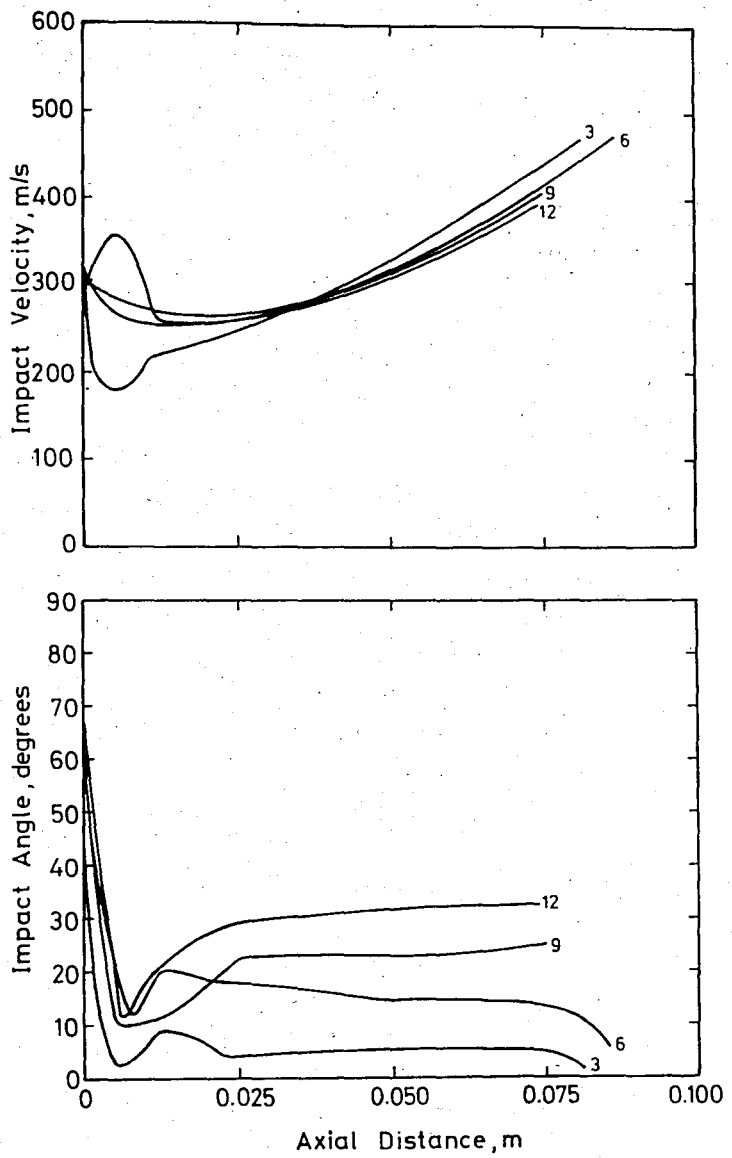

FIGURE 14 - Particle impact angles and velocities for the first stage rotor

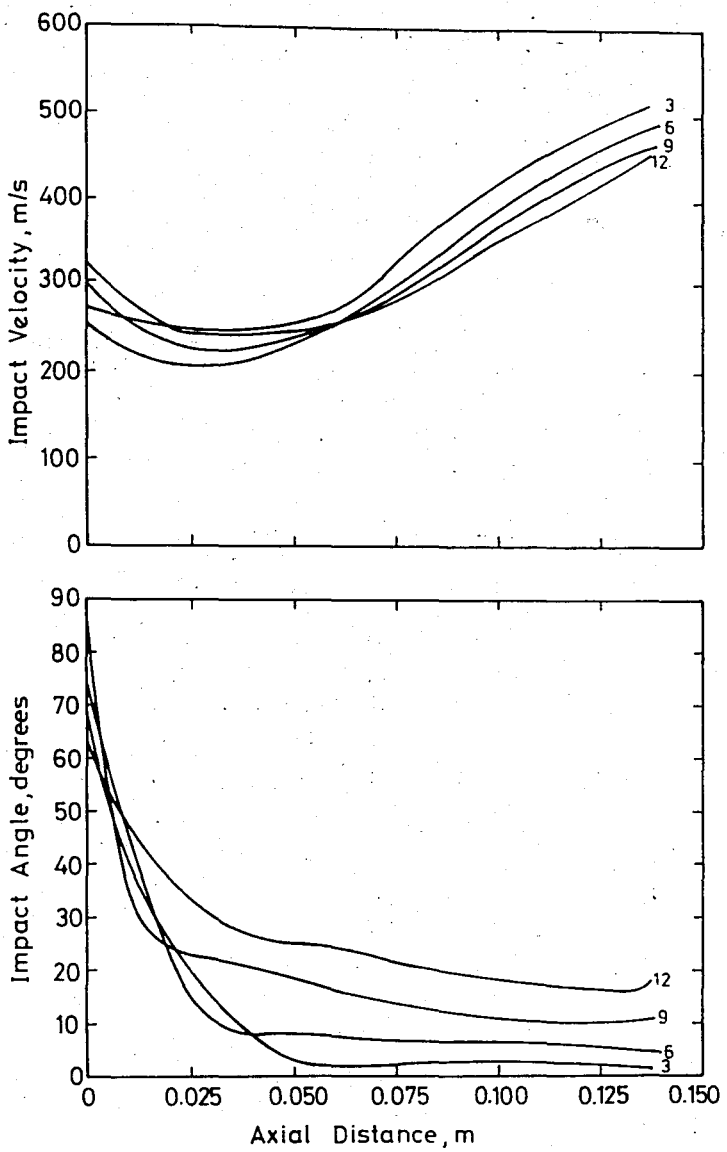

FIGURE 15 - Particle impact angles and velocities for the second stage stator

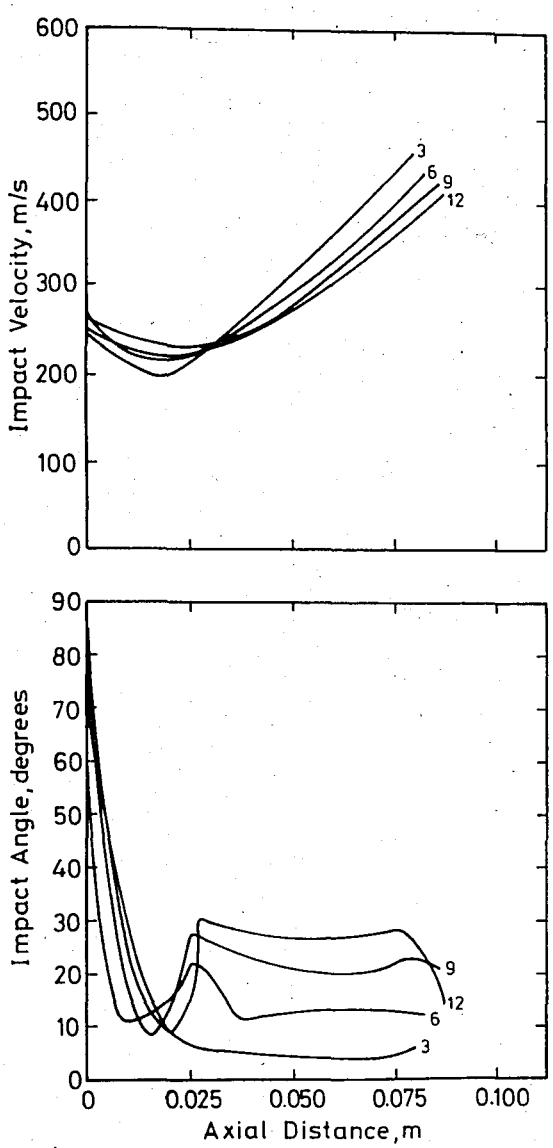

FIGURE 16 - Particle impact angles and velocities for the second stage rotor

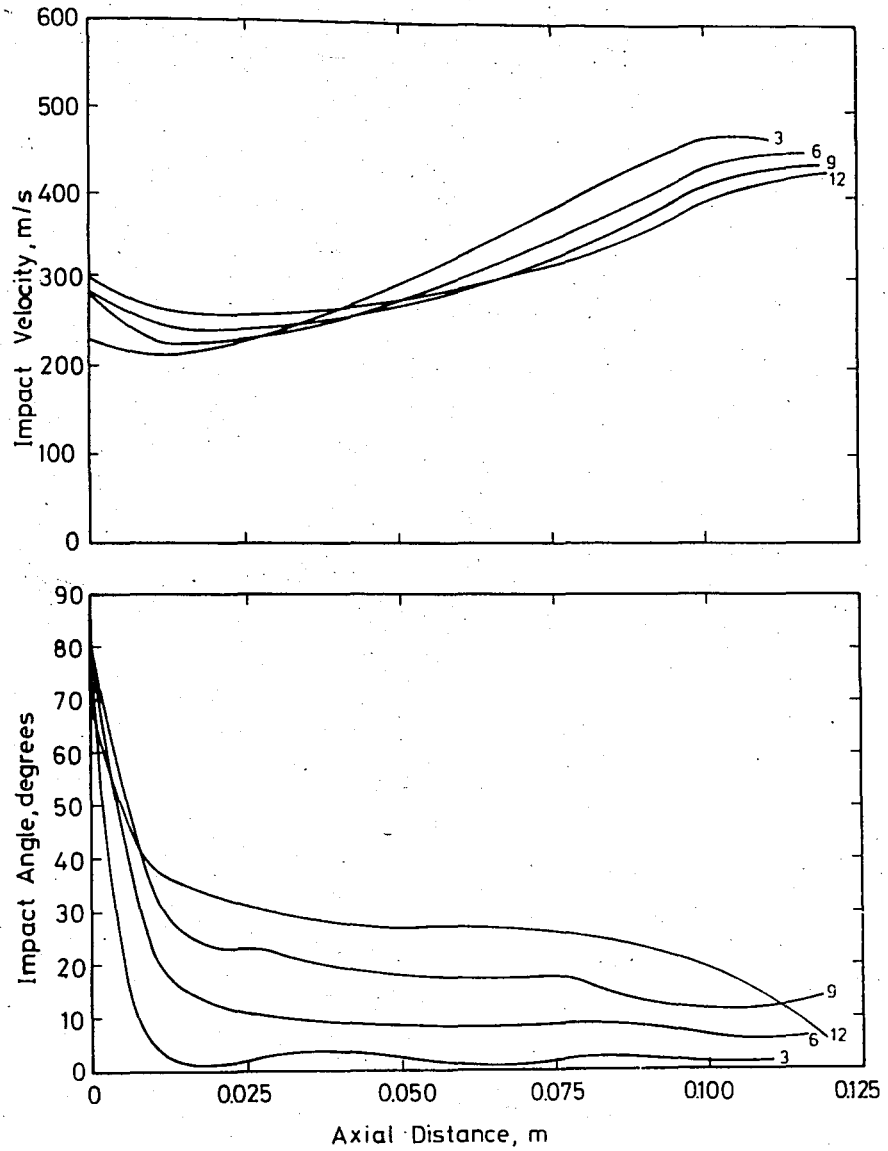

FIGURE 17 - Particle impact angles and velocities for the third stage stator

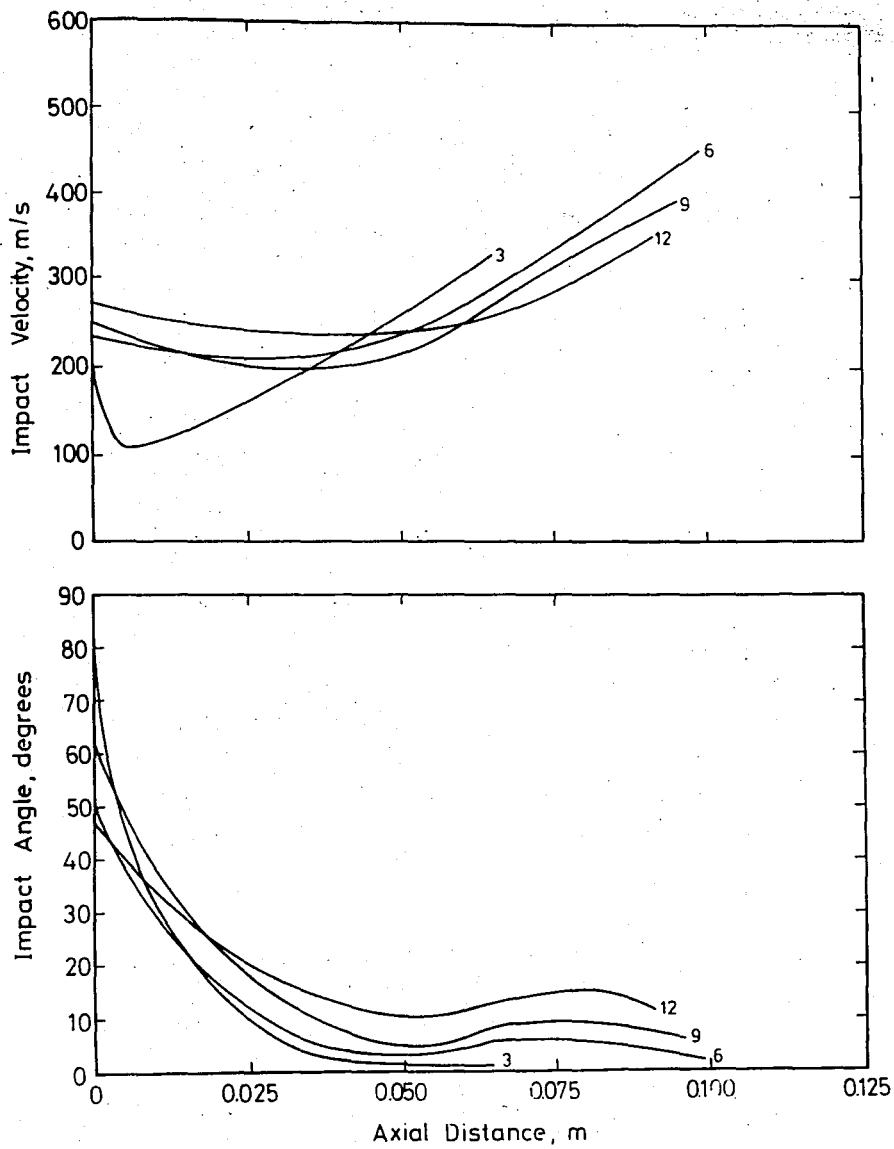

FIGURE 18 - Particle impact angles and velocities for the third stage rotor

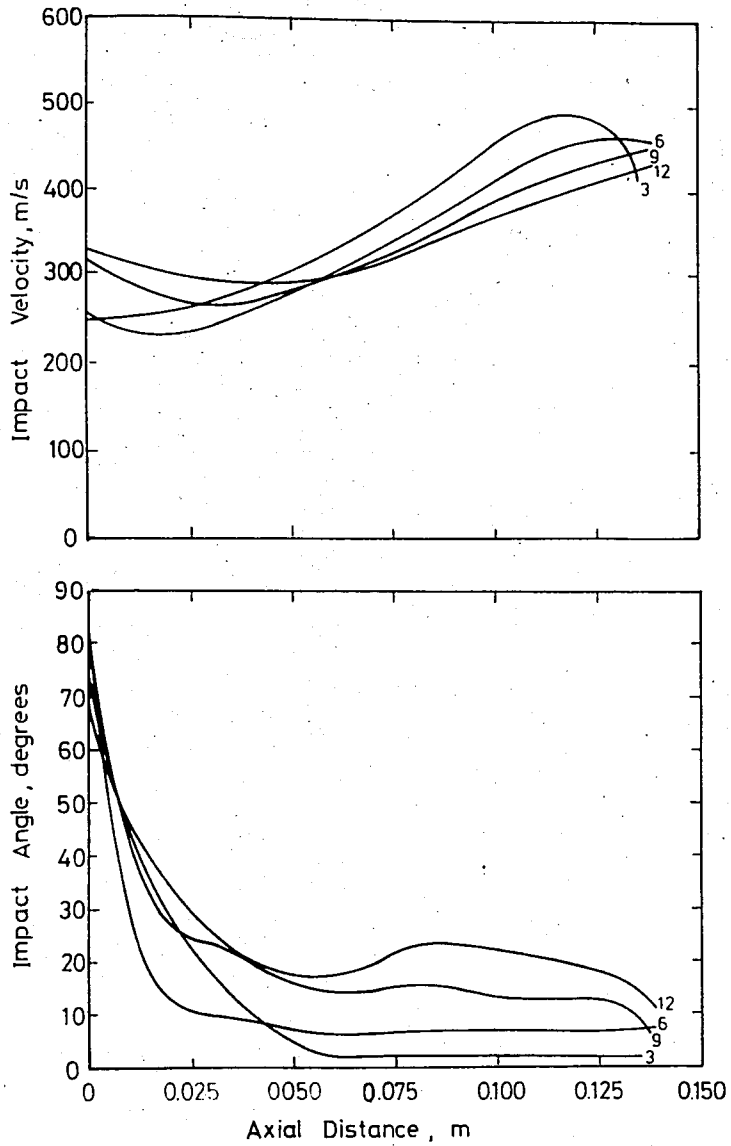

FIGURE 19 - Particle impact angles and velocities for the fourth stage stator

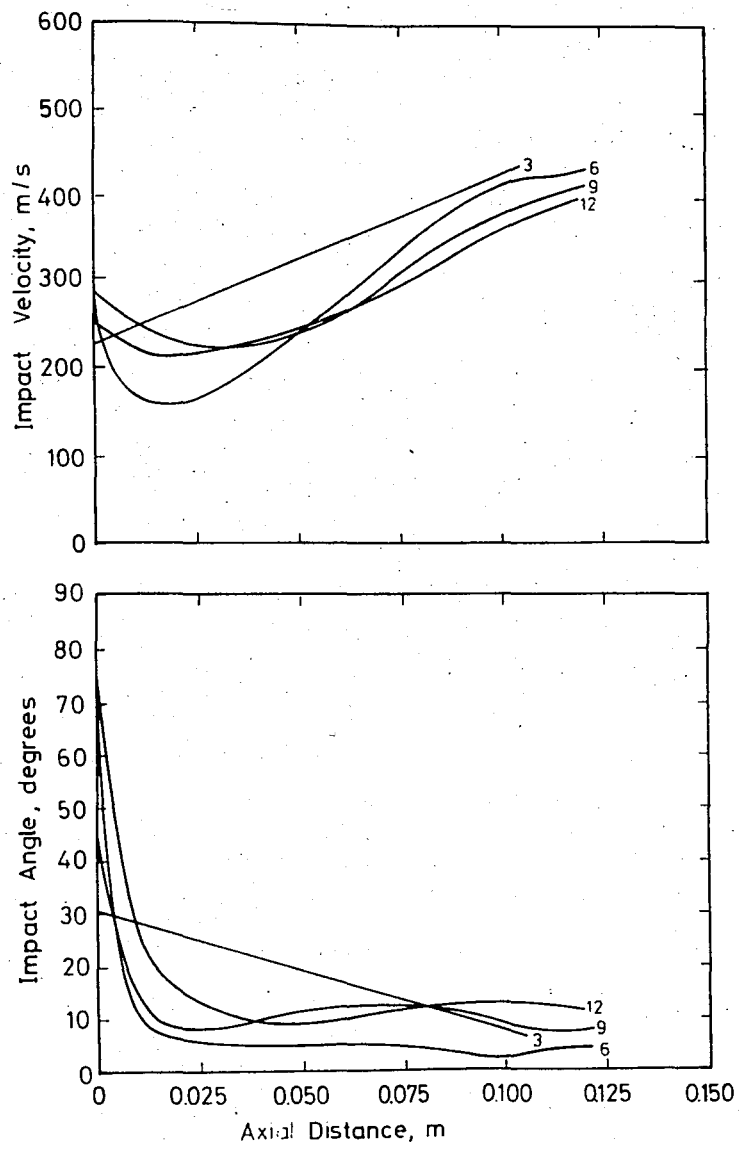

FIGURE 20 - Particle impact angles and velocities for the fourth stage rotor

It is observed that particles collide the leading edge of the blade with an angle close to 90 degrees. On the other hand, particle collisions with the trailing edge occur at smaller angles and larger velocities.

Before presenting the erosion results it is worthwhile to critically review the basic erosion models used in the calculations.

It should be remembered that the erosion responses of two of the materials were calculated from Eqs. (27) with the model coefficents (see Table 2) deduced from a set of constant temperature experimental data for silicon carbide particles eroding a nickel-cobalt alloy based on the rough estimate that silicon carbide particles are 25 times as erosive as coal ash particles eroding "typical" blade materials. Therefore, it is highly questionable whether these models can represent the behavior of some real blade materials to an acceptable accuracy and it is clear that they do not reflect the effect of temperature variations through the turbine. The reason for including these cases in the present study, as well, is to establish a basis of comparision between a ductile material and a brittle material that have similar maximum erosion levels but different angular responses.

Accurate assesment of multistage turbine erosion is dependent on the availability of basic erosion data for the specific blade material used and in the complete operational range of temperatures and velocities. In this respect, the interpolative models used to describe the erosion behavior of 304 stainless steel and Rene 41 are more realistic. These models were based on the basic erosion data obtained by Tabakoff et al {41},{52} in their high temperature material erosion facility at the University of Cincinati.Nevertheless, these data (shown in Figures D3 and D4) cover temperatures up to 649 ^{0}C and velocities up to 305 m/s which are low in comparision to the maximum temperatures of about 1082^{0}C and the

maximum velocities of about 657 m/s encountered in our turbine. In the present application, erosion rates at velocities above the experimental range were estimated by extrapolation. However, for temperatures above the experimental range the erosion data obtained at the maximum experimental temperature (649 ^{0}C) was assumed, because it was felt that the erosion response could drastically change near the melting temperatures of the materials that extrapolation would be misleading.

Figures 21 through 28 illustrate the total erosion damage per blade as a function of particle size. The total erosion damages per blade caused by 3,6,9 and 12 μm particles are also illustrated in Figures 29 through 32 as a function of the stage number. The axis on the left (E) gives the total damage per blade in terms of the volume of material (m^3) removed per kilogram of particles entering the turbine. The axis on the right (E^*) indicates the material volume (m^3) removed from each blade in a given row in 10,000 hours of continous operation for a reference turbine inlet concentration of 0,00023 gm/m^3 standard (0,0001 grain/ft^3 standard). It is noted that stator and rotor blade total erosion rates exhibit different trends. As we go downstream, the total damage per blade generally increases for the stationary rows but decreases for the rotating rows. It is interesting that damage inflicted on 304 stainless steel and Rene 41 is very similar in both trend and magnitude. Comparision between the "hypothetical" materials with 20^0 and 90^0 maximum erosion angles shows that ductile materials as blade material are much more susceptible to erosion damage than brittle materials of comparable basic erosion resistance. This is mainly because in the particle diameter range considered most particle-blade impacts occur at small angles to which brittle materials are inherently resistant. It is also interesting to note that the ductile material erosion calculated by the semiempirical erosion model is considerably lower than the 304 stainless

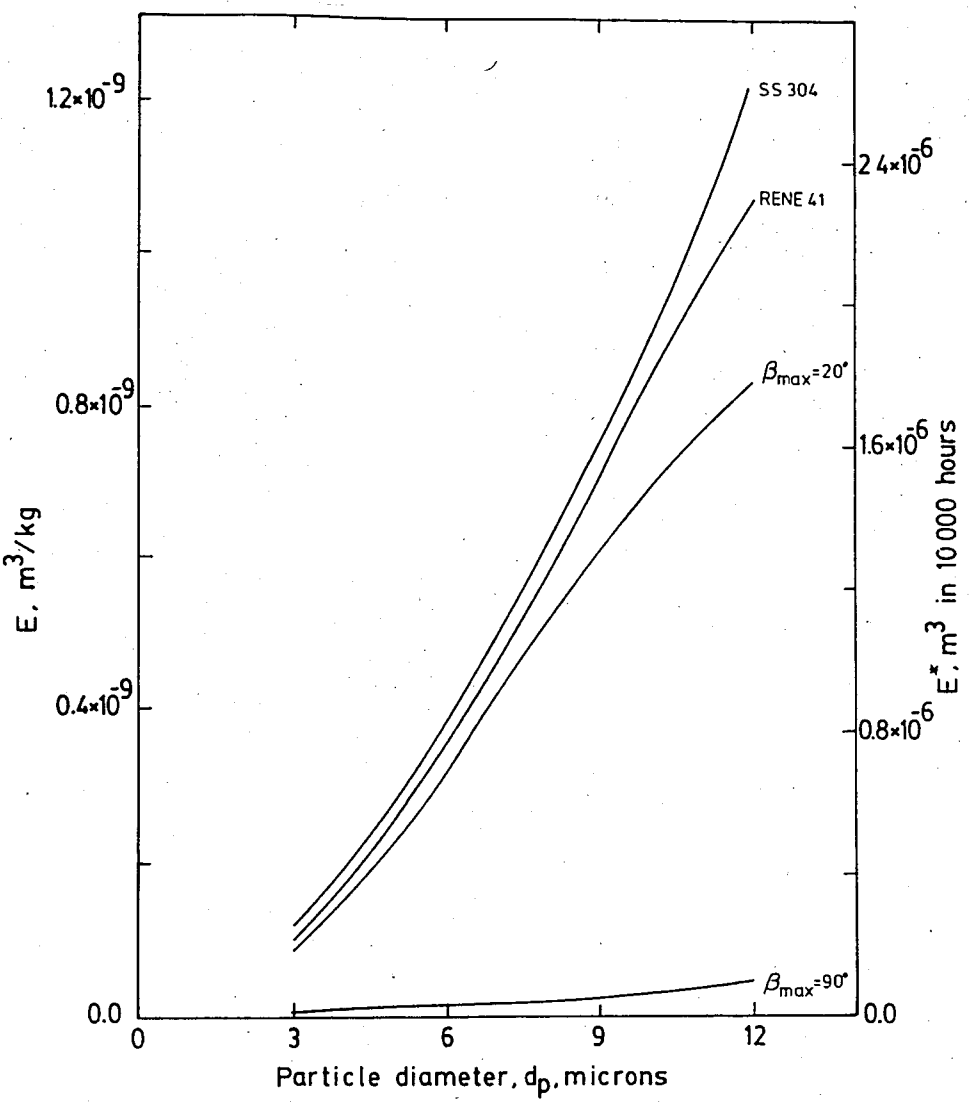

FIGURE 21 - Total erosion damage per blade as a function of particle size for the first stage stator

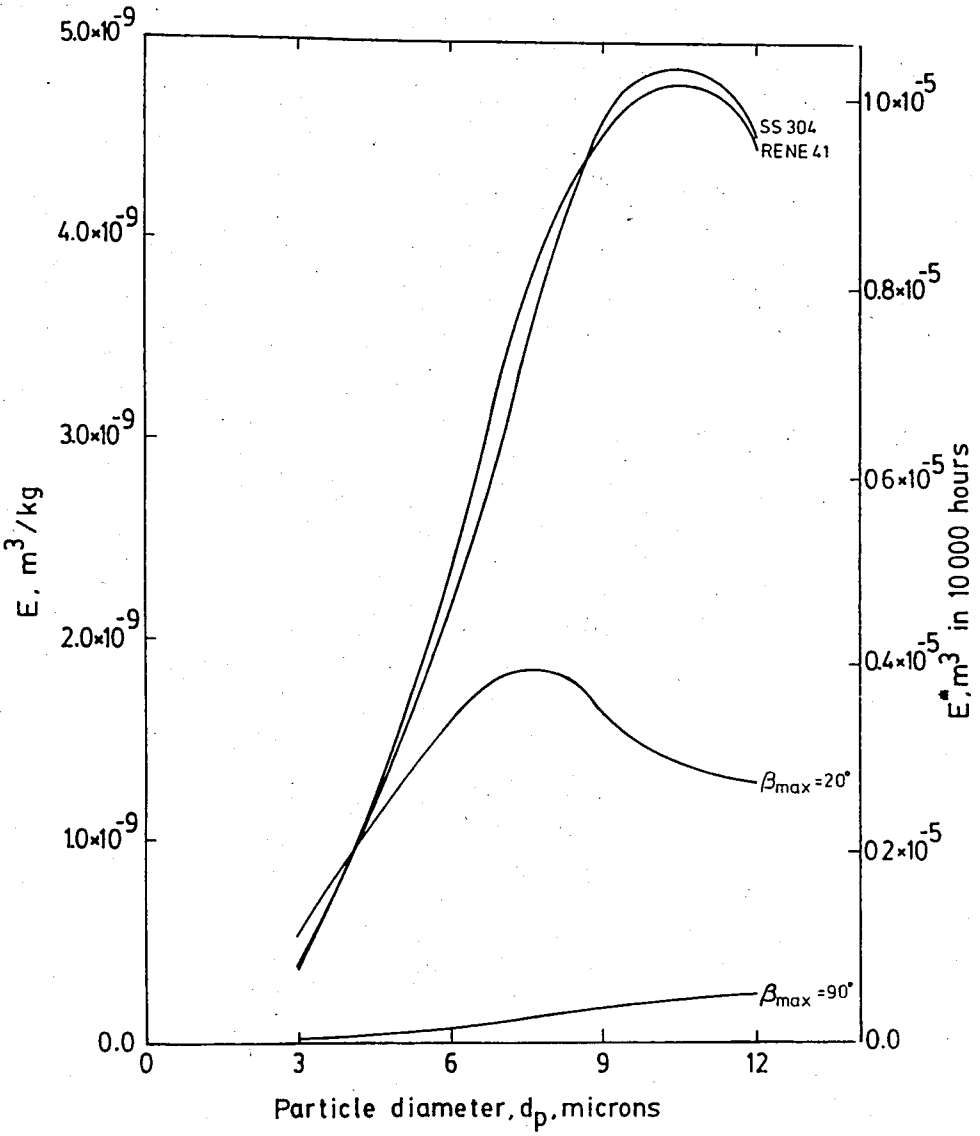

FIGURE 22 - Total erosion damage per blade as a function of particle size for the first stage rotor

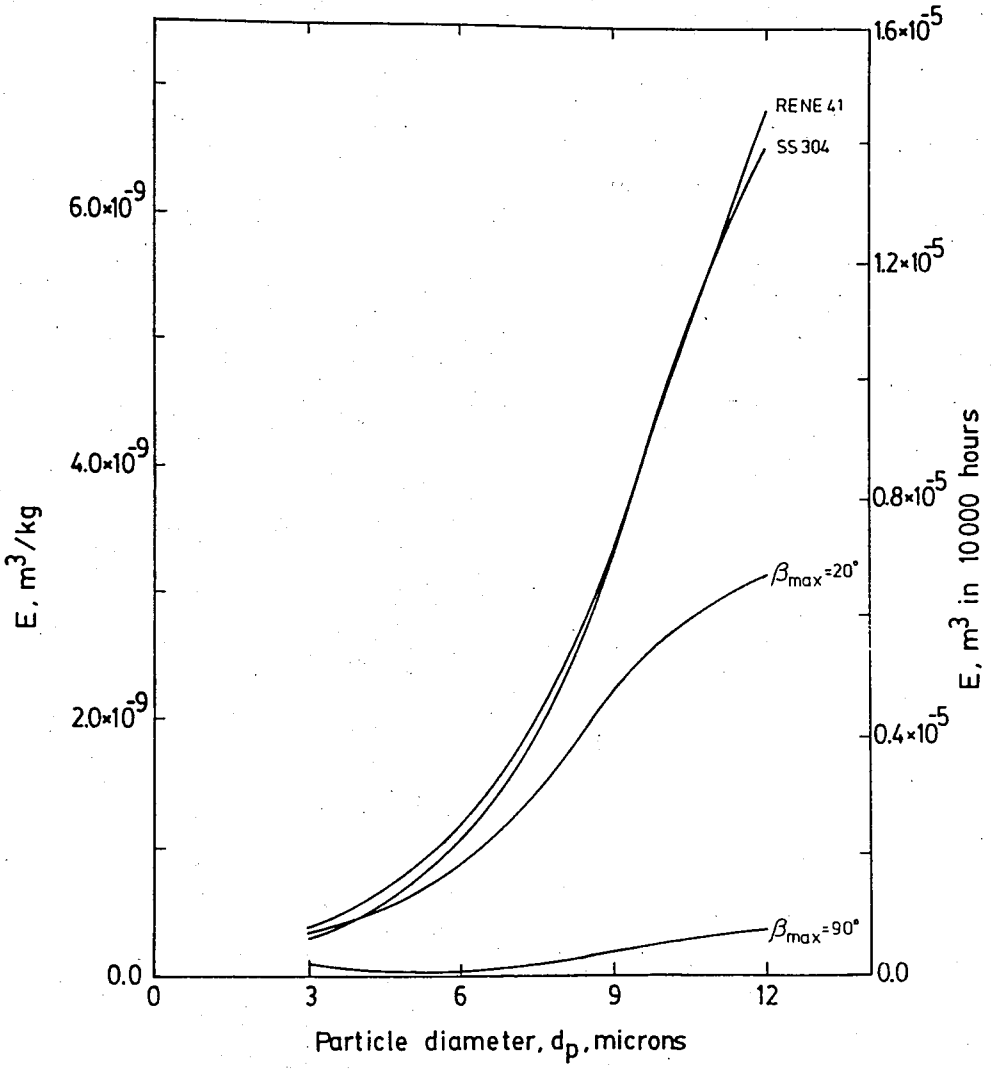

FIGURE 23 - Total erosion damage per blade as a function of particle size for the second stage stator

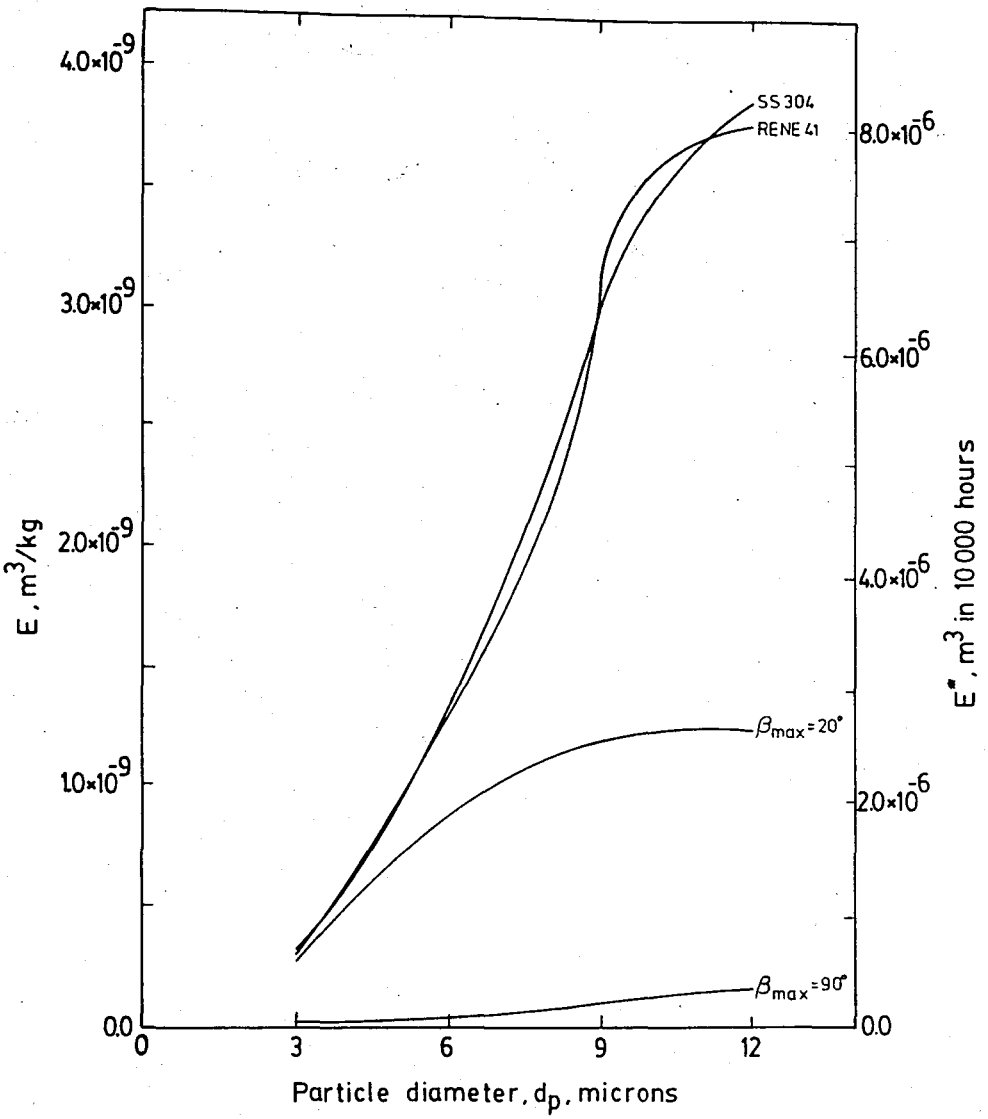

FIGURE 24 - Total erosion damage per blade as a function of particles size for the second stage rotor

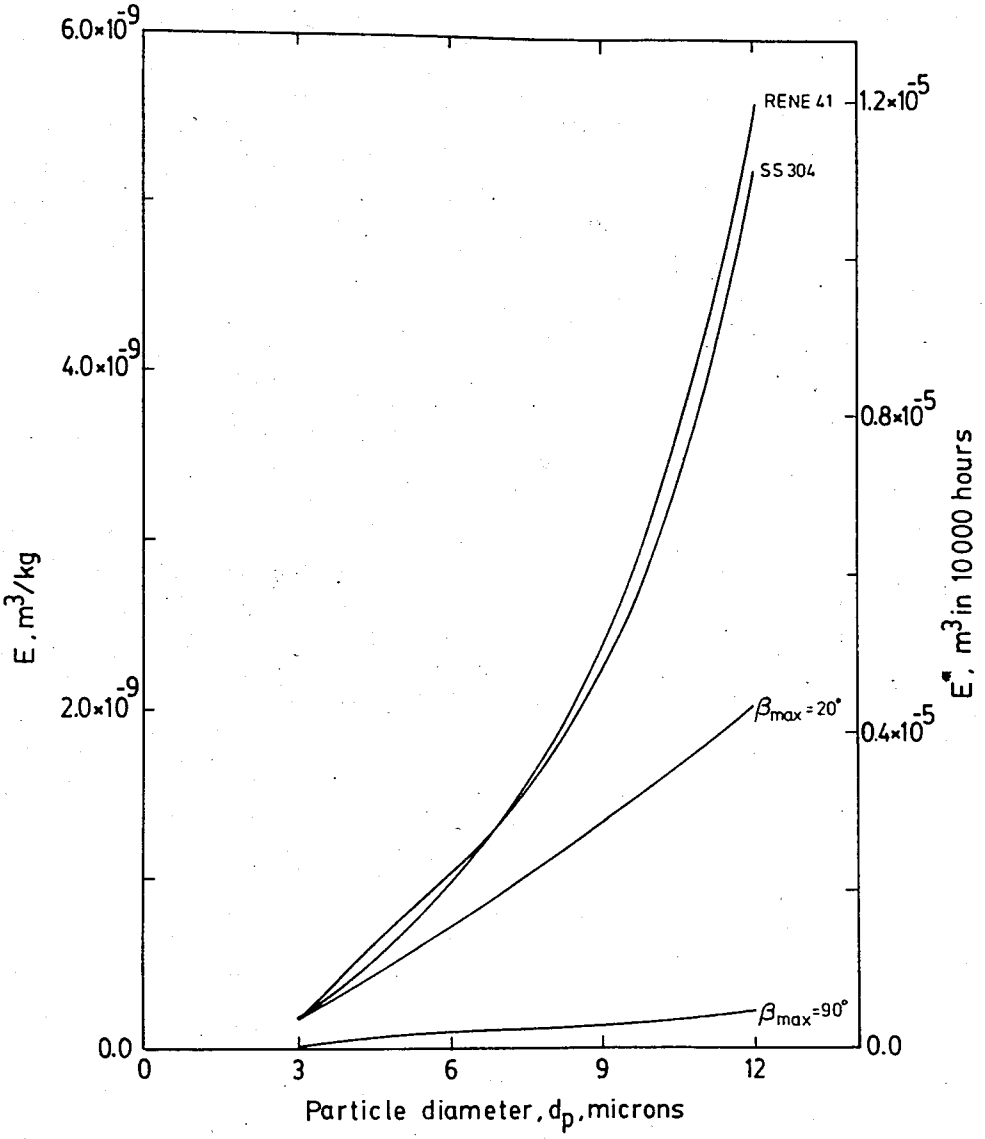

FIGURE 25 - Total erosion damage per blade as a function of particle size for the third stage stator

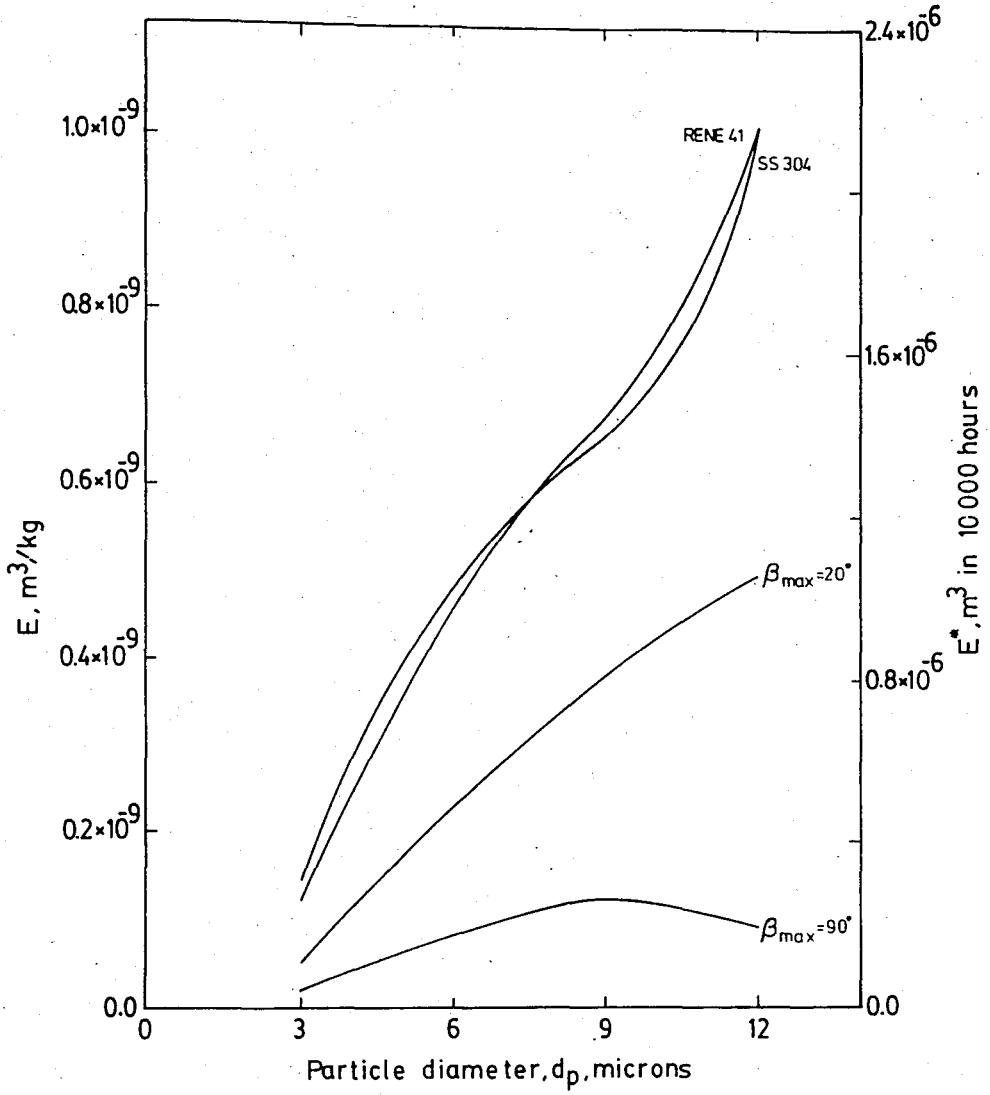

FIGURE 26 - Total erosion damage per blade as a function of particle size for the third stage rotor

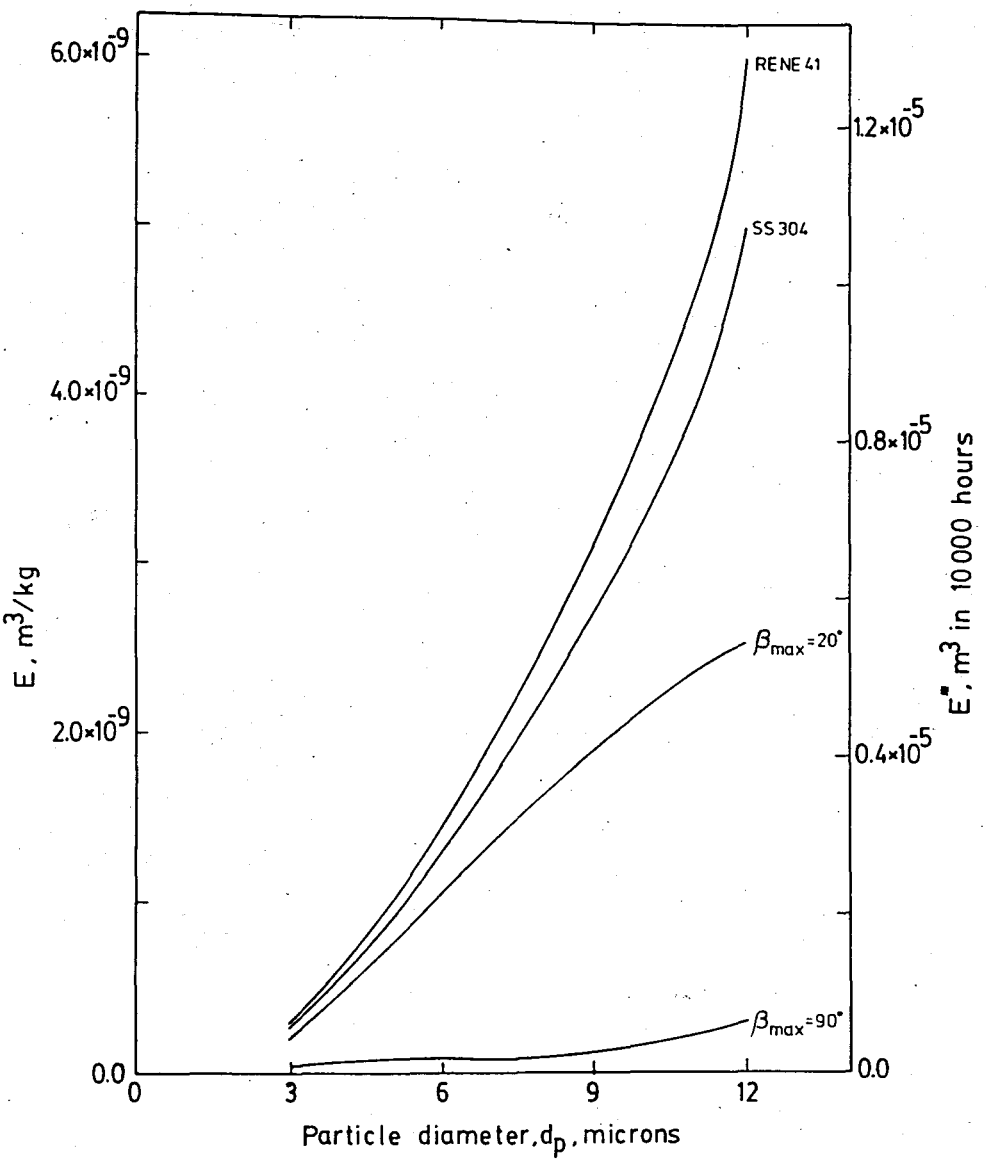

FIGURE 27 - Total erosion damage per blade as a function of particle size for the fourth stage stator

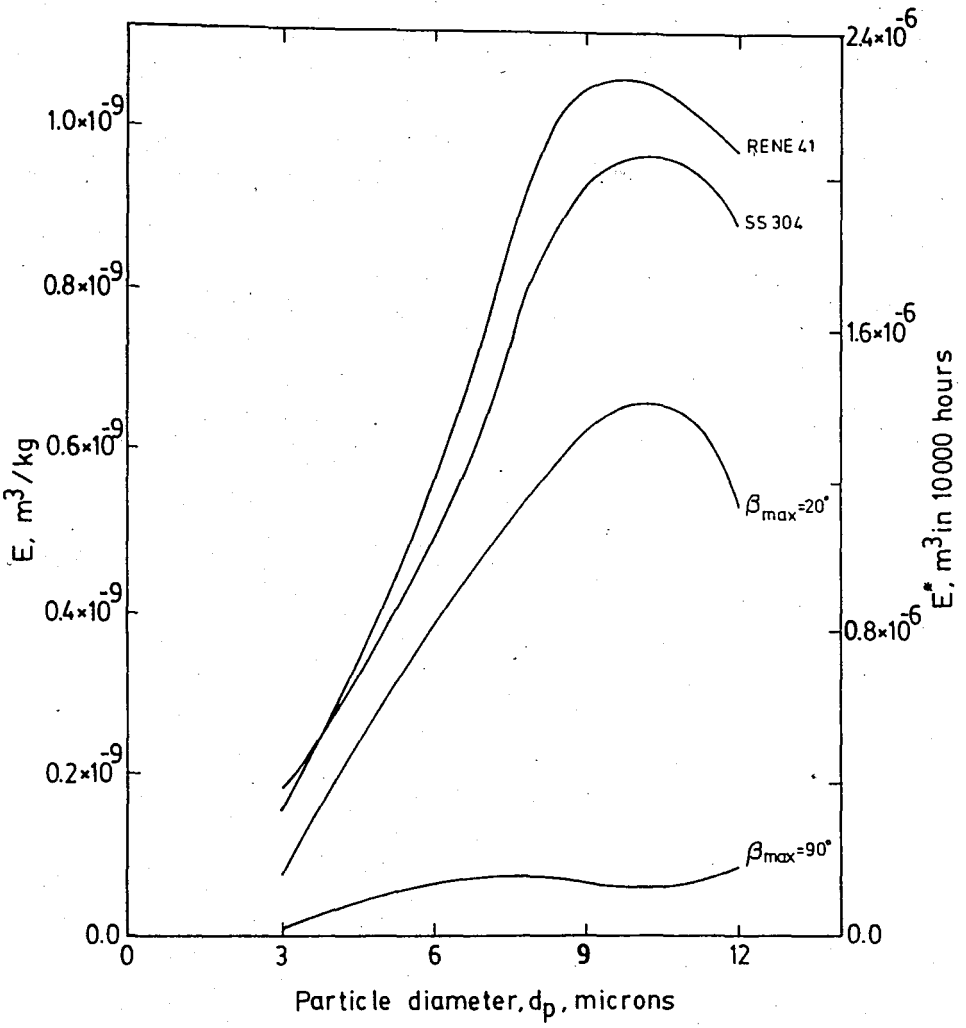

FIGURE 28 - Total erosion damage per blade as a function of particle size for the fourth stage rotor

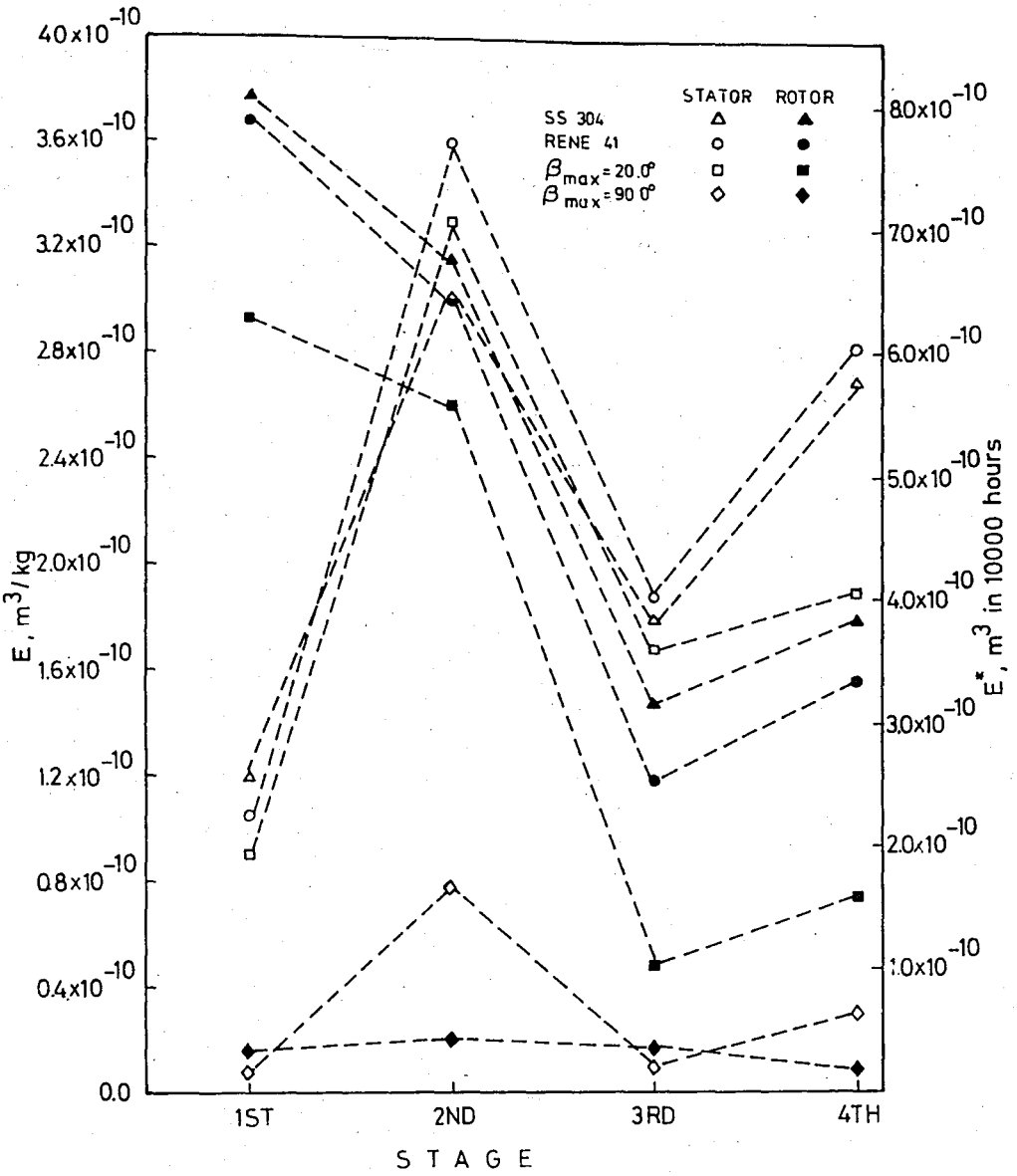

FIGURE 29 - Total erosion damage per blade by 3μm particles as a fuction of the stage number

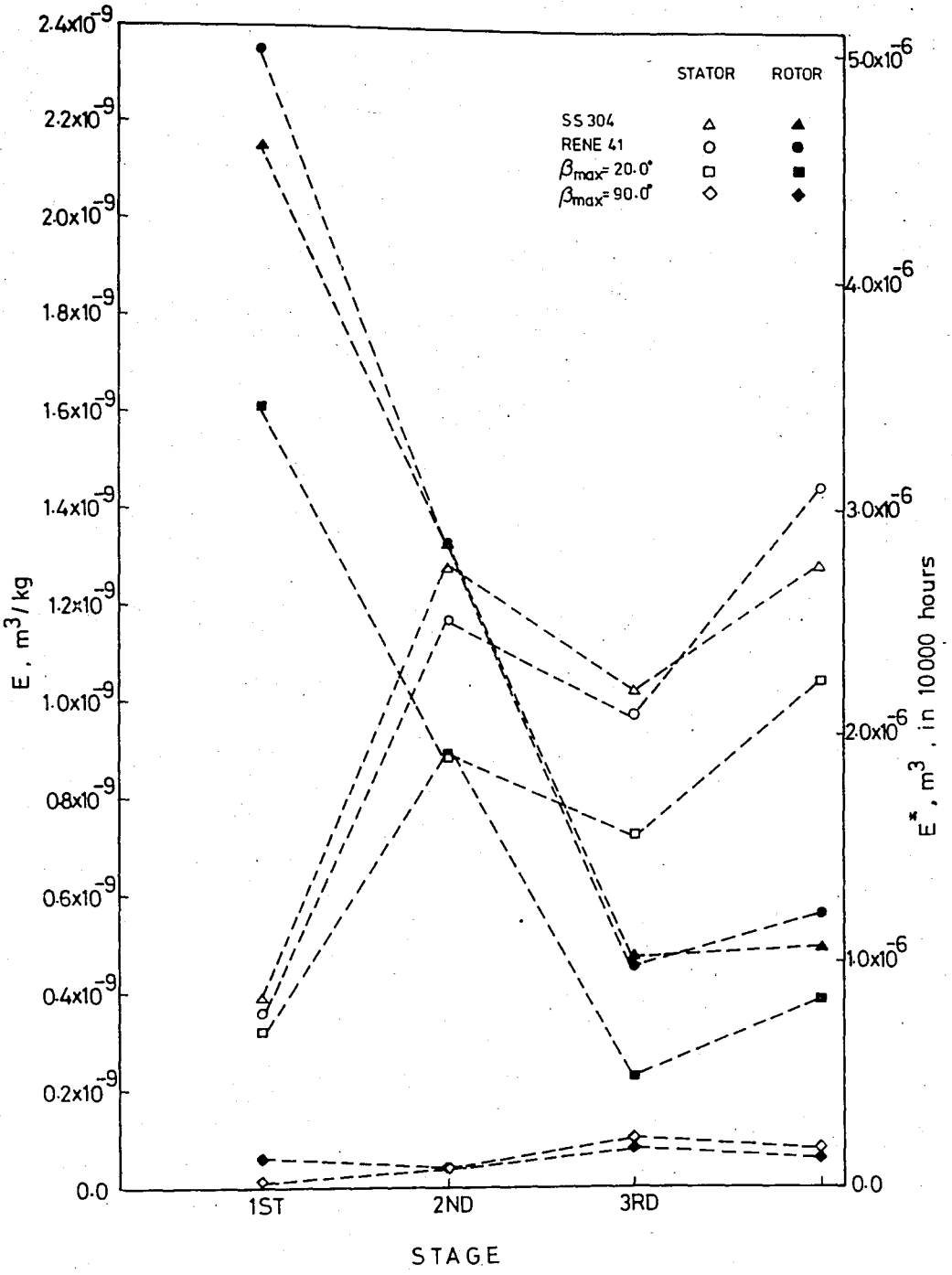

FIGURE 30 - Total erosion damage per blade by 6μm particles as a function of the stage number

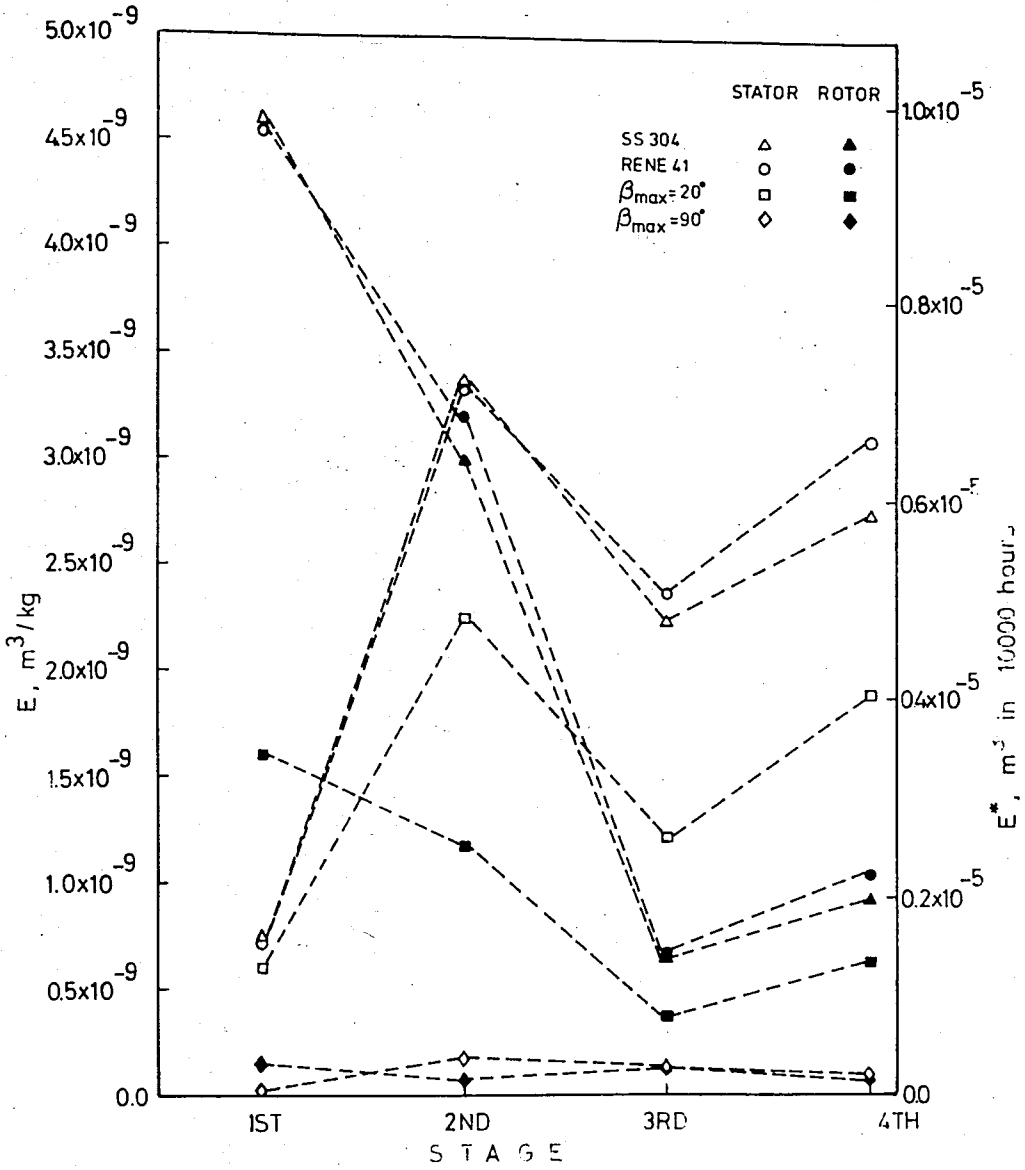

FIGURE 31 - Total erosion damage per blade by 9µm particles as a function of the stage number

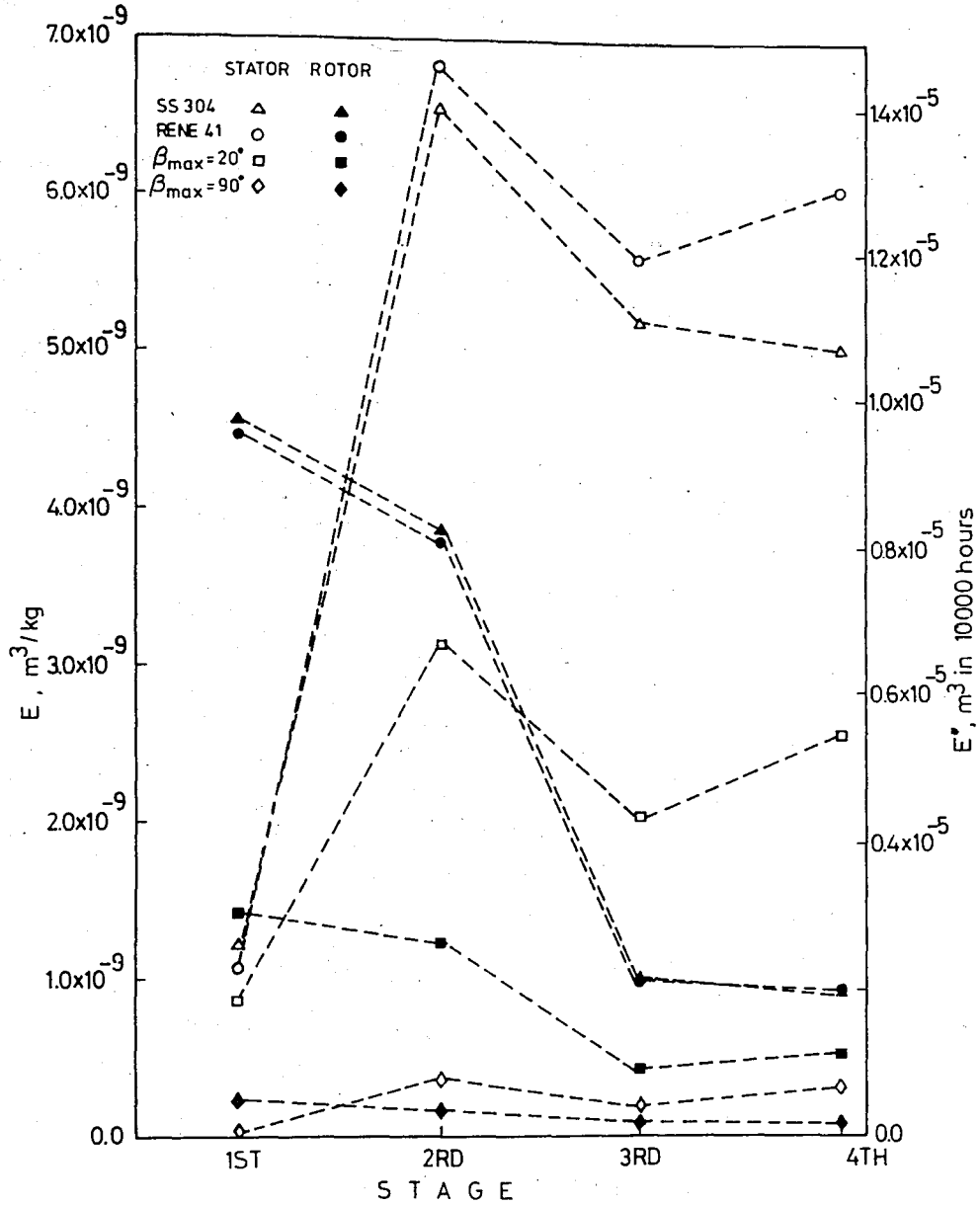

FIGURE 32 - Total erosion damage per blade by 12μm particles as a function of the stage number

steel and Rene 41 erosion calculated by the interpolative model, for all particle diameters considered (3-12μm).

Figure 33 summarizes the effect of particle size on the total erosion rates of 304 stainless steel. As expected, damage increases greatly with increasing particle diameter. For long blade life, large particles must be effectively removed from the gas. Another point of interest in these curves is that the total damage on the first stage stator and the second and forth stage rotor blades is considerably lower than in the remaining rows.

Figures 34 through 37 shows the predicted material recession rates due to erosion of 304 stainless steel blades as a function of the axial distance measured from the blade leading edge of each row. These results are given for four particle diameters (3,6,9 and 12 μm) in millimeters of material recession after 10,000 hours of operation with a reference inlet particle loading 0,00023 gm/m^3 standard (0,0001 grain/ft^3 standard). It is noted that the recession rate curves are quite sensitive to particle diameter and display considerable trend and magnitude variations between blade rows. These curves are usually characterized by two notable peaks which occur near the leading and trailing edges the exact locations depending upon the diameter of particles and the blade row under consideration. The trailing edge recession rates are usually larger than the leading edge recession rates for the larger particles (9μm and 12μm), but the reverse is usually true for the smaller particles (3 μm and 6 μm).

As an example to the blade erosion pattern of a typical brittle material, Figures 38 through 41 show the recession rates calculated for the case with $\beta_{max} = 90^0$. Here, the leading edges exposed to particle impacts at relatively large angles erode at much faster rates than the trailing edges, in general.

Figure 42 shows the leading edge and trailing edge recession rates of 304 stainless steel as a function of

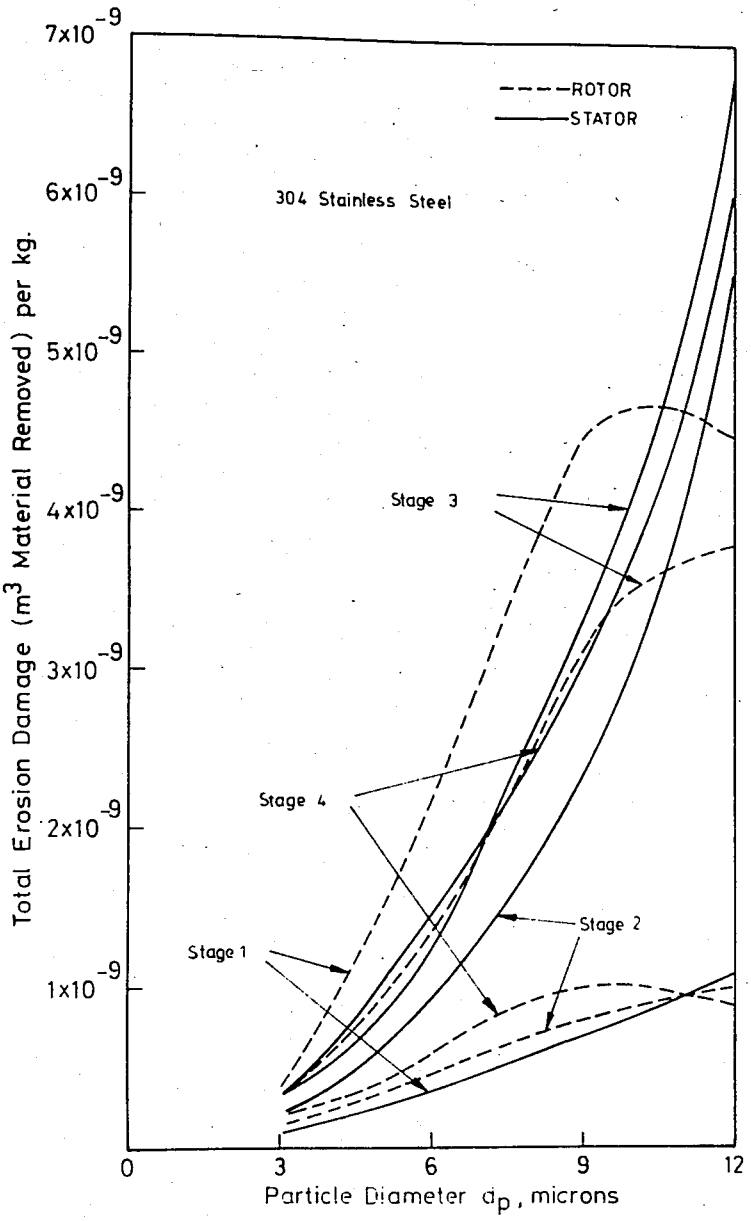

FIGURE 33 - Total erosion damage per blade of 304 stainless steel as a function of particle size

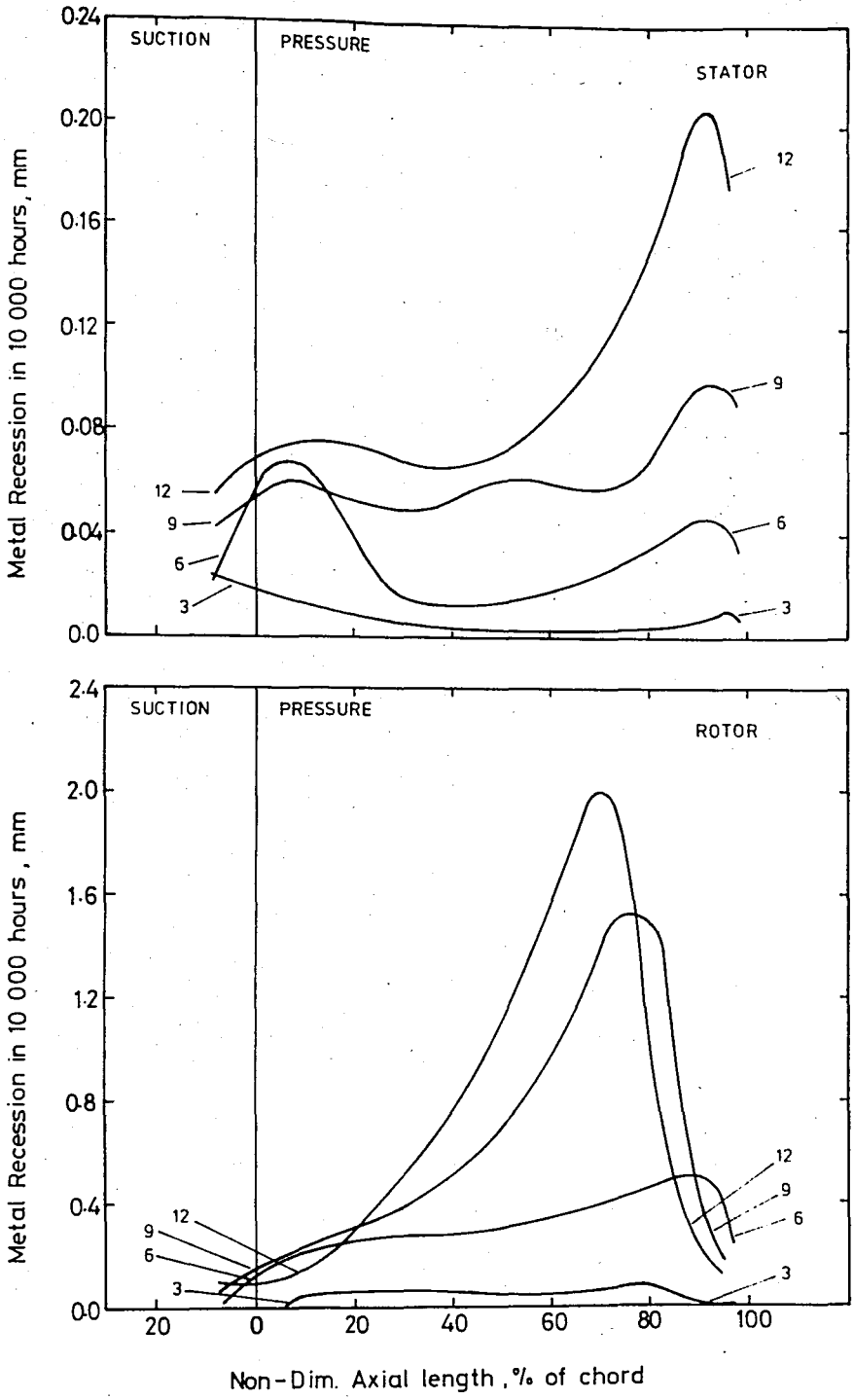

FIGURE 34 - Metal recession rates for 304 stainless steel (first stage) as a function of axial position

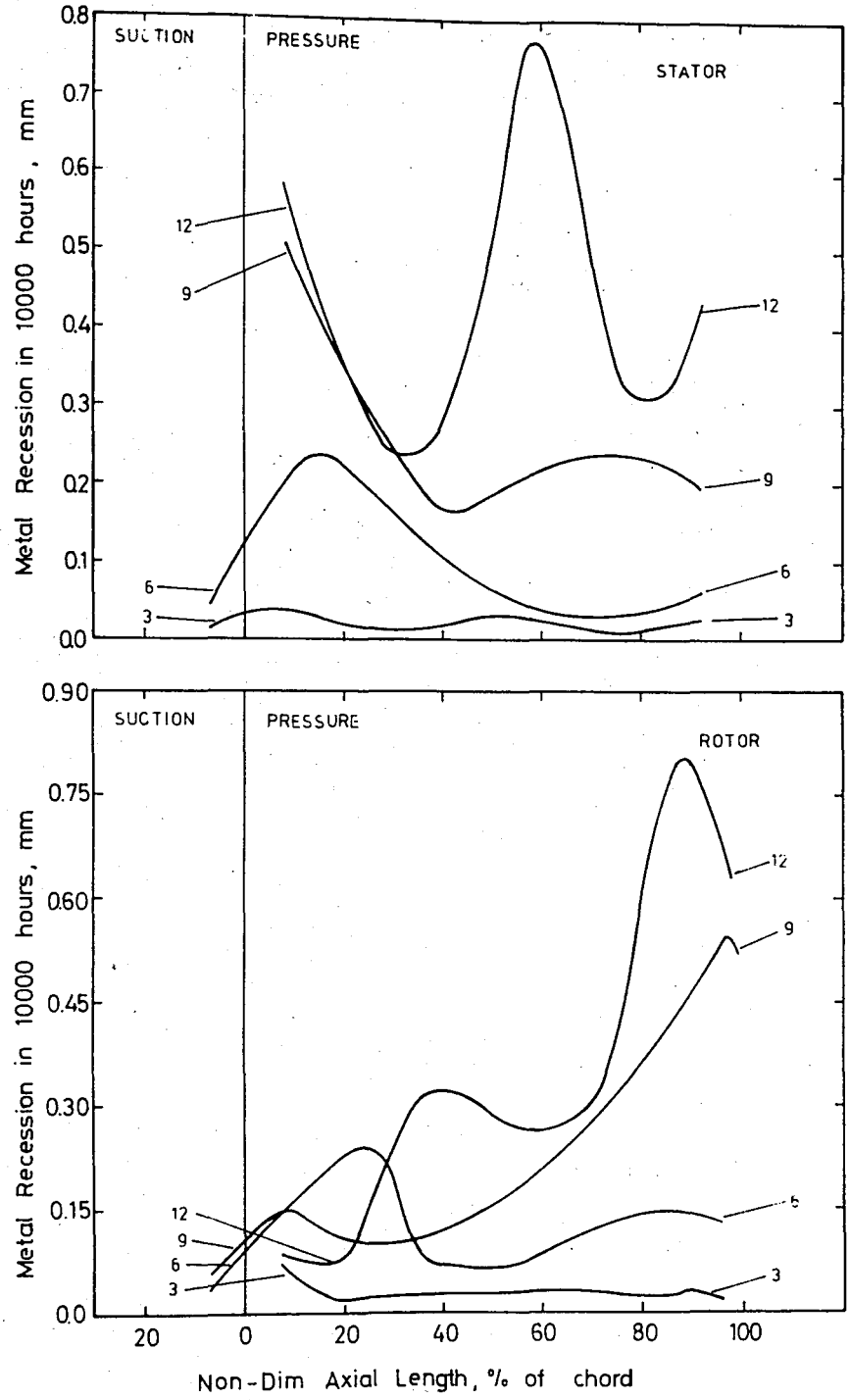

FIGURE 35 - Metal recession rates for 304 stainless steel (second stage) as a function of axial position

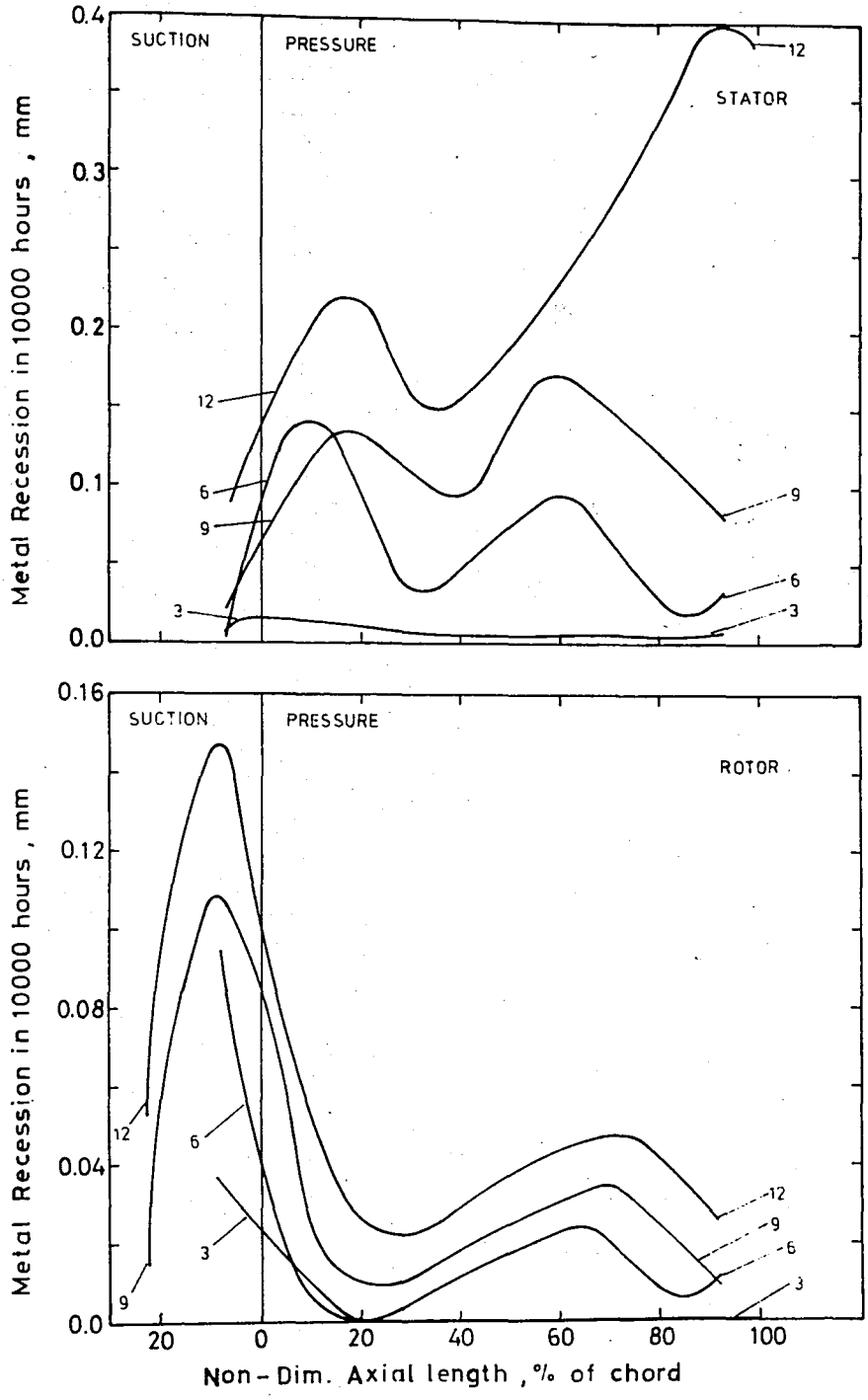

FIGURE 36 - Metal recession rates for 304 stainless steel (third stage) as a function of axial position

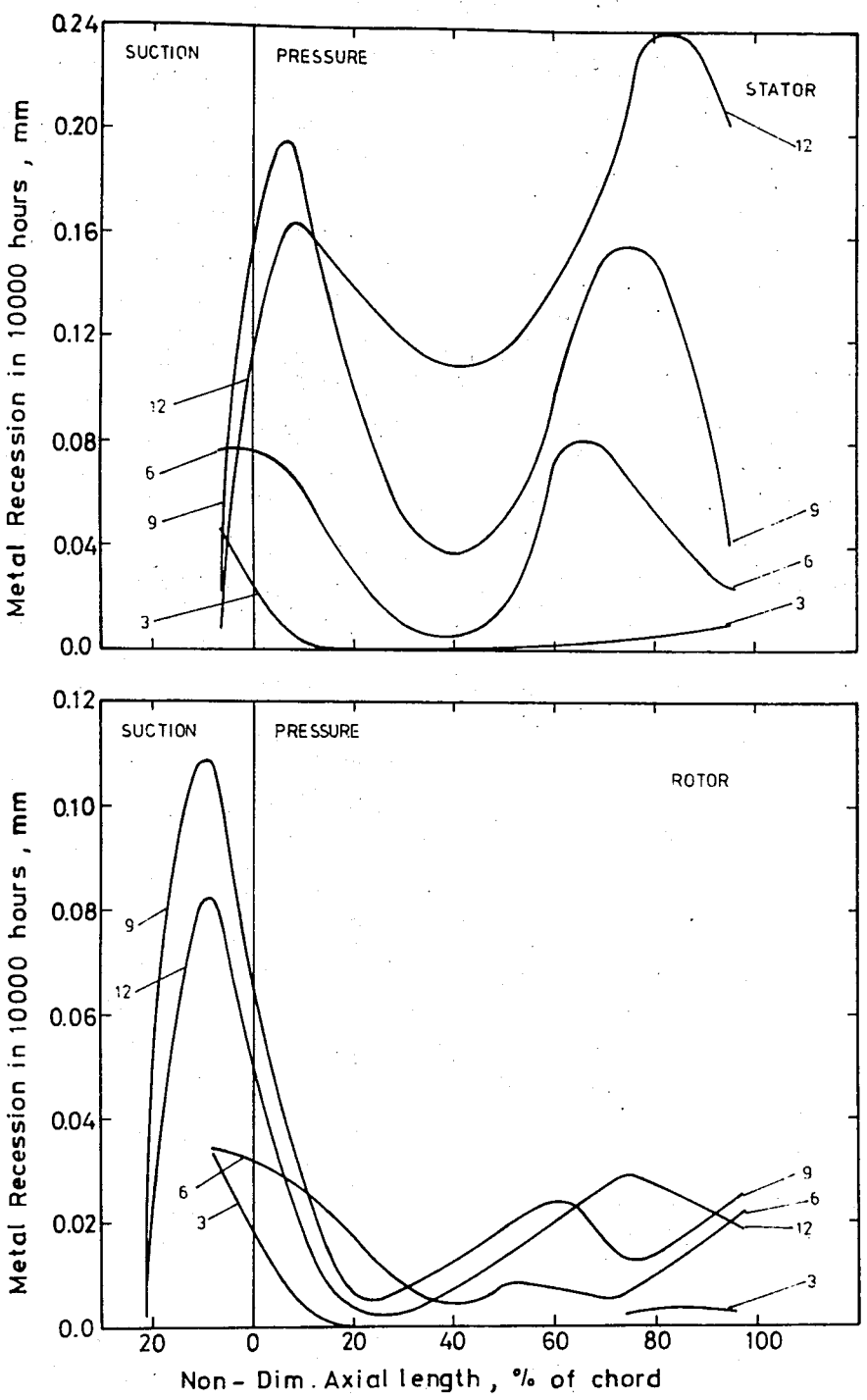

FIGURE 37 - Metal recession rates for 304 stainless steel (fourth stage) as a function of axial position

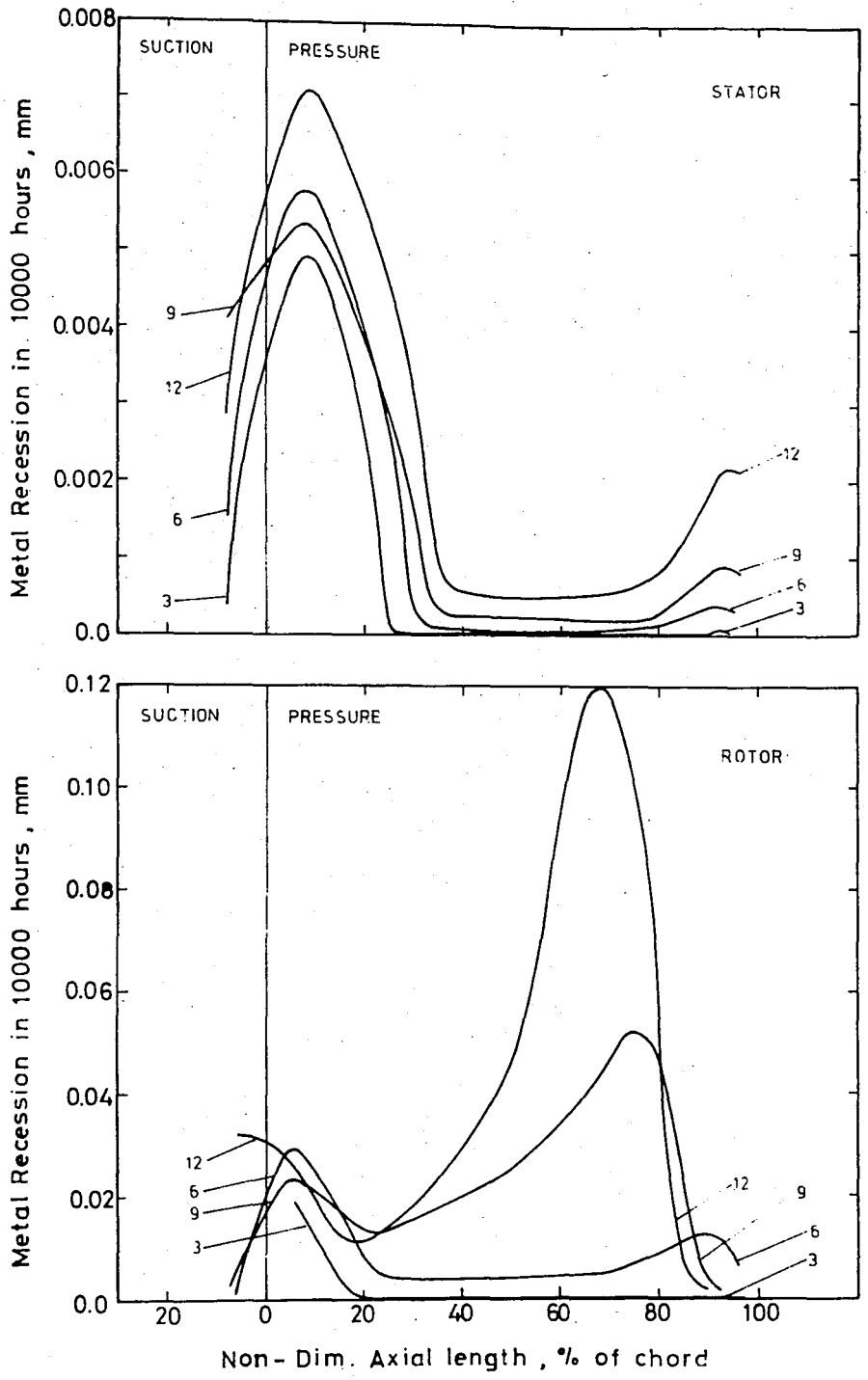

FIGURE 38 - Metal recession rates for brittle material, $\beta_{max}=90^{0}$ (first stage) as a function of axial position

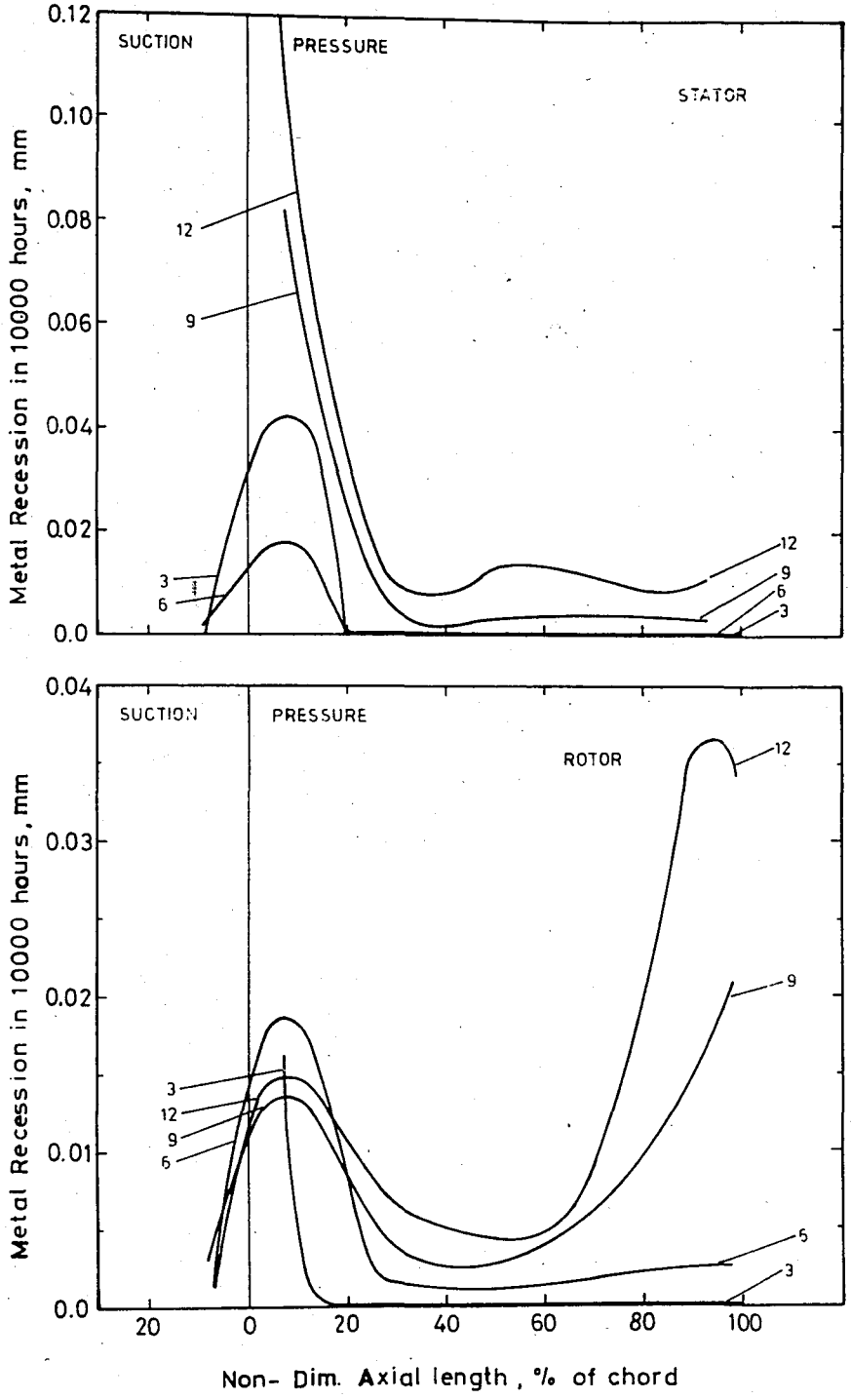

FIGURE 39 - Metal recession rates for brittle material $\beta_{max}=90^0$ (second stage) as a function of axial position

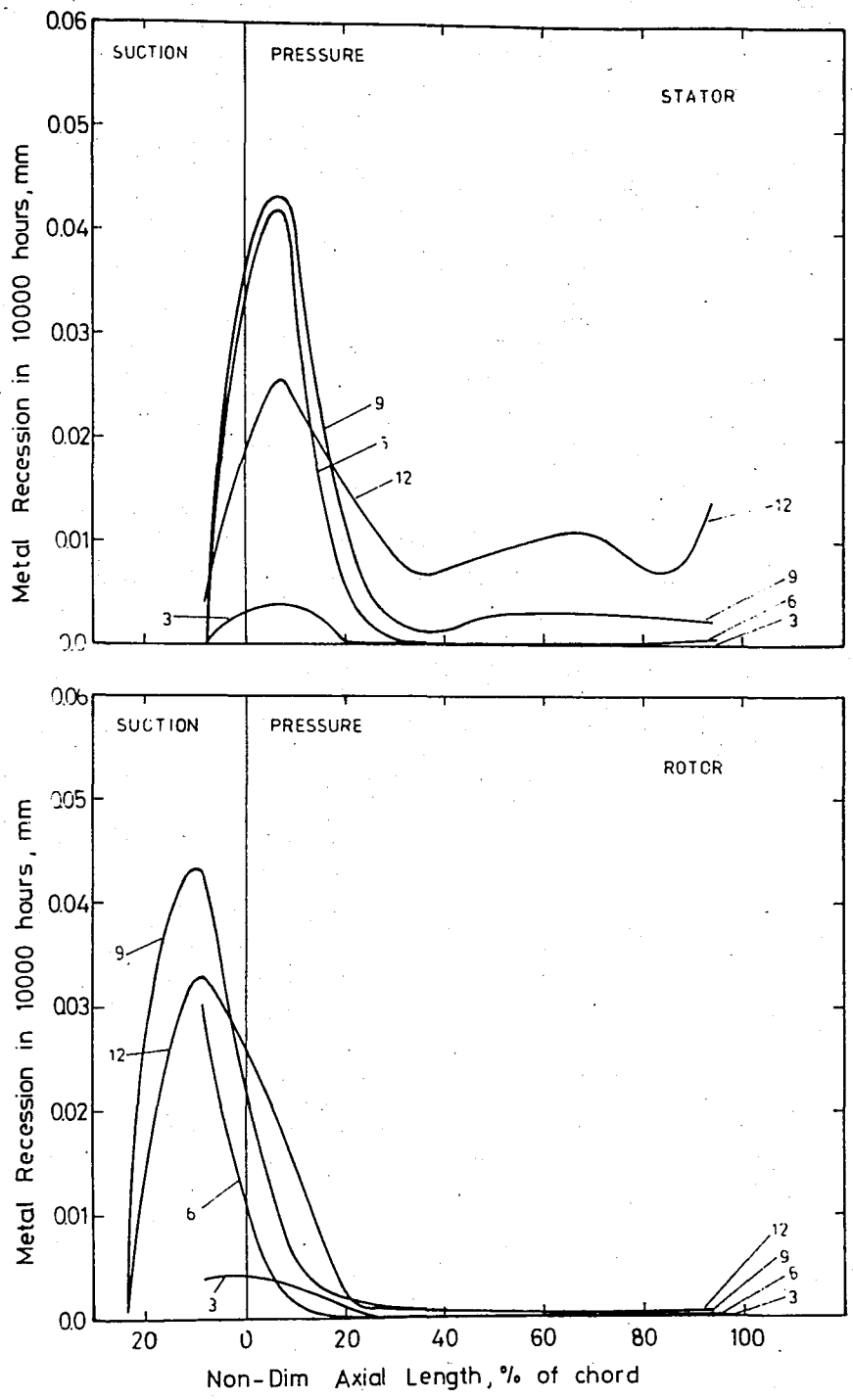

FIGURE 40 - Metal recession rates for brittle material $\beta_{max}=90^0$ (third stage) as a function of position

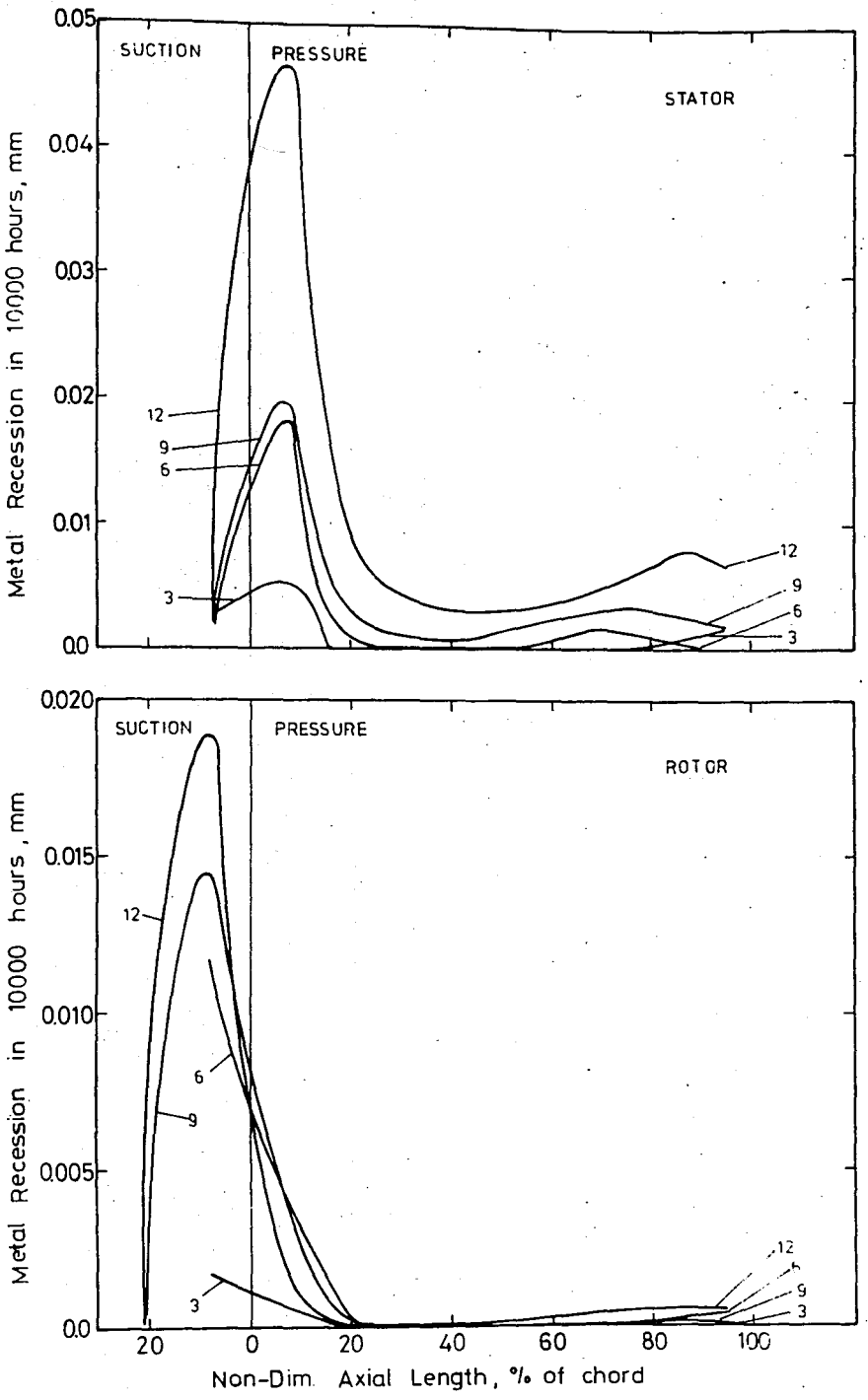

FIGURE 41 - Metal recession rates for brittle material, $\beta_{max}=90^0$ (fourth stage) as a function of axial position

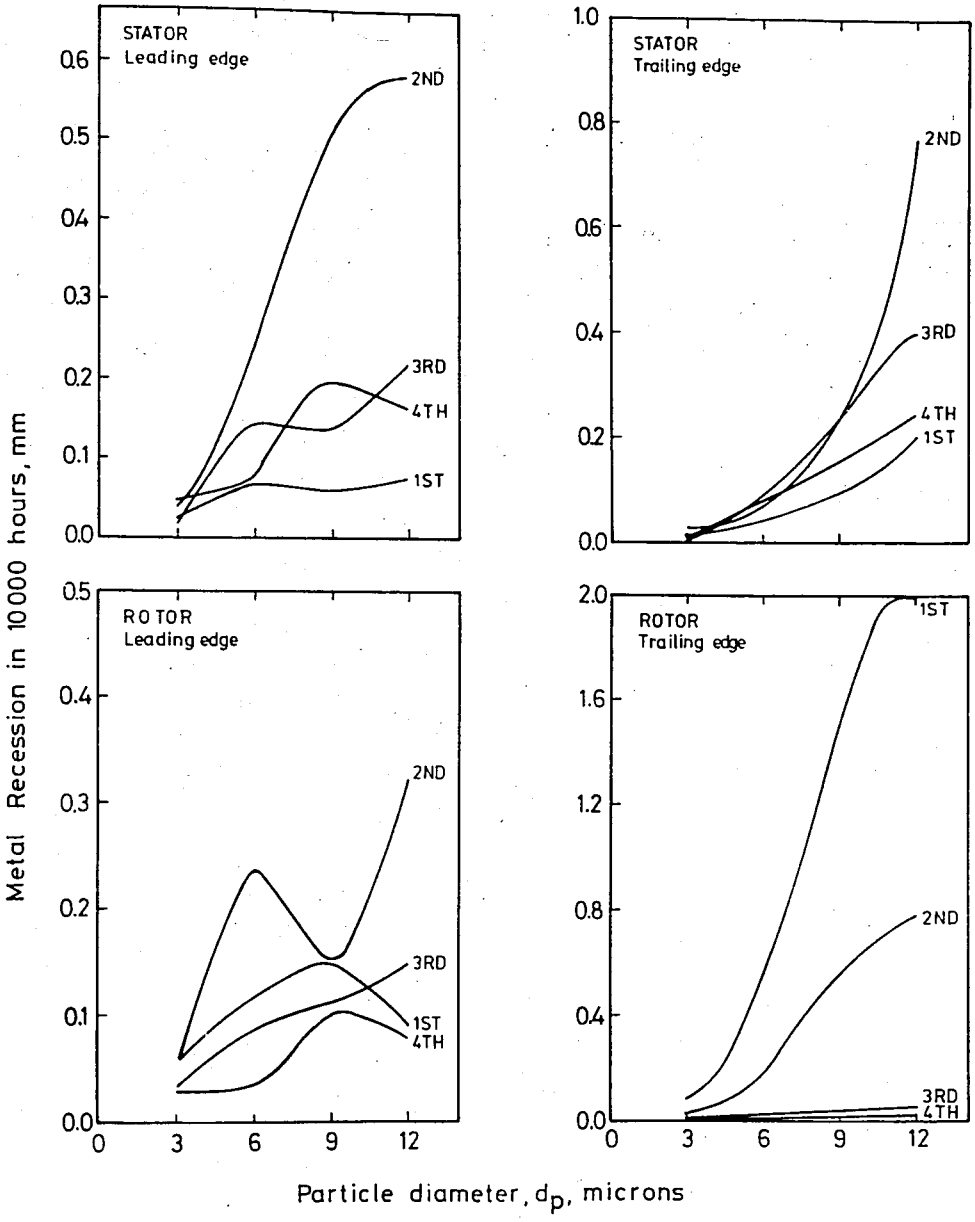

FIGURE 42 - Maximum metal recession rates as a function of particle size for 304 stainless steel

particle diameter. It appears from these results that the useful life of the machine will be dictated by the thinning of the first stage rotor trailing edge. In addition, the trailing edge regions of the second stage stator and rotor blades and the third stage stator blades and the leading edge regions of the second stage rotor blades are subject to high erosion rates.

Figure 43 illustrates the leading edge and trailing edge recession rates of the brittle material with $\beta_{max}=90^0$.

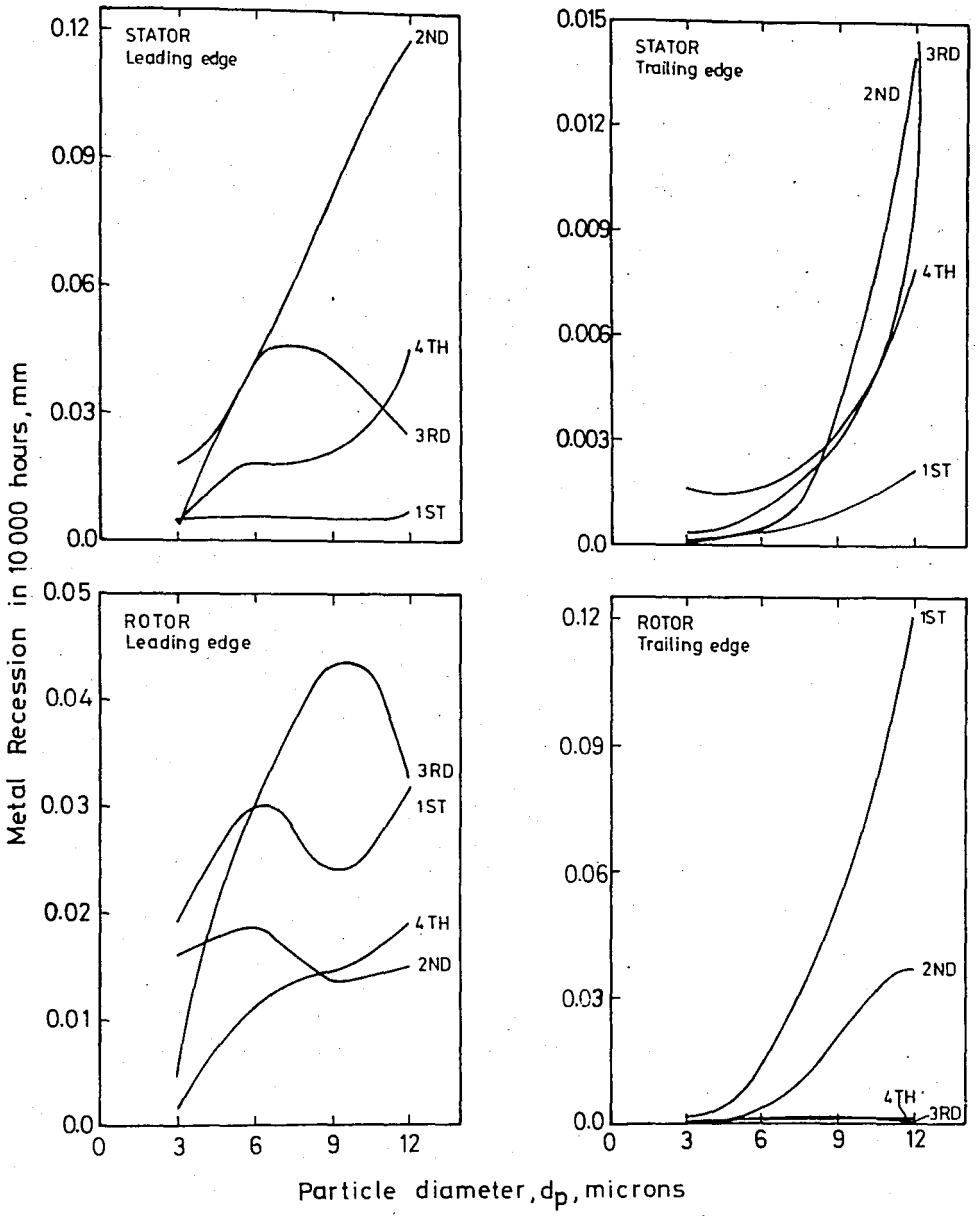

FIGURE 43 - Maximum metal recession rates as a function of particle size for brittle material, $\beta_{max}=90^0$

V. CONCLUSIONS AND RECOMMENDATIONS

1. A computer program package has been developed to calculate the blade erosion damage in a multistage turbine resulting from the particulate matter contained in the hot expansion gases

2. The following conclusions have been obtained from the application of this program package to a modern multistage gas turbine.
   a. Erosion damage primarily occurs at the leading and trailing edges of the blades and is usually confined to the pressure surfaces
   b. Erosion damage has been noted to generally increase with increasing particle diameter and density, flow turning, gas velocity, and number of blades in a row and with decreasing blade size.
   c. The useful life of the machine will be dictated by the thinning of the first stage rotor trailing edge. In addition, the trailing edge regions of the second stage stator and rotor blades and the third stage stator blades and the leading edge regions of the second stage rotor blades are subject to high erosion rates. Erosion of this turbine may be controlled by armoring these high erosion points with field-replaceable erosion shields or by hard facing. Erosion life of a blade may also be increased by increasing the trailing edge thickness.

d. Ductile materials as blade material are much more susceptible to erosion damage than brittle materials of comparable basic erosion resistance. Use of brittle materials (e.g. ceramic blade) appears to be a promising solution to the blade erosion problem. Erosion of blades made of a brittle material tends to peak around the leading edges. Hard facing or shielding of these areas may prove to be necessary.

3. The models used to simulate the gas particle flow need improvement in the following areas

a. The present gas flow model is 2-D and does not describe the flow in those stages having small hub-to-tip radius ratios accurately. A 3-D flow solution is required.

b. It is known that blade and end-wall boundary layers and secondary flows have important effects on the motions of small particles and the resulting erosion damage. For reliable assessment of turbine erosion these effects should be taken into account.

c. Accurate assesment of multistage turbine erosion is dependent on the availability of basic erosion data for the specific blade material used and in the complete range of temperatures and velocities typical of modern high-temperature gas turbines. Experimental studies to obtain such data should be encouraged.

APPENDICES

APPENDIX A

TSONIC PROGRAM INPUT DESCRIPTION

A description of input variables of the TSONIC program used for gas flow solution are given below:

GAM	specific heat ratio, C_p/C_v
AR	gas constant, J/(kg)(K)
TIP	inlet stagnation temperature, K
RHOIP	inlet stagnation density, kg/m^3
WTFL	mass flow rate per blade, kg/sec
OMEGA	rotational speed, rad/sec
ORF	overrelaxation factor, ORF=0, program calculates optimum ORF 1<ORF<2, ORF calculated by program is used for subsequent runs using the same mesh spacing
BETAI	inlet flow angle, deg
BETAO	outlet flow angle, deg
CHORDF	axial length of blade,m
STGRF	distance between leading and trailing edge circles, rad.
REDFAC	weight flow reduction factor to assure subsonic flow, 0.5 < REDFAC < 0.9
DENTOL	density change tolerance per iteration DENTOL 0.001(high), 0.01(medium), 0.1 (loose tolerance)

CUTOFF	percent of axial blade length were extrapolation of surface velocities start.
MBI	number of vertical mesh lines up to leading edge
MBO	number of vertical mesh lines up to trailing edge
MM	total number of vertical mesh lines, MM<100
NBBI	number of horizontal mesh lines, NBBI<50
NBL	number of blades
NRSP	number of MR, RMSP, and BESP coordinates, NRSP<50
RI1,2	leading edge radius(1 for upper, 2 for lower surface), m
RO1,2	trailing edge radius(1 for upper, 2 for lower surface), m
BETI1,2	true angle at tangent points of leading edge radius with blade surface, deg
BETO1,2	true angle at tangent points of trailing edge radius with blade surface, deg
SPLNO1,2	number of MSP1,2 and THSP1,2 coordinates
MSP1,2	meridional blade coordinate, m
THSP1,2	tangential blade coordinate, rad.
MR	meridional channel coordinate, m
RMSP	radial mid-channel coordinate, m
BESP	stream channel thickness, m

Control variables

BLDAT	=1, print geometrical information
AANDK	=0
ERSOR	=0
STRFN	=1, print stream function values
SLCRD	=1, print streamline coordinates
INTVL	=1, print interior flow data
SURVL	=1, print surface flow data
ICONT	=1
NLAST	=0
JFLOW	=1, subsonic and 2, transonic
JOUT	=1, print and 2, store on disc unit
IPLOT	=0

TSONIC program stores the gas solution necessary for TPART program on unit 18(with JOUT 2)

APPENDIX B

TPART PROGRAM INPUT DESCRIPTION

All formats are free.

Card 1 : Title

Card 2 : DPART, RHOP

DPART : particle diameter, microns

RHOP : particle density, gm/cm^3

Card 3 : NSTAGE, NPAR, DSR (1), DSR(2), SSK, IDIST, PERCNT

NSTAGE: Stage number of current run

NPAR : number of particles to be studied

SSK : scale factor, usually 1

PERCNT: Capture zone, percent of pitch for full pitch run PERCNT=100.

IDIST : first stage stator particle distribution
0, no given distribution(usually)
1, some given distribution

DSR : gap size between blades, ft

Card 4 : (for first stage IDIST=0)
XRE, ZRE, VPARRE, BETPRE, ALPPRE

XRE : Partical starting position in stator, x-direction, ft

ZRE : Partical starting pasition in stator, θ-direction, ft

VPARRE: Partical starting velocity (ft/sec)

BETPRE: 0 (usually)

ALPPRE: 0 (usually)

Card 4 : (for first stage IDIST=1)
the above quantities for each particle entering.

Card 4 : (for other stages) and Card 5 :(for first stage)

IPPRINT, INP

IPPRINT : 1, particle integration history printed.
0, no print

INP : 1, passage gas properties printed.
0, no print.

TPART program reads stator and rotor data stored by TSONIC program on units 21 and 23 respectively. During calculations stores data necessary on unit 23 and 24 temporarily. TPART program also reads proceding stage exit data from unit 25 (except for first stage) and stores current stage exit data on unit 26. TPART program stores impact data on unit 27.

APPENDIX C

TPER PROGRAM INPUT DESCRIPTION

All formats are free.

Card 1 : Title

Card 2 : NDEP

NDEP : number of impacts of each particle considered

Card 3 : ((TESURS (I,J), I=1,2), J=1,9)

TESURS : stator blade surface temperature distribution

I=1,2 denotes upper and lower surfaces respectively.

J=1,9 denotes number of data readed for each surface

Card 4 : ((TESURR (I,J), I=1,2),J=1,9)

TESURR : rotor blade surface temperature distribution

I and J as explained above.

TPER program reads impact data stored by TPART program on unit 28.

APPENDIX D

EROSION MODELS USED

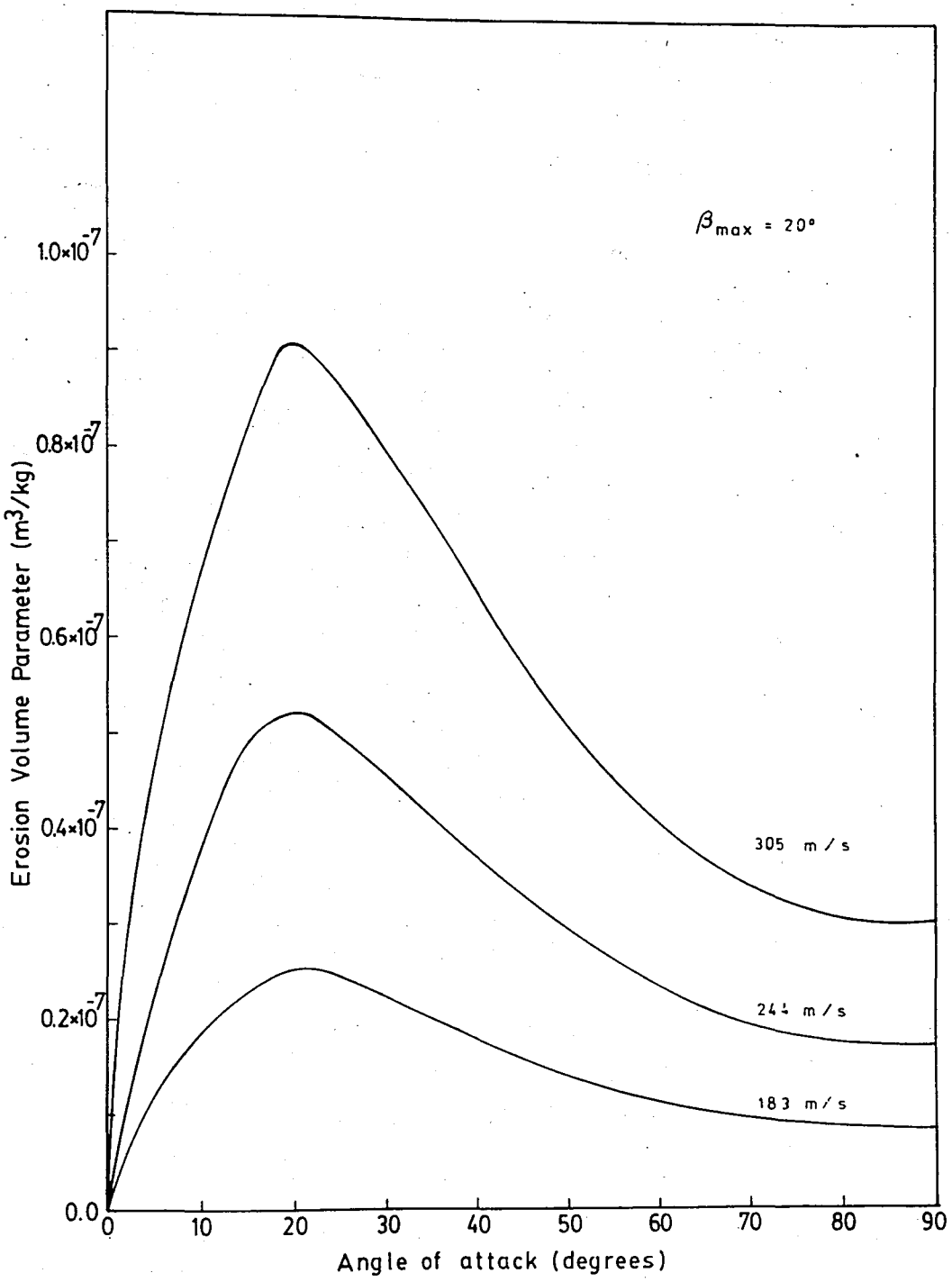

FIGURE D-1 - Erosion volume paremeter as a function of angle of attack for ductile material, $\beta_{max}=20^0$

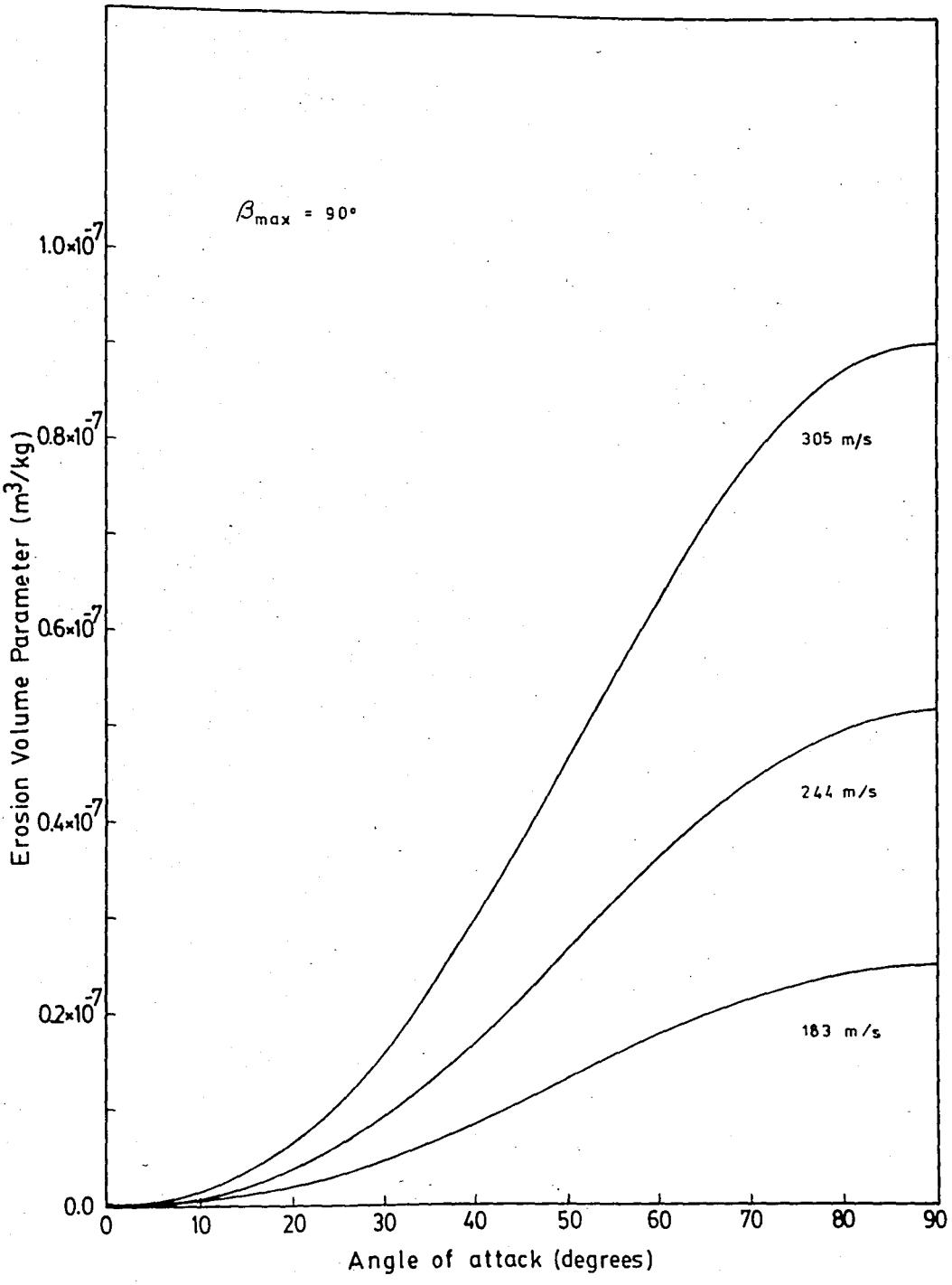

FIGURE D-2 - Erosion volume parameter as a function of angle of attack for brittle material, $\beta_{max}=90^0$

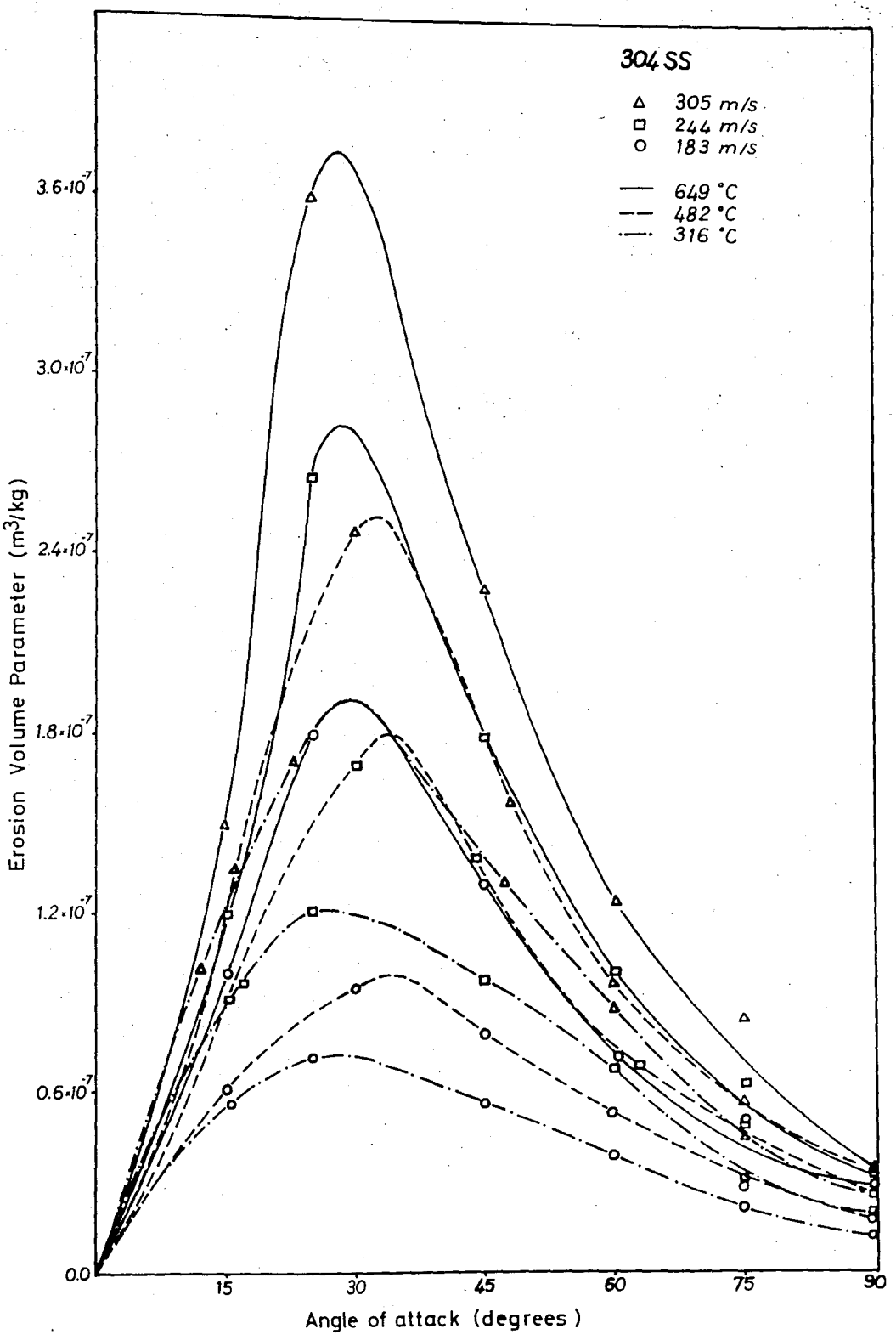

FIGURE D-3 - Erosion volume parameter as a function of angle of attack for 304 stainless steel

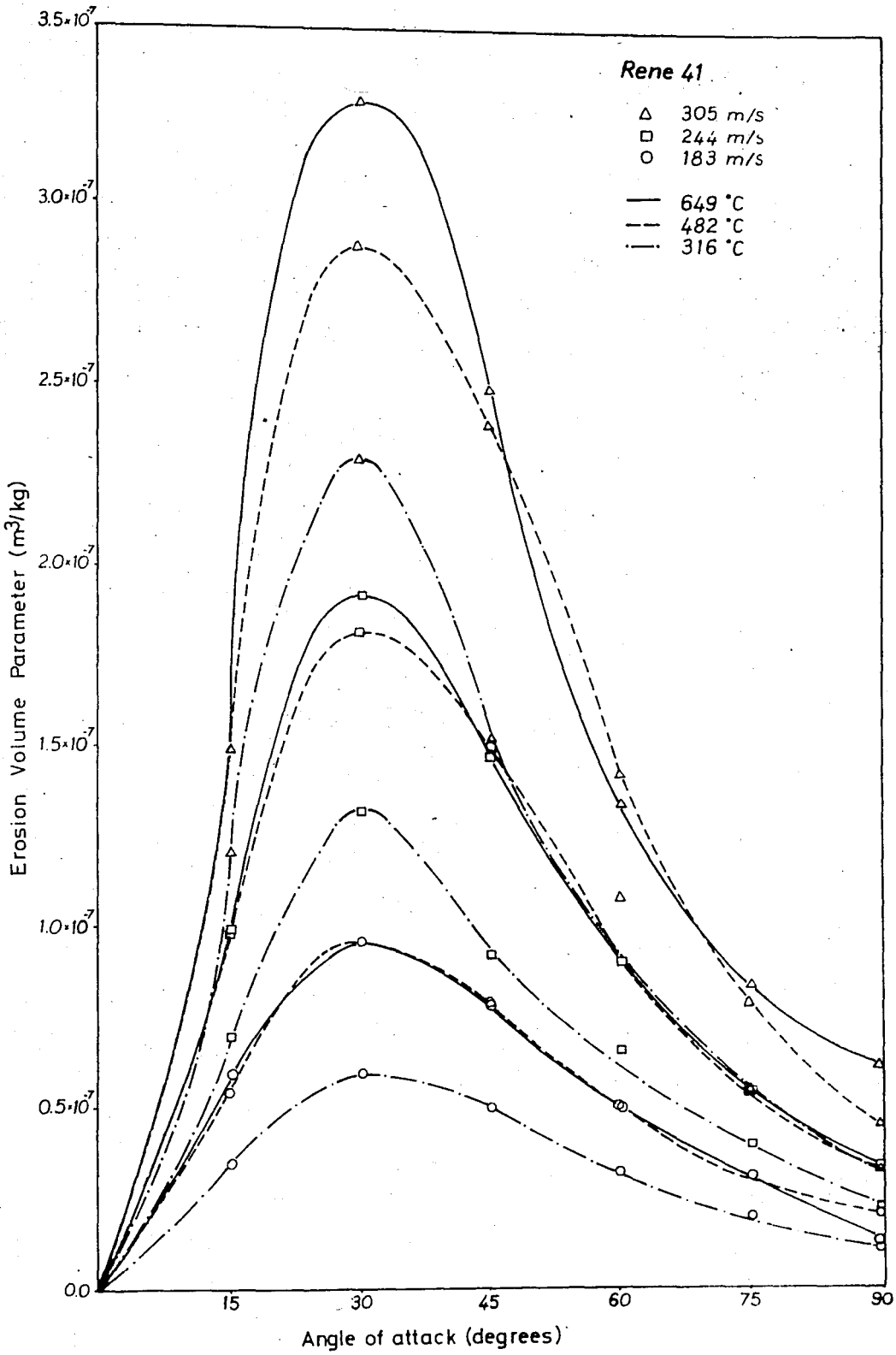

FIGURE D-4 - Erosion volume parameter as a function of angle of attack for Rene 41

APPENDIX E

TURBINE OPERATIONAL AND GEOMETRIC DATA

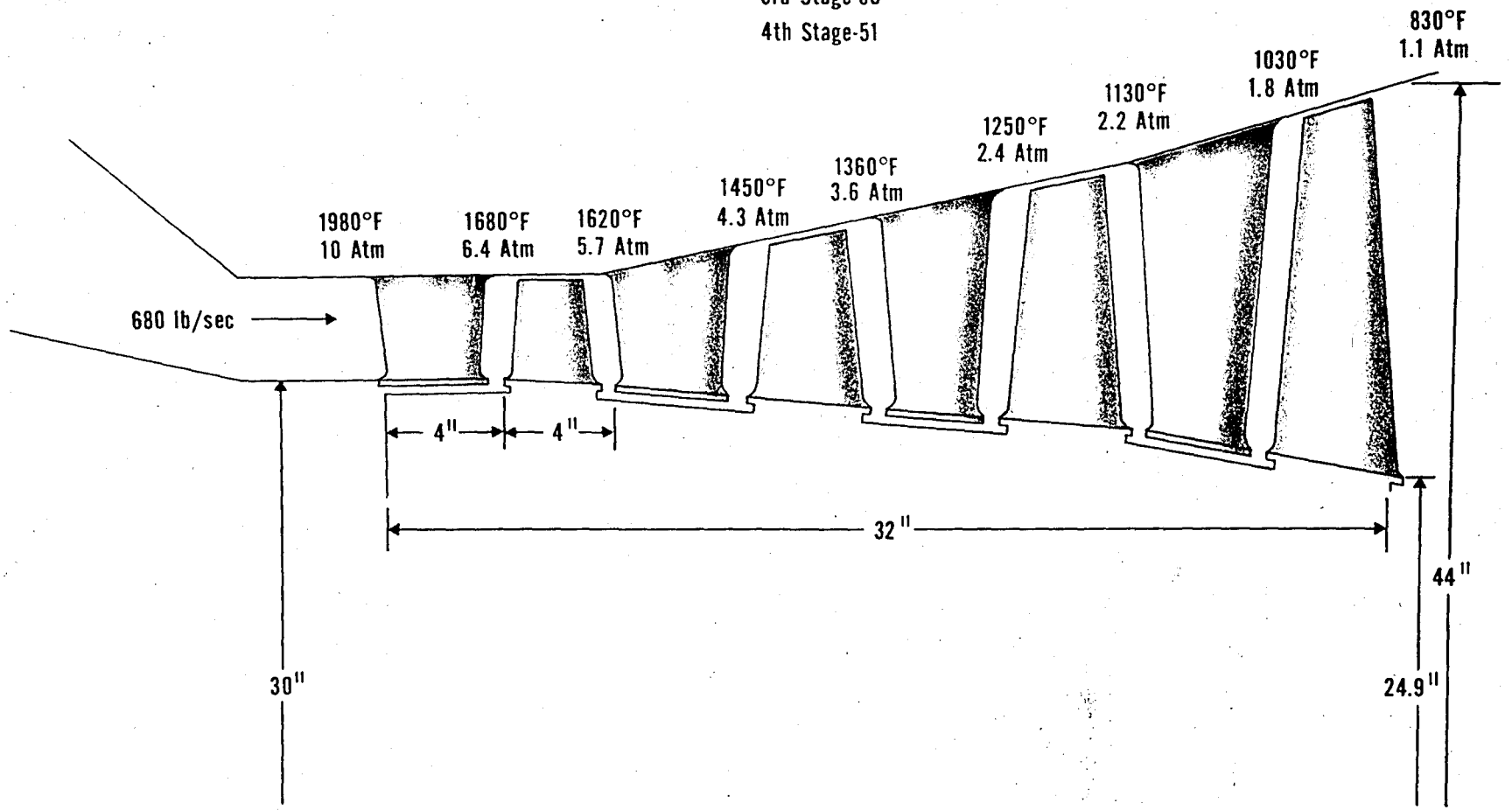

FIGURE E-1 - Turbine geometrical and operational data

LOCATION	V Absolute Velocity m/s	U Blade Velocity m/s	W Relative Velocity m/s	β Angle Relative to Rotor Blade	α Angle Relativ Stator Blade
Enter Rotor 1	597.3	312.7	371.1	47.87	66.7
Leave Rotor 1	281.4	311.5	474.3	57.3	15.5
Enter Rotor 2	509.5	315.2	308.1	27.5	61.2
Leave Rotor 2	275.8	318.5	457.9	53.5	14.
Enter Rotor 3	426.9	323.7	261.3	5.9	53.4
Leave Rotor 3	251.2	326.7	465.2	54.9	14.1
Enter Rotor 4	458.3	336.5	280.3	8.7	54.4
Leave Rotor 4		337.1	366.5	50.	

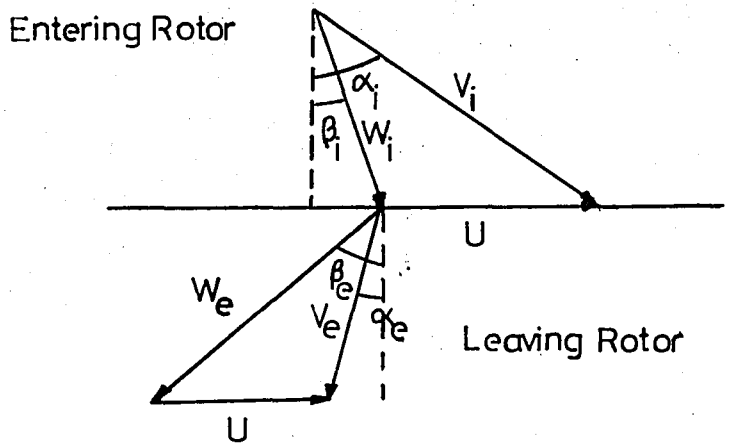

FIGURE E-2 - Velocity triangles on mid-span stream surface

REFERENCES

1. Mengütürk, M.and Sverdrup, E.F.,"Calculated Tolerance of a Large Electric Utility Turbine to Erosion Damage by Coal Gas Ash Particles," Erosion Prevention and Useful Applications, ASTM Special Technical Publication 664, pp. 193-224,1979

2. Katsanis, T., "Fortran Program for Calculating Transonic Velocities on a Blade-to-Blade Stream Surface of a Turbomachine," NASA T No. D-5427, 1969

3. Mengütürk, M. and Güneş, D., "Piecewise Exact Solution (PES) Method of Calculating Particle Trajectories in Various Applications," to be published.

4. Lapple, C.E. and Shepherd, C.B.,"Calculation of Particle Trajectories," Industrial and Engineering Chemistry, Vol.32, No.5, pp.605-617, 1940

5. Davies, C.N. and Peetz C.V.," Impingement of Particles on a Transverse Cylinder," Vol.234, pp.269-295, 1955

6. Heywood, H., "Uniform and Nonuniform Motions of Particles in Fluids, "Inst. Chem. Engrs., 1962

7. Holland-Batt, A.B., "Two Dimensional Motion of Particles Accelerating in Fluids, "Trans. Instn. Chem. Engrs., Vol.50, pp.156-167, 1972

8. Tabakoff, W. and Hussein, M.F., "Trajectories of Particles Suspended in Fluid Flow Through Cascades," AIAA Journal of Aircraft, Vol.8, No.1, pp. 60-62, Jan 1971

9. Tabakoff,W. and Hussein, M.F.,"Gas Particle Suspension Properties in a Cascade Nozzle, "JSME and ASME Paper, No.14, Joint International Gas Turbine Conference, Tokyo, Japan, Oct 1971

10. Hussein, M.F and Tabakoff, W., "Calculation of Particle Trajectories in a stationary Two Dimensional Cascade," Project Themis Report, No.72-27, University of Cincinati, Cincinati, Ohio, 1972

11. Morsi, S.A. and Alexander, A.J., "Theortical Low-Speed Particles Collision with Symmetrical and Cambered Aerofoils, "ASME paper, No.72-WA/FE-35, 1972

12. Ulke, A. and Rouleau, W.T., "The Effects of Secondary Flows on Turbine Blade Erosion, " ASME paper No.76-GT-74, 1976

13. Dring, R.P., Caspar, J.R. and Suo, M., "Particle Trajectories in Turbine Cascades, " AIAA Journal of Energy, Vol.3, No.3, pp. 161-166, 1979

14. Lord, M.J. and Singh, U.K.,"Theoretical Study of Potential Turbine Erosion Hazard by means of Particle Trajectory Calculation, "Proc. 5 th Int. Conf. on Erosion by Solid and Liquid Impact, Paper 54, Cambridge, U.K., Sept 1979

15. Suo, M., Patrick, W.P. and Johnson, B.V., "Particle Trajectories Near an Airfoil with a Film-Cooled Leading Edge," AIAA Journal of Energy, Vol. 3, No.3, pp.156-160, 1979

16. Mengütürk, M., Güneş, D., Mimaroğlu, H.K. and Sverdrup, E.F., "Blade Boundary Layer Effect on Turbine Erosion and Deposition," Proc. of ASME Gas Turbine Conference,June 1982/also to be published in J.of Fluids Eng., Fall 1983

17. Finnie, I., Wolak, J. and Kabil, Y., "Erosion of Metals by Solid Particles, "Journal of Materials, Vol.2, No.3, pp.682-700, Sept 1967

18. Stoker, R.L., "Erosion due to Dust Particles in a Gas Stream, "Industrial and Engineering Chemistry, Vol.41, No.6, pp.1196-1199, 1949

19. Finnie, I., "The Mechanism of Erosion of Ductile Materials, "Third U.S. Natl. Congr. of Applied Mechanics, pp.527-532, 1958

20. Finnie, I., "Erosion of Surfaces by Solid Particles, " Wear, No.3, pp.87-103, 1960

21. Bitter, J.G.A, "A Study of Erosion Phenomena," Part I, Wear, No.6, pp. 5-21, 1963

22. Bitter, J.G.A., "A Study of Erosion Phenomena," Part II, Wear, No.6, pp.169-190, 1983

23. Wood, C.D. and Espenschade, P.W., "The Mechanism of Dust Erosion, "SAE Trans. Vol.73, pp.515-523, 1965

24. Sheldon, G.L. and Finnie, I., "The Mechanism of Material Removal in the Erosive Cutting of Brittle Materials, " Journal of Engring for Industry, Trans.of ASME,pp.393-400, No 1966

25. Neilson, J.H. and Gilchrist, A., "Erosion by a Stream of Solid Particles," Wear, No.11, pp.111-123, 1968

26. Sage, W., "The Erosive Characteristic of Natural Sands and Abrasive Dusts, "National Gas Turbine Establishment, Note No. NT699, May 1968

27. Tilly, G.P. and Sage, W., "The Interaction of Particle and Material Behaviour in Erosion Process, "Wear, No.16, pp.447-465, 1970

28. Brasinikas, G., "Erosion by Particle Impact-Experiments with Callide Coal Ash, "Australian Aeronautical Research Laboratories, July 1970

29. Head, W.J. and Harr, M.E.," The Development of a Model to Predict the Erosion of Materials by Natural Contaminants," Wear, No.15, pp.1-46, 1970

30. Smeltzer, C.E., Gulden, M.E. and Crompton, W.A., "The Mechanism of Metal Removal by Impacting Dust Particles," Trans. of ASME, pp. 639-654, Sept. 1970

31. Finnie, I., "Some Observations on the Erosion of Ductile Metals,"Wear, No.19, pp.81-90, 1972

32. Sheldon, G.L. and Kanhere, A., "Investigation of Impingement Erosion Using Single Particles, "Wear, No.21, pp.195-209, 1972

33. Grant, G. and Tabakoff, W., "Erosion Prediction in Turbomachinery due to Environmental Solid Particles," AIAA 12 th Aerospace Sciences Meeting, Feb.1974

34. Frass, A.P.,"Survey of Turbine Bucket Erosion, Deposits and Corrosion," Asme Paper, No.75-GT-123, 1975

35. Ives. L.K., Young, J.P. and Ruff, A.W., "Particle Erosion Measurements on Elevated Temperatures," Prevention of Failure in Coal Conversion Systems, NBS Special Publication, pp.145-157, 1977

36. Young, J.P. and Ruff, A.W., "Particle Erosion Measurements on Metals, "Journal of Engineering Materials and Technology, pp.121-125, April 1977

37. Tabakoff, W., Kotwal, R. and Hamed, A., "Erosion Study of Different Materials Affected by Coal Ash Particles", Wear, No.52, pp.161-173, 1979

38. Maji, J and Sheldon, G., "Mechanism of Erosion of a Ductile Material by Solid Particles, "ASTM, pp.136-142, 1979

39. Wakeman, T.and Tabakoff, W.,"Erosion Behavior in a Simulated Jet Engine Environment, "Journal of Aircraft., Vol. 16, No.12, pp.823-883, Dec 1979

40. Raask, E., "Impact Erosion Wear Caused by Pulverized Coal and Ash, "Proc. 5th Int. Conf. on Erosion by Solid and Liquid Impact, Sept 1979

41. Tabakoff, W., Ramachandran, J. and Hamed, A., "Temperature Effects on Erosion of Metals used in Turbomachinery, " Proc. 5 th Int. Conf. on Erosion by Solid and Liquid Impact, Sept 1979

42. Raj, R. and Moskowitz, S., "Erosion Characteristics of Transpiration Cooled Materials," Asme Paper, No. 80-GT-186, 1980

43. Kotwal, R. and Tabakoff, W., "A New Apprach for Erosion Prediction due to Fly Ash," Asme Paper, No.80-GT-96, 1980

44. Tilly, G.P., "Erosion Caused by Airborne Particles," Wear, No, 14, pp.63-79, 1969

45. Neilson, J.H. and Gilchrist, A., "An Experimental Investigation into Aspects of Erosion in Rocket Tail Nozzles, "Wear, No.11, pp.111-123, 1968

46. Gat, N. and Tabakoff, W., "Some Effect of Temperature on the Erosion of Metals, "Wear, No.50, pp.85-94, 1978

47. Gat, N. and Tabakoff, W., "Effects of Temperature on the Behavior of Metals under Erosion by Particulate Matter," ASTM J. of Testing and Evaluation, Vol.8, No.4, pp.177-186, 1980

48. Newhart, J.E., "Evaluating and Controlling Erosion in Aircraft Turbine Engines,"

49. Sheldon, G.L., "Effects of Surface Hardness and Other Material Properties on Erosive Wear of Metals," J. of Engineering Materials and Technology, pp.133-137, April 1977

50. Hussein, M.F., "The Dynamic Characteristics of Solid Particles in Particulate Flow in Rotating Turbomachinery", Ph.D Dissertation, University of Cincinati, 1972

51. Tabakoff, W. and Hamed, A., "Aerodynamic Effects on Erosion in Turbomachinery, " JSME and ASME Paper, No. 70 Joint Gas Turbine Conference, Tokyo, Japan, May 1977

52. Tabakoff, W., Hamed, A. and Ramachandran, J. "Study of Metals Erosion in High Temperature Coal Gas Streams," Transactions of ASME, J. of Engg for Power, Vol 102, pp.148-152, Jan. 1980